THE PROCEEDINGS OF
THE PHYSICAL SOCIETY

VOL. 60, PART 6 — 1 June 1948 — No. 342

A Further Study of the γ-Radiation from Polonium

BY B. ZAJAC, E. BRODA AND N. FEATHER
Department of Natural Philosophy, University of Edinburgh

MS. received 7 *February* 1948

ABSTRACT. Absorption experiments using lead, gold and tungsten have shown that, in addition to the known γ-radiation of 0·77 MEV. energy, polonium emits other (soft) radiations of which the most intense has a quantum energy of 84 ± 4 kev. The intensity of this radiation is of the same order of magnitude as that of the hard radiation (roughly one quantum per 10^5 disintegrations). Experiments by the recoil method indicate that the emission of the polonium γ-radiation is not delayed by more than 10^{-1} sec. The results of Chang (1946) concerning the fine-structure of the α-particles of polonium remain uncorrelated with all other experimental evidence. Whilst present information regarding γ-ray energies and intensities may be reasonably explained, satisfactory explanation of the α-particle fine structure " data " appears as remote as ever.

§1. INTRODUCTION

INTEREST in the γ-radiation of polonium has recently been revived by the publication by Chang (1946) of quite unexpected evidence for a many-lined fine structure in the α-particle spectrum of this body. Two experimental studies of the polonium γ-radiation have since been described (de Benedetti and Kerner 1947, Siegbahn and Slätis 1947) and a critical discussion of Chang's results in relation to earlier information on the γ-radiation (Bothe and Becker 1930, Webster 1932, Bothe 1935, 1936) has been given by one of us (Feather 1946). The experiments now to be described were, like the others already mentioned, prompted by a consideration of Chang's results; they deal more particularly with the question whether a true nuclear radiation of quantum energy less than that of the now (Siegbahn and Slätis 1947) well-established "line" of 0·77 MEV. energy is in fact emitted, and secondly whether or not the emission of the polonium γ-radiation is measurably delayed in relation to the primary α-disintegration process. It should be remarked that the absorption measurements of Siegbahn and Slätis (1947) and de Benedetti and Kerner (1947) would appear to rule out the possibility of any significant emission of quantum radiation in the energy range 0·1 to 0·7 MEV. (or even of somewhat lower energy); on the other hand the only possible remaining way of explaining Chang's results on the basis of nuclear excitation followed by γ-ray emission is to postulate the relatively frequent emission of quanta of low energy (Feather 1946). It may be said in anticipation that no adequate low-energy quantum emission could be established in our experiments, although we have shown, in apparent contradiction of a statement of de Benedetti and Kerner, that weak nuclear radiations of about 84 kev. energy are present. No evidence that any appreciable fraction of the polonium γ-radiation is delayed by as much as 10^{-1} sec. after α-emission was obtained. It will be recalled that the possibility of such delayed emission was discussed in an attempt to interpret (Feather 1946) the reported observation

of γ-radiation of quantum energy 0·2 to 0·43 MeV. (Bothe 1935, 1936) in terms of excitation of nuclear states of corresponding energy only to the extent of a few times per million disintegrations. Now that the emission of such γ-radiation has been effectively disproved (de Benedetti and Kerner 1947, Siegbahn and Slätis 1947) the reason behind this suggestion obviously disappears.

§2. ABSORPTION EXPERIMENTS

Absorption of the γ-rays in lead was investigated over a range of thickness from zero to 3·4 gm/cm², and in a separate experiment a careful comparison of the absorption in lead, gold and tungsten was made up to thicknesses of 450 mg/cm². The first experiment extended over a period of 15 days, and the second (comparison) experiment over 48 days. No significant discrepancy appeared in the process of correlating all the observations in these experiments by simple correction for decay, taking $\lambda = 5{\cdot}74 \times 10^{-8}\,\text{sec}^{-1}$. The strength of the source at the beginning of the absorption measurements was about 6 mc., and a rough estimate based on β-particle counting showed that at this stage the radium (D + E) contamination was responsible for about 10^{-5} disintegrations per disintegration of polonium. The source was deposited by evaporation of an HCl solution, drop by drop, on a polythene disc 50 mg/cm² thick over an area 0·5 cm. in diameter.

A thin (end) windowed counter was employed for detection of the γ-radiations, the polythene disc carrying the source being supported on wood at a distance of approximately 2 cm. from the counter window, which was 1·4 cm. in diameter and 2·6 mg/cm² thick. The window material was mica. A standard argon–alcohol filling was employed and the counter pulses were registered by a "scale of 32" counting set. The average background counting rate of the (unshielded) counter was about 26 min^{-1}. Throughout the experiments aluminium absorbers of 480 mg/cm² thickness were placed directly over the source to cut out the primary β-particles from the radium E "impurity", and a further absorber of aluminium of 30 mg/cm² was invariably inserted immediately in front of the counter window so that the secondary electrons entering the counter should always originate in the same material. All absorbers were square foils of 3·2 cm. side.

The lead absorption curve obtained with this experimental arrangement is given in figure 1. Analysis of this curve by "least square" and graphical methods indicates component radiations as follows :

hard component $(\mu/\rho) = 0{\cdot}086$ cm²/gm., intensity 75%,
soft component $(\mu/\rho) = 2{\cdot}2$ cm²/gm., intensity 16%,
more absorbable radiation, intensity 9%.

The value of the mass absorption coefficient of the hard component is to be compared with 0·0815 cm²/gm. obtained by de Benedetti and Kerner in measurements up to 62 gm/cm², and 0·081 cm²/gm. deduced by Siegbahn and Slätis from observations over 33 gm/cm² absorber thickness *. It should be entirely unnecessary to point out that our value cannot claim anything approaching the independent weight of either of these other two determinations, made with much stronger sources under better geometrical conditions, but the numerical agreement is at least satisfactory. On the other hand, our observation of softer components of quantum radiation, transmitted through 0·5 gm/cm² of aluminium and res-

* As long ago as 1931 rough absorption experiments extending to 51 gm/cm² of lead were made by Blau and Karz-Michailova (1931).

ponsible for 25% of the total γ-ray effect in our counter, is a matter of more interest. It is explicitly stated by de Benedetti and Kerner that they could detect no radiation softer than the main component of about 0·8 MEV. energy until their aluminium absorber thickness was reduced below 0·5 gm/cm². Likewise the lead absorption curve of Siegbahn and Slätis shows little or no trace of any softer component. However, these authors used a counter with a gold cathode, and if this counter was the same as that later employed by Slätis (1947) in another investigation then, from information provided in the later paper, it would appear that absorption of our soft components in the wall of the counter would have amounted to at least 75% in the arrangement used. It cannot be held, therefore,

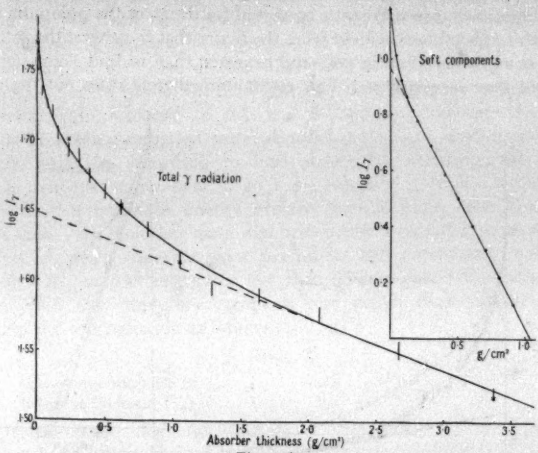

Figure 1.

× Observations with 50 mg/cm² polythene above the source.

that serious conflict with the results of Siegbahn and Slätis is established, and without further information as to the degree of attention given to the initial portion of their absorption curve by de Benedetti and Kerner (their published curve shows no plotted point below 1 gm/cm² thickness of lead) it is impossible to say whether there is any outstanding disagreement with their observations, either. It can, however, be stated quite definitely that the total intensity of the soft components observed in our experiments is at least 7 times that of any effect which might be attributed to quantum radiations from the radium (D + E) impurity in the source—and in any case the absorbability of our soft components is quite different from that of the general quantum radiations from a source of radium (D + E + F) in equilibrium. With such a source, under conditions similar to those obtaining in the present experiments, the effective mass absorption coefficient of the radiation transmitted by 0·5 gm/cm² of aluminium is roughly 1·1 cm²/gm. in aluminium, or about 25 cm²/gm. in lead. This is entirely different from $(\mu/\rho)_{Pb} = 2{\cdot}2$ cm²/gm. which characterizes the main soft component now under discussion.

It should also be stated that there is no possibility that the soft radiations arise from disintegration effects, or as a result of inelastic scattering of the

α-particles, in the aluminium absorber placed over the source. Observations made with 50 mg/cm² of polythene directly above the source (see figure 1) showed that these radiations still persisted with the same intensity as before.

The comparison measurements with absorbers of lead, gold and tungsten were carried out in an attempt to reach more definite conclusions concerning the quantum energies of the soft components. On the basis of the lead absorption measurements alone it would be possible to assign an energy of about 145 kev. or 84 kev. to the main soft component, depending on whether or not it were assumed that *K*-shell absorption was involved. Figure 2 shows the results of the comparison measurements, corrected for decay of the polonium as already described. It is at once evident from the figure that in general the soft radiation is more strongly absorbed in gold and tungsten than in lead—and slightly more so in gold than in tungsten. This result immediately rules out the possibility

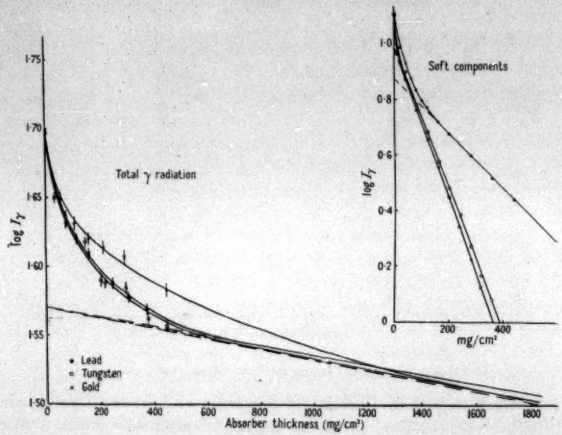

Figure 2.

that the main component of soft radiation has quantum energy greater than 87·9 kev., the *K*-absorption energy for lead or less than 80·7 kev., the *K*-absorption energy for gold. A more detailed (graphical) analysis of the curves of figure 2 was carried out on the following assumptions :

(i) the hard component, deduced from figure 1 as responsible for 75% of the total γ-ray effect in our first experiment, was responsible for the same fraction of the total effect in the comparison experiment (figure 2);

(ii) the mass absorption coefficients of the hard component in gold and tungsten could be calculated from the value obtained in the first experiment for absorption in lead, using standard theoretical expressions. Values of 0·084 cm²/gm. (gold) and 0·079 cm²/gm. (tungsten) were deduced on this assumption.

The results of this further analysis are summarized in table 1 which includes the corresponding results from the previous analysis of the lead absorption curve of figure 1 for additional comparison.

Table 1

Experiment	I	II	II	II
Absorber	Pb	Pb	Au	W
Main soft component μ/ρ (cm²/gm.)	2·2	2·2	6·1	5·7
Main soft component effective intensity (%)	16	15	19	19
More absorbable radiation—effective intensity (%)	9	10	6	6

It is at once evident from the figures given that it is impossible to provide a complete explanation of all these results in terms of two monochromatic soft components only; the term "main soft component" which has been used hitherto has obviously no unique reference to a single radiation. This latter conclusion derives from two considerations, first that the apparent intensity of this hypothetical component is greater on the basis of gold (or tungsten) absorption than on the basis of lead absorption measurements, and secondly that corresponding to $(\mu/\rho)_{Pb}=2{\cdot}2\,cm^2/gm.$ we should expect $(\mu/\rho)_{Au}=8{\cdot}4$ and $(\mu/\rho)_W=6{\cdot}8\,cm^2/gm.$, instead of 6·1 and 5·7 cm²/gm. respectively. Clearly there must be present radiation more absorbable than the most prominent soft component radiation according to lead absorption measurements, but less absorbable than that component in gold and tungsten. Such a radiation must obviously have a quantum energy greater than 87·9 kev., the *K*-absorption energy of lead. On the other hand, the presence of a radiation more absorbable in all three elements than the most prominent soft component must also be postulated. A quantum energy of less than 35 kev. would thus appear to be indicated. We may therefore accept a very rough three-component interpretation of the soft radiation as follows (table 2)

Table 2

Quantum energy (kev.)	<35	84±4	105±15
Effective intensity (%)	6	15	4

Further discussion of this interpretation is reserved for a later stage, here it should merely be re-emphasized that the figures given under heading "effective intensity" in table 2 represent percentages of the total γ-ray counting rate in our experimental arrangement, not absolute, or even relative, values of true quantum intensities per disintegration of polonium.

§3. DELAY EXPERIMENTS

These experiments were designed in the first instance to investigate the possibility that the residual nucleus ^{206}Pb, which results from the α-disintegration of polonium, is occasionally produced in a metastable state of lifetime of the order of minutes; they were later extended to search for possible γ-ray lifetimes as short as a few milliseconds. The first experiment originated in the suspicion (Feather 1946) that the unidentified activity of 1·6 m. half-value period, which Waldman and Collins (1940) have reported as produced by the action of high-energy x-rays on lead, might result naturally in a rare mode of the disintegration $^{210}Po\rightarrow{}^{206}Pb$. As already stated, this experiment gave a negative result. It was carried out by exposing a brass disc collector of 1·4 cm. diameter at a distance of 1 cm. and at a potential of −700 v. with respect to a "clean" source of about 12 mc. of polonium deposited on a platinum foil of 4 cm² area. Exposures lasted for a standard time of 12 minutes. Any activity collected by the disc was then observed over a period of 10 minutes immediately following the end of the exposure, using a thin-windowed counter and an absorber of 15 mg/cm² paper to cut out the effect of the α-radiation of the polonium which was collected

by aggregate recoil. As a result of 14 exposures it was concluded that the collector carried no activity giving an initial counting rate of more than 1 count per minute under our experimental conditions. The α-activity of the polonium collected by aggregate recoil was estimated, by removing the paper absorber, as $1{\cdot}4\,\text{min}^{-1}$ per minute exposure in the same geometrical arrangement, this figure corresponding roughly to one polonium atom collected per 3000 α-disintegrations of the source.

The next experiment, on possible short-period delays, was carried out in two different arrangements exemplifying the same basic principle. This principle was to examine the activity of a collector permanently exposed to a polonium source, the source and collector being so disposed in the neighbourhood of the end-windowed counter that the counter was considerably more sensitive to γ-radiation emitted by atoms disintegrating on the collector than to γ-radiation from the primary source.* Transference of recoiling atoms from the source to the collector in the applied field was calculated to take place in an average time of $2{\cdot}4\times10^{-3}$ sec. in the first arrangement and 5×10^{-2} sec. in the second. In spite of the longer transference-time the second arrangement had the great advantage over the first that the collector subtended a much greater solid angle at the counter window than before: in the second arrangement, in fact, the collector was separated from the window only by a 0·5 cm. air gap and an aluminium absorber $30\,\text{mg/cm}^2$ thick. In each arrangement the counting rate with source and collector in position was determined both when the source and collector were at the same potential and also when the collecting field was applied. A "genuine" increase in the counting rate on the application of the field would in this experiment provide clear evidence for the production of an activity in the recoil nucleus ^{206}Pb of any lifetime between a few milliseconds and 1 minute. In fact, the mean increase in three sets of observations using the first arrangement, was $0{\cdot}80\pm0{\cdot}53\,\text{min}^{-1}$ and, in five sets of observations using the second arrangement, $0{\cdot}40\pm0{\cdot}56\,\text{min}^{-1}$. The γ-ray counting rate determined with the primary source in the collector position in arrangement (i) was $20{\cdot}5\pm2{\cdot}4\,\text{min}^{-1}$, and it was estimated that in arrangement (ii) it would have been at least $60\,\text{min}^{-1}$. (As already implied a direct determination of the γ-ray effect of the polonium source through only $30\,\text{mg/cm}^2$ aluminium could not easily be made on account of the radium (D + E) impurity). The efficiency of collection of ^{206}Pb recoil atoms was estimated—in the only way available, in terms of the efficiency of aggregate recoil collection—as about $\frac{2}{3}$ of the efficiency in the standard exposure arrangement of the long-period delay experiment (see above) in arrangement (i), and as about $\frac{1}{3}$ of this standard efficiency in arrangement (ii). The latter result was all the more gratifying since the average distance travelled by a recoil atom in the field—and that not in a straight line—was about 10 cm. in this arrangement, as against 1 cm. under "standard" conditions.

§4. DISCUSSION

In discussing the experimental results described above we may deal first, quite briefly, with the results of the delay experiments. Always assuming that the recoil efficiency of the primary polonium source was high—which the appearance of the activated platinum foil and our observations on aggregate recoil might be held to justify—it is obvious that these results show that not more

* Essentially the same principle was used by Ellis (1932) and also by Wright (1932) in work on ThC and RaC′, respectively.

than 10% of the γ-ray effect in our counter arises from activities of lifetime greater than 5×10^{-3} sec. and not more than about 3% of the total effect from activities of lifetime greater than 10^{-1} sec. It is significant to remark that this second statement includes γ-ray activities which because of a high degree of internal conversion might show up only through the emission of *L* x-rays (Curie and Joliot 1931), since the aluminium absorber in the second arrangement was sufficiently thin to transmit a considerable fraction of such fluorescent radiation.

Turning to the results of the absorption experiments one important conclusion can be stated at the outset. Because of the close similarity of the absorption curves obtained with gold and tungsten absorbers it must be concluded that no significant component of the "soft" radiation from polonium has quantum energy intermediate between the *K*-absorption energies of tungsten and gold, i.e. in the energy range between 69·4 and 80·7 kev. Now the $K\alpha_1$ and $K\alpha_2$ radiations of elements 81 to 84 inclusive lie within this range, thus we have the important result that the soft radiations which we have detected do not include the *K*-radiations of lead. That these radiations must be emitted following the internal conversion of the 0·77 Mev. polonium γ-ray is undeniable, but they are evidently below the limit of detection with our arrangement : present considerations, in fact, support previous estimates of the absolute intensity of the photoelectron lines (Feather 1946) and show that the internal conversion coefficient for the 0·77 Mev. radiation cannot be abnormally large (not greater than about 10^{-2}). Since they are not *K* x-rays obviously the soft radiations of table 2 must be predominantly of nuclear origin. Before we can make much progress towards an understanding of their mode of emission, however, we must make some attempt to estimate their intensity. This can only be done in the present instance by a rough comparison with the harder radiation.

Let us consider first the intensity of the main hard component. The "best" estimate in this case would appear to be $(1{\cdot}0 \pm 0{\cdot}4) \times 10^{-5}$ quanta per disintegration (Feather 1946)—and no difficulty would ensue if this were the only γ-radiation emitted. For, if the same change of spin were involved in an α-disintegration leading to the 0·77 Mev. excited state as in that leading to the ground state of the nucleus ^{206}Pb, we should expect an excitation of the 0·77 Mev. state of $(1{\cdot}8 \pm 0{\cdot}5) \times 10^{-5}$ per disintegration (Feather 1948). The agreement between this figure and the observed γ-ray intensity is remarkably close, and in the absence of the soft radiation we might well be satisfied that the rare nuclear processes were completely understood. We have now to see whether it is possible to explain at the same time the emission of the softer γ-radiations in terms of the excitation of other states having spin values consistent with our observation that the soft γ-radiation is not appreciably "delayed". In this connection we should note the estimate of Curie and Joliot (1931) that the intensities of the *L*- and *M*-radiations of polonium (or lead) which they observed were about 4×10^{-4} and $1{\cdot}5 \times 10^{-3}$ quanta per disintegration, respectively.

Now it is certain from our results that the soft radiations are not considerably more intense (in quanta emitted per disintegration) than the hard component. Using the results of Bradt and collaborators (1946) in making our comparison we should in fact conclude that our 84 ± 4 kev. soft component has roughly the same intensity as the 0·77 Mev. (hard) radiation.* Our other soft components

* Bradt *et al.* found that an aluminium counter is roughly five times as sensitive to γ-rays of 0·8 Mev. energy as to 0·1 Mev. radiation.

would then appear as less intense than this. As concerns the main soft component two possibilities must now be considered: either the major portion of the *L*-radiations of Curie and Joliot follows the internal conversion of this soft γ-radiation (of 84 ± 4 kev. energy) or it does not. On the first assumption the 84 kev. nuclear transition has an intensity of roughly 4×10^{-4} per disintegration, the radiation has an internal conversion coefficient of about 40, and because of intensity considerations it cannot be coupled in any way with the emission of the 0·77 Mev. radiation. Separate excitation of a nuclear state of 84 kev. energy has thus to be assumed, and a difference of spin between excited and ground states of some 5 units is necessary to explain the intensity. The assumption has therefore to be ruled out if the radiation is not appreciably delayed.

The second assumption avoids this particular difficulty by allowing coupling of the hard and soft radiations—and so permitting a single high energy state excitation. We might, in fact, on this view, imagine that the 0·77 Mev. state was fed chiefly by γ-ray transitions from a state of 84 kev. higher energy (and possibly to a smaller extent from other states in the same energy range) excited directly by α-disintegration. The difference of 84 kev. in the energy available for α-disintegration would be expected to introduce an adverse factor of no more than 3·5 in the partial disintegration probability (which would not seriously disturb the numerical agreement already noted), and if it were assumed, for example, that the ground state of ^{206}Pb and the excited state of 0·85 kev. each had zero spin, and the 0·77 Mev. state had spin of 2 units, no major interpretative difficulty need remain—except the explanation of the intensity of the *L*- and *M*-radiations observed by Curie and Joliot and the whole problem of the fine-structure spectrum of Chang (1946). Concerning the first difficulty it might be possible to accept the suggestion, frequently put forward in the past, that the fluorescent radiations arise in the (infrequent) internal ionization of the radioactive atom by the escaping α-particle, having no connection, therefore, either with the appearance of discrete lines in the α-particle energy spectrum, or with nuclear γ-ray transitions, but the problem posed by Chang's results would seem as far from solution as ever. Amongst the rare effects associated with the polonium disintegration only the fluorescent X-ray emission itself appears to have an intensity of the same order of magnitude as the fine-structure lines in Chang's spectrum.

REFERENCES

de Benedetti, S., and Kerner, E. H., 1947, *Phys. Rev.*, **71**, 122.

Blau, M., and Kara-Michailova, E., 1931, *Sitzungsber. Akad. Wiss. Wien*, II *a*, **140**, 615.

Bothe, W., 1935, *Z. Phys.*, **96**, 607; 1936, *Ibid.*, **100**, 273.

Bothe, W., and Becker, H., 1930, *Z. Phys.*, **66**, 307.

Bradt, H., Gugelot, P. C., Huber, O., Medicus, H., Preiswerk, P., and Scherrer, P., 1946, *Helv. Phys. Acta*, **19**, 77.

Chang, W. Y., 1946, *Phys. Rev.*, **69**, 60.

Curie, I., and Joliot, F., 1931, *J. Phys. et Radium*, **2**, 20.

Ellis, C. D., 1932, *Proc. Roy. Soc.* A, **136**, 396.

Feather, N., 1946, *Phys. Rev.*, **70**, 88; 1948, *Nuclear Stability Rules* (Cambridge: University Press) (in preparation).

Siegbahn, K., and Slätis, H., 1947, *Arkiv Mat. Ast. Fys.*, **34 A**, (15).

Slätis, H., 1947, *Arkiv. Mat. Ast. Fys.*, **35 A** (3).

Waldman, B., and Collins, G. B., 1940, *Phys. Rev.*, **57**, 338.

Webster, H. C., 1932, *Proc. Roy. Soc.* A, **136**, 428.

Wright, P., 1932, *Proc. Camb. Phil. Soc.*, **28**, 128.

The Semi-Diurnal Variation in Cosmic Ray Intensity

By PHYLLIS NICOLSON and V. SARABHAI
Cavendish Laboratory, Cambridge

MS. received 2 *September* 1947

ABSTRACT. The experimental data on the daily variation in cosmic-ray intensity are first surveyed. It appears to be established by Rau's experiments that the energetic meson component at sea level shows a marked semi-diurnal variation which is in phase with the semi-diurnal variation shown by the barometric pressure. Several authors have suggested that this phenomenon is explicable in terms of the Pekeris theory of atmospheric oscillations. The implications of this explanation on the process of meson formation are here examined quantitatively. It is concluded that the explanation is only possible if mesons arise mainly at about 60 or 70 km. above sea level, which is highly unlikely since the corresponding cross-section for meson production would be much larger than appears plausible.

In addition the experimental data on the diurnal variation are briefly discussed. This variation seems to be more complicated in character than is usually assumed and not attributable to factors such as a heliomagnetic field and fluctuations in the geomagnetic field, which are often held responsible.

§ 1. INTRODUCTION

If the experimentally observed solar daily variation in cosmic-ray intensity is analysed into Fourier components, it is usually found that the only important components are the diurnal (24-hour period) and the semi-diurnal (12-hour period). It is with the semi-diurnal component that we are chiefly concerned here.

Certain observers (Regener and Rau 1939, Ehmert 1939, Rau 1940, Sarabhai 1945) have found a daily variation in meson intensity which is mainly semi-diurnal and shows a strong positive correlation with that in atmospheric pressure, and have pointed out that the theory of atmospheric oscillations outlined by Pekeris (1937) and described in § 3 below provides at least a qualitative explanation of this phenomenon, which is difficult to understand on any other basis. If this explanation is valid, then the experimental data on the amplitude of the cosmic-ray effect, together with the quantitative predictions of the Pekeris theory, provide a means of determining the approximate height at which mesons are mainly produced and hence the approximate value of the average cross-section for meson production. At the present stage of theory and experimental data relating to meson creation, even a very rough estimate of the value of this cross-section would be useful.

It was clear from the general features of the oscillation predicted by Pekeris that this method of explaining the semi-diurnal variation in meson intensity would certainly lead to rather a large value for the cross-section, but whether this value would be too large to be plausible could not be decided without quantitative investigation. The main purpose of this paper is to describe such investigations and their result (§ 3). One of the subsidiary purposes is to make clear the implications of the Pekeris theory, for the results of this theory have been incorrectly interpreted by certain writers on the semi-diurnal variation in cosmic-ray intensity.

Since there is much apparently conflicting evidence on the daily variation of cosmic radiation, it is essential to survey all the experimental data before proceeding to consider theories to explain any part of these data. We shall now make such a survey and then consider what facts may be looked upon as experimentally established.

§ 2. EXPERIMENTAL DATA

It is important to classify the various experimental results according to the nature of the intensity to which they refer, for the daily variation may be expected to depend upon the constitution of the radiation observed. For example the mesonic and electronic components may not be affected in the same way by short-period fluctuations in meteorological conditions, since these fluctuations may be entirely different in character in the upper atmosphere where the mesons mainly arise and in the lower atmosphere where most of the electrons recorded at sea-level arise.

In addition it is important to make clear whether the observer in presenting his results has tried to allow for changes in meteorological factors such as temperature and pressure, for it often happens that the so-called "corrections" applied are so large that they completely change the character of the daily variation. For example, the "external temperature" correction, applied by many workers in an attempt to eliminate the effect of fluctuations in the temperature of the air above the recording apparatus, may be sufficient to shift the phase of the diurnal variation by eight hours; it is therefore important to consider the justification for this correction. The correction is usually made before harmonic analysis is carried out, by adjusting the hourly recordings by means of a temperature coefficient determined from the correlation of long period (usually average monthly) variations of intensity with temperature. Now the variations in monthly mean intensity at sea level are probably caused mainly by changes in the average height of origin of mesons; this height depends upon the temperature distribution throughout the atmosphere below it and also on the pressure at sea level. Consequently, even in these long period variations, there is not always a simple dependence of the intensity on the temperature at the ground; even if there were it would have little bearing on the relation between hour-to-hour changes in intensity and ground temperature. Test made by Forbush at Cheltenham (U.S.A.) suggest that at this location at least, no external temperature correction ought to be made. Consequently the value of results to which this correction has been applied seems very doubtful.

The practice, often adopted, of correcting hourly readings for fluctuations in barometric pressure by using a barometric coefficient based on comparison of the mean daily intensity and barometric pressure, may not be entirely justified either; for although the barometric effect is certainly due partly to mass absorption, it may also depend upon factors such as movement of meson-producing layers, which are differently related to short and long period pressure changes. A third correction is sometimes applied for fluctuations in the internal temperature of the apparatus, but in the best designed experiments this is made unnecessary by thermostatic control.

2.1 *Collection of results*

Results are collected in table 1. The notation used therein is as follows :—

λ = geomagnetic latitude of the station.

h = altitude of station in metres above sea level.

ϕ = angle of cone formed by observed radiation; since information on this is not very precise it will be classified simply as wide or narrow.

θ = inclination of axis of observed cone to the vertical.

$D(b,c)$; $S(b,c)$ = diurnal (semi-diurnal) variation of amplitude $b\%$ and maximum at c hours. In cases where the harmonic dial method of analysis has been used the probable error in b is also given.

+S; −S imply that the maximum of the variation is displaced by less than one hour from the maximum (minimum) of the semi-diurnal pressure variation.

I.C.; G.C. indicate use of ionization chamber; Geiger counter apparatus.

B.; E.T.; I.T. indicate correction for barometer effect; external temperature effect; internal temperature effect.

2.2 *Discussion of the experimental evidence on the S variation*

In view of the smallness of the daily variation, observations over a very long period are required before one can be certain that the variation obtained is of physical significance. For this reason the reliability of many of the results quoted above is somewhat doubtful. In the case of the S variation the only results of convincing statistical significance are those of Duperier (1945), based on three years' observations and those of Rau (1939), although the results found by Hoerlin under 10 cm. Fe do carry some conviction on account of the large amplitude of the S effect recorded and the closeness with which it follows the pressure variation.

Rau used two independent ionization chambers of different size suspended under 40 metres of water in a narrow vertical fissure in the rock forming the floor of Lake Constance. The dimensions of this fissure were such that the intensity observed was mainly vertical. The data from the two chambers showed a similar variation. The results given above were obtained with the larger chamber. The first result S ($0{\cdot}18 \pm 0{\cdot}04$, $11^h\,30$) was found by a harmonic dial analysis of the data recorded on 192 days, while the second result S ($0{\cdot}14$, 10^h) was obtained by taking the average of the hourly readings over a period of 15 months, and then harmonically analysing the resulting daily variation curve. The two results when considered together, suggest that the amplitude lies between $0{\cdot}14$ and $0{\cdot}18\%$, and we shall in numerical work take $0{\cdot}16\%$ as the amplitude established by Rau.

The interpretation of Rau's results is much less ambiguous than that of Duperier's for the following reasons: (i) Only mesons are measured instead of the total intensity made up of mesons and soft component. (ii) The angle ϕ is small and consequently the radiation can be regarded as entirely vertical to a good approximation. (iii) Only particles of initial energy $>10^{10}$ ev. can penetrate the absorber above Rau's apparatus (50 m. water including the atmosphere), which means that the effect of magnetic variations has been eliminated. This is confirmed by the absence of any change in intensity during magnetically disturbed days in the case of Rau's experiments.

In view of the difference in nature of the intensity measured in the two cases, it is not surprising that the variations found by Rau and Duperier are of very different character.

At the equator there are no completely convincing results. Thompson's are uncertain on account of their short duration (only about 6 day's readings for a zone $2\frac{1}{2}°$ in latitude) and the fact that a relatively large correction is made necessary

Table 1

(i) Variation of radiation

Observer	λ	h	Apparatus	ϕ	θ
Barnothy and Forro (1939)	47° N.	124	G.C.	wide	0
Duperier (1945)	54° N.	0	G.C.	wide	0
Alfvén and Malmfors (1943)	58° N.	0	G.C.	narrow	30° N. 30° S. 60° N. 60° S.
Hoerlin reported by Rau (1940)	2° N.	5500 to 6100 2500 to 5500	I.C. I.C.	wide wide	0 0
Kolhorster (1941) (1)	52·4° N.	0	G.C.		45° N. 45° S. 45° E. 45° W.
Sarabhai (1945)	3° N.	900	G.C.	wide	0

(ii) Variation of total

Steinmaurer (1935)	47° N.	590	I.C.	wide	0
Hess and Graziadei (1936)	47° N.	2300	I.C.	wide	0
Doan (1936) (2)	52° N.	150	I.C.		0
Forbush (1937) (3)	50° N.	72	I.C.	wide	0
Schonland, Delatizky and Gaskell (1937) (4)	32° S.	122	I.C.	wide	0
Thompson (1938) (5)	40–55° N. 25–40° N. 10–25° N. 10° S.–10° N. 10–25° S. 25–40° S.	0	I.C.	wide	0
Sarabhai (1945)	3° N.	900	G.C.	narrow	0

(iii) Variation of

Barnothy and Forro (1936) (6)	47° N.	124	G.C.		0 50°
Rau (1939) (7)	50° N.	360	I.C.	narrow	0

(iv) Variation of

Barnothy and Forro (1939)	47° N.	124	G.C.		0

(1) Results not Fourier-analysed. Appreciable variation with θ; time of maximum varies from about 7 to 15h.
(2) Very small barometric variation on 10 days selected. Results from 7 identical recording meters running simultaneously.
(3) D variation well established.
(4) Results made uncertain by large temperature fluctuations of apparatus itself.
(5) Recording made during 12 voyages. On average 6 days readings for each zone 2½° in latitude. Uncertainty introduced by necessity of correcting for latitude effect.

under little or no absorber

Absorber	Duration of Expts.	Corrections applied	Results	
			D	S
0	2 months	B.		
0	3 years	None B.	(0·25, 17h 20) (0·22, 17h 20)	−(0·18, 03h12)
0	2½ years	B.	(0·12±0·03, 10h) (0·08±0·03, 13h) (0·16±0·02, 13h) (0·17±0·02, 19h)	
0	10 days	B., I.T.		−(0·06, 04h 30)
10 cm. Fe	8 weeks	B., I.T.		+(0·78, 10h 47)
0	8 months	None		
0	15 days	None	(0·3, 14h 30)	
meson component				
10 cm. Pb	9 months	B. B., E.T.	(0·25, 8h) (0·25, 12h)	
12 cm. Pb	3 years	B., E.T.	(0·2, 10h 40)	(0·5, 00h)
12 cm. Pb	10 days	B.	(0·19±0·04, 09h)	
12 cm. Pb	273 days	B.	(0·17±0·02, 11h)	(0·04±0·01, 00h 30)
12 cm. Pb	3 years	B. B., I.T. B., I.T., E.T.	(0·2, 16h) (0·2, 6h) (0·2, 14h)	
12 cm. Pb	11 months in all	B.	(0·33, 14h 20) (0·22, 14h 30) (0·26, 14h 20) (0·23, 13h 50) (0·21, 14h 30) (0·17, 13h 10)	
8 cm. Pb*	12 days	None	0	+(3·0, 10h 30)
energetic meson intensity				
36 cm. Pb	4 months	B.		
36 cm. Pb	3 months	B.		
40 m. H_2O	15 months	None	0	(*a*) +(0·18±0·04, 11h 30) (*b*) +(0·14, 10h)
electronic shower intensity				
?	12 months	B.	(0·41, 15h)	

(6) Curves suggest reversal of phase of S variation as θ changes from 0 to 50°, but physical significance of these results is not convincing.

(7) (*a*) Harmonic dial method used on 192 days observations.
(*b*) By harmonic analysis of mean of 15 months observations. A second smaller, independent I.C. was used simultaneously and showed similar variation.

* In this case the method of shower anticoincidences was actually used for excluding the soft component, but the arrangement is essentially equivalent to a counter telescope with about 8 cm. Pb absorber.

by the latitude change in a 24-hour period. Sarabhai's experiments are unfortunately also too brief to give convincing results; they suggest the presence of a large +S variation. Hoerlin's results, obtained during the 1932 Cordillera Blanca Expedition and re-examined by Rau (1940), carry the greatest conviction. They suggest very strongly that the variation under an absorber of 10 cm. Fe is semi-diurnal, with large amplitude and phase strikingly close to that of the semi-diurnal pressure variation (meson maximum at 10^h47, pressure maximum at 10^h50). It seems likely, therefore, that at the equator the meson component shows a large +S variation but further experiments are necessary to establish this.

However this may be, Rau's conclusion that at latitude 50° the energetic mesons are characterized by a +S variation, appears to have good foundation and it seems worth while to examine quantitatively whether such a variation can be explained in terms of the Pekeris theory of atmospheric oscillations, particularly as this explanation of the effect has been given in several independent papers.

§3. EXPLANATION OF THE +S VARIATION

A predominant semi-diurnal variation is not likely to result either from temperature or from magnetic variations, as both would produce mainly diurnal rather than semi-diurnal effects. Apart from this consideration, Rau's results show clearly that magnetic fluctuations are not responsible, as the particles he observes have energies too high to be influenced by them *.

It has already been pointed out independently by Rau and Ehmert (1940) and by Sarabhai (1945) that a +S variation would result from atmospheric oscillations of the kind predicted by Pekeris, provided that the bulk of the mesons arise above 30 km., at which height the Pekeris oscillation has a nodal surface. Before working out the implications of this interpretation we will briefly indicate the nature of these atmospheric oscillations.

3.1 *The theory of atmospheric oscillations*

The diurnal component of the daily variation in atmospheric temperature is considerably larger than the semi-diurnal component, as one would expect. In spite of this, however, in the variation of the barometric pressure at sea-level, the semi-diurnal component is dominant, being about $1\frac{1}{2}$ times as large as the diurnal component. An explanation of the large semi-diurnal pressure variation has long been sought. Kelvin suggested that the atmosphere has a free oscillation of period about 12 hours, so that the semi-diurnal tide excited by the sun is magnified by resonance. Since then many attempts have been made to determine the period of free oscillation of the atmosphere.

G. I. Taylor (1929, 1932, 1936) showed that this period can be calculated from the speed of propagation of waves of explosion such as that caused by the Krakatau eruption in 1883, and that for this eruption the speed with which the wave was propagated corresponds to a free period of about $10\frac{1}{2}$ hours; a similar speed was found by Whipple (1934) for the wave of the Great Siberian Meteor. A period of $10\frac{1}{2}$ hours is, however, fatal to the resonance theory of atmospheric oscillation. In 1937 Pekeris extended the theory which had been outlined by Taylor in 1936,

* In the case of Rau's experiments, tides in Lake Constance provide a possible cause for an S effect, since any change in surface level of the lake alters the thickness of the water absorber above the apparatus. The change in intensity produced by such tides appears to be negligible however, as their magnitude is very small indeed—the change in level from high to low water being of the order of 0·1 inch.

and was able to prove that, when the temperature distribution with height suggested by experimental data is assumed, the atmosphere can have a free oscillation of 12-hour period in addition to one of 10½-hour period.

As early as 1924 Chapman discussed the semi-diurnal oscillation excited partly tidally and partly thermally by the sun, and concluded that if the atmosphere has a natural period of 12 hours, then this oscillation will be magnified about a hundredfold by resonance. Recently a more detailed investigation of the magnitude of the semi-diurnal pressure oscillation at different heights has been carried out by K. Weekes and M. V. Wilkes, who have extended the basic theory outlined by Pekeris and have used the Cambridge Differential Analyser to obtain numerical solutions of the equations involved. An account of this work together with detailed numerical results is to be published shortly. Meanwhile, Weekes and Wilkes have very kindly made their results available to the present writers.

The mode of oscillation of 12-hour period is characterized by a horizontal nodal surface at a height of about 30 km., the atmosphere above and below this level swinging in opposite directions. The changes in pressure and the horizontal velocity of winds caused by the oscillations are reversed in phase in crossing this level; the vertical velocity of winds has the same phase at all levels.* The amplitude of the pressure oscillation is small and almost uniform up to nearly 30 km.; at high altitudes it increases rapidly with increasing rarefaction of the atmosphere. The feature of particular significance in considering the effect of such pressure oscillations upon meson intensity at sea level is the variation Δh in the height of an isobaric surface situated at mean height h. Table 3 shows the values of Δh as a function of h calculated by Weekes and Wilkes for an atmosphere having the temperature distribution given in table 2, a distribution based as far as possible upon experimental data. The values given for Δh correspond to an oscillation of amplitude 1 mm. Hg at sea level at the equator, which is very close to that experimentally observed. The amplitude of the oscillation decreases with increasing latitude by a factor approximately $\cos^3\lambda$; Δh is given for $\lambda = 0$ and 50°.

Table 2. The variation of temperature with height adopted in the calculation of table 3

Height (km.)	Temperature (° K.)	Evidence
0– 10	288–220 ; linear fall.	Up to about 25 km. well established by radio-sonde data.
10– 30	220	
30– 55	220–350 ; linear rise.	Inferred from the abnormal propagation of sound (Whipple 1935).
55– 60	350	Suggested by radio exploration (Budden, Ratcliffe and Wilkes 1939)
60– 77	350–190 ; linear fall.	
77–100	190	

Table 3. The semi-diurnal oscillation of isobaric levels at various altitudes

h (km.)		0	10	20	30	40	50
Δh (km.)	$\lambda=0$	+0·010	+0·012	+0·012	−0·002	−0·086	−0·272
	$\lambda=50°$	+0·003	+0·003	+0·003	−0·001	−0·023	−0·072
h (km.)		60	70	80	90	100	
Δh (km.)	$\lambda=0$	−0·49	−0·51	−0·60	−1·05	−2·22	
	$\lambda=50°$	−0·129	−0·135	−0·160	−0·28	−0·59	

* It is interesting to note that this type of oscillation is compatible with that suggested by the "dynamo" theory developed by Chapman (1919) to account for the semi-diurnal variation of the earth's magnetic field. Chapman finds that the pressure oscillations in the upper conducting layer where the dynamo effect is produced are nearly 180° out of phase with those observed at the ground.

These values do not agree with those calculated by Mailvaganam (1946). From the following considerations it seems that Mailvaganam's results cannot be valid. It can be seen from the results of Pekeris' own analysis that near resonance the horizontal velocity is proportional to the pressure oscillation at any height, and consequently that the curve given by Pekeris (1937, figure 1) for the horizontal velocity also represents the pressure oscillation. Now the pressure oscillation calculated by Mailvaganam does not agree even in character with that given by Pekeris. The most obvious discrepancy is that Mailvaganam's results do not show the node at 30 km. which characterizes all Pekeris' results. One of the causes of the discrepancy seems to be that Mailvaganam has used incorrect numerical values for constants (C and D in his notation). We are indebted to Weekes and Wilkes for investigations on this point.

It is apparent from the nature of the oscillation described above that mesons created above 30 km. will show a + S variation at sea level, for if the isobaric levels in the lower atmosphere move down, corresponding to a fall in sea level barometric pressure, isobaric levels above 30 km. move up; mesons are therefore formed at higher levels and the meson intensity at sea level is decreased as the probability of decay is enhanced. Also the + S variation arising in this way should be much more pronounced at the equator than at latitude 50°, as the pressure oscillation increases by about a factor 4 in going from $\lambda = 50°$ to $\lambda = 0°$. The experimental data at present available at the equator are compatible with the occurrence of such an increase in amplitude of the S variation, although not sufficient to establish it.

We shall now calculate the average height at which mesons would have to arise to produce a + S variation of the magnitude observed by Rau.

3.2 *Calculation of the average height of creation of energetic mesons*

3.2.1 *Treatment assuming all mesons arise at one height*

In this calculation we shall assume that all mesons arise at height X above sea-level, and that at this height they have a differential energy spectrum proportional to E^{-n}. It seems probable that mesons at a high level will have a spectrum of this form; the assumption is unlikely to introduce a large error, as the results do not appear to depend critically upon the energy spectrum. Usually n will be taken equal to 3, but one case with $n = 2$ has been worked out to test the dependence of the result upon n.

The probability $P(E, X)$ that a meson of energy E will travel distance X without decaying is

$$\exp\left(-\int_0^X \frac{\mu \mathbf{c}}{\tau} \frac{dx}{E(x)}\right),$$

where μ, τ are the mass and the lifetime at rest of the meson. The only mesons we shall be concerned with in interpreting Rau's results have $E \geqslant 10^{10}$ ev. and for these the energy loss in penetrating the atmosphere may be neglected so that $P(E, X) = \exp(-\alpha X/E)$ where α is constant $(= \mu \mathbf{c}/\tau)$.

The total number $M(X)$ of mesons recorded at sea level

$$= K \int_{E_0}^{\infty} E^{-n} \exp(-\alpha X/E)\, dE,$$

where E_0 is the lowest energy recorded by the apparatus and K is a constant.

The change δM in M produced by a change δX in height of creation of the mesons is

$$\left[K\alpha\delta X\int_{E_0}^{\infty} E^{-(n+1)}\exp\left(-\alpha X/E\right)dE\right], \qquad \ldots\ldots(1)$$

so that

$$\frac{\delta M}{M}=\frac{\alpha\delta X\int_{E_0}^{\infty} E^{-(n+1)}\exp\left(-\alpha X/E\right)dE}{\int_{E_0}^{\infty} E^{-n}\exp\left(-\alpha X/E\right)dE}$$

$$=\alpha\delta X\,.\,F(E_0,X) \quad \text{say.}$$

or

$$\delta X=\delta M/(\alpha M\,F(E_0,X)). \qquad \ldots\ldots(2)$$

For n an integer the integrands involved in $F(E_0,X)$ can be integrated by parts and the function F can be readily tabulated against X for a given E_0.

If $\delta M/M$ is put equal to the amplitude of the semi-diurnal variation experimentally observed, then δX gives the movement of the meson-producing layer required to account for the observed variation at sea level. On the average, mesons will be produced when the primary particles have penetrated a certain mass of air, i.e. at a certain isobaric level in the atmosphere. The mean height of this level may be found by comparing the δX determined from equation (2) with Δh given in table 3.

As Rau's results represent the most accurate determination, this process was carried out using his value for $\delta M/M$ and E_0. For $E_0=10^{10}$ ev. and $n=3$, $F(E_0,X)$ is a very slowly varying function of X and δX is about 160 metres for all values of X between 30 and 100 km. * Using table 3 this gives about 80 km. as the mean height of meson production.

Ehmert (1940), in a very rough calculation using a mean decay coefficient, estimated that a movement of 270 m. in the meson-producing layer was necessary to give a variation of 0·18% in meson intensity at sea level. The discrepancy between this value and δX found above seems to be largely due to the fact that Ehmert, following Euler and Heisenberg (1938), has taken different values for μ and τ (160 instead of $180\times$ mass of electron for μ, and $2{\cdot}7\times10^{-6}$ instead of $2{\cdot}1\times10^{-6}$ sec. for τ). If Ehmert's value for δX is used however, the height of meson formation is only altered by about 8 km.

In the above calculation it has been assumed that mesons all arise at the same height, but in actual fact meson production will be spread over a considerable range in height. The effect of this spread will be to lower the height at which maximum production occurs, for the oscillation of the isobaric levels given in table 3 increases rapidly with height above 65 km., and mesons produced higher than the average have a much greater effect on the variation at sea level than those produced lower. Although the result of the simple calculation described above is not seriously modified by this consideration, a more accurate calculation can be made as shown in the next section.

* All mesons are assumed to have the same mass ($200\times$ mass of electron) and the same lifetime at rest ($2{\cdot}15\times10^{-6}$ sec.).

3.2.2 *Treatment taking account of the distribution of meson production with height*

Suppose that

$P(h)$ = number of primary particles per unit area at height h above sea level.

σ = cross section (assumed constant) for production of mesons by these primary particles.

$\rho(h)$ = number of nuclei per unit volume at height h.

$f(h)$ = number of mesons produced per unit length.

Then

$$f(h) = dP/dh = \sigma P(h)\rho(h). \qquad \ldots\ldots (3)$$

For an isothermal atmosphere,

$$\rho(h) = \rho_0 e^{-h/H}, \qquad \ldots\ldots (4)$$

where H is a constant often called the scale height; in this case

$$dP/dh = \rho_0 \sigma P(h) e^{-h/H}. \qquad \ldots\ldots (5)$$

By integrating (5),

$$\ln P = -Ae^{-y} \quad \text{where} \quad A = H\rho_0\sigma;\ y = h/H. \qquad \ldots\ldots (6)$$

Hence

$$dP/dy = Ae^{-y}\exp(-Ae^{-y}) = ze^{-z}, \qquad \ldots\ldots (7)$$

where

$$z = Ae^{-y} \quad \text{and} \quad \ln z = \ln A - y = -y + \text{constant}. \qquad \ldots\ldots (8)$$

It follows that a plot of ze^{-z} against $\ln z$ will represent the rate of meson production, $f(y)$, as a function of y; this is shown in figure 1. The position of sea level ($y = 0$) in this diagram is determined by the value of $\ln A$ which depends only upon the cross-section—a change in cross-section displaces the curve horizontally but does not alter its shape. The fact that the same curve applies for all values of σ greatly simplifies the numerical work involved.

The curve shown in figure 1 strictly applies only for an isothermal atmosphere (H constant). The calculation of this curve is considerably more complicated when H is a varying function of height as in the true atmosphere; it has been carried out for the true atmosphere for one particular value of σ. As the curve obtained in this case was very similar in shape to that for H constant and only displaced slightly in height, it has been assumed that the variation in H may be neglected for present purposes.

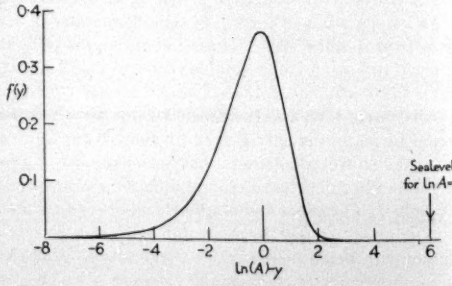

Figure 1. Rate of meson production per unit length as a function of height.

Figure 1 gives the rate of meson production for a production process with a particular cross-section σ. In actual fact σ will depend upon the energy of the primary particle and also upon the energy of the meson it produces, and the meson production actually occurring in the atmosphere will be the result of superposing curves corresponding to a whole range of values of σ. However, as there is no reliable theoretical or experimental knowledge of the dependence of σ on energy, it seems reasonable to assume for the entire produc tion an average cross-section independent of energy.

Suppose the mesons have a differential energy spectrum E^{-n} at their point of origin (n will be taken equal to 3 in numerical work). Then M, the total number of mesons reaching sea level

$$= \int_{h=0}^{\infty} dh\, f(h) \int_{E_0}^{\infty} E^{-3} \exp(-\alpha h/E)\, dE. \qquad \ldots\ldots(9)$$

We require to find the change in M resulting from a movement Δh of the isobar, whose mean position is at height h above sea level. We shall assume that the rate of production of mesons remains the same at a particular isobaric level throughout the semi-diurnal atmosphere oscillation. This is justified provided the density at a given isobaric level does not vary significantly, which is the case below 90 km. at least. With this assumption

$$\delta M = \alpha \int_{h=0}^{\infty} f(h) \Delta h\, dh \int_{E_0}^{\infty} E^{-4} \exp(-\alpha h/E)\, dE, \qquad \ldots\ldots(10)$$

so that

$$\frac{\delta M}{M} = -\alpha \frac{\int_0^{\infty} f(h) \Delta h\, F_1(h)\, dh}{\int_0^{\infty} f(h)\, F_2(h)\, dh}, \qquad \ldots\ldots(11)$$

where
$$F_1 = \int_{E_0}^{\infty} E^{-3} \exp(-\alpha h/E)\, dE, \qquad F_2 = \int_{E_0}^{\infty} E^{-4} \exp(-\alpha h/E)\, dE. \qquad \ldots\ldots(12)$$

F_1 and F_2 can be found by integration by parts and are readily tabulated as functions of h. The integrals occurring in (11) are then evaluated by numerical integration. This evaluation has been performed for three different values of σ, using the values of Δh provided by Weekes and Wilkes at latitude 50° and taking $E_0 = 10^{10}$ ev., in accordance with Rau's measurements. The results are given in table 4.

Table 4. The semi-diurnal variation in meson intensity at sea level for three different values of σ

$\ln A$	6	8	9
A	$e^6 \sim 400$	$e^8 \sim 3000$	$e^9 \sim 8100$
Ht. of max. meson production (km.)	48	64	72
$\delta M/M$	0·0008	0·0014	0·0017

Rau's measurements give $\delta M/M = 0{\cdot}0016$, and so to explain these measurements by means of the Pekeris theory the mesons have to be created mainly at a height of about 70 km.*

* Before the calculation which resulted in table 4 was carried out it was thought that the height of meson formation might be reduced to as low as 50 or 60 km. by taking account of the spread in height of meson formation, and in a brief statement on this work at a Physical Society Conference in July 1946, about 50 km. was suggested as the mean height of meson formation required to explain Rau's results (Sarabhai and Nicolson 1947).

3.3 *The high cross-section*

It is concluded above that the bulk of the mesons must arise at about 70 km. above sea level if Rau's results are to be accounted for. At 70 km. the pressure is about 0·01 cm. Hg, which is roughly 1/8000 of atmospheric pressure. This means that primary particles have to create mesons in traversing an amount of air equivalent to only 1/8000 of the atmosphere. The corresponding cross-section for the production process is considerably larger than seems likely if protons are the meson primaries. The maximum conceivable cross-section in this case, in air, is of the order of the geometrical cross-section of the oxygen nucleus and corresponds to a mean free path for the proton of about 1/20 of the atmosphere, so that the cross-section derived above is over 100 times the largest reasonable value for proton primaries.

It has been suggested (Hoyle 1947) that the primary hard radiation is not composed of protons but of very heavy nuclei of atomic number Z about 80. Since the energy a particle needs to penetrate the earth's magnetic field is proportional to its charge, such a nucleus would need energy about 10^{12} ev. to reach the equator. Its fate upon impact with oxygen and nitrogen atoms at the top of the atmosphere is unknown. It is probable that collisions with air nuclei will lead to rapid disintegration of the heavy nucleus but it is uncertain whether mesons will arise directly from these disintegrations or only indirectly through the agency of protons and neutrons which will be liberated. For direct collisions involving meson interaction, the maximum cross-section for meson production by nuclei with Z about 80 cannot be much larger than about twelve times that for production by protons. (This estimate corresponds to the appropriate geometrical cross-section, on the assumption that the nuclear radius is proportional to (atomic weight)$^{\frac{1}{3}}$). This is smaller than the cross-section required to explain the $+S$ variation by a factor of more than 10. Larger cross-sections for meson production by a heavy nucleus might arise as a result of the Coulomb interaction, but it seems very unlikely that for $Z=80$ the cross-section could be as large as that needed to account for the $+S$ effect.

It is hard to see how this serious difficulty in the explanation of the $+S$ effect may be resolved. The Pekeris theory of atmospheric oscillations appears to be well-established; Weekes and Wilkes believe that the results quoted in table 3 are substantially correct up to about 60 km. On the other hand, for a semi-diurnal variation which is positively correlated with pressure, it is difficult to think of an alternative explanation to that in terms of the Pekeris theory. The first need is for more experimental evidence of a reliable kind on the existence and magnitude of this $+S$ variation. Since the pressure oscillation decreases rapidly with increase in latitude, reliable evidence is most readily obtained at the equator. One of us (Sarabhai) hopes to obtain such evidence in India shortly.

§4. THE $-S$ VARIATION

The experimental data suggest that, although the intensity measured under a thick absorber shows a $+S$ variation, that measured without an absorber shows a $-S$ variation. This implies that the easily absorbed radiation, consisting of the soft component and low energy mesons, is characterized by a $-S$ variation which is large enough to swamp the $+S$ variation shown by the energetic mesons.

If the soft radiation arises in the lower atmosphere as is certainly the case for the electronic component observed at sea level, it will tend to show a $-S$ variation

on account of the ordinary mass absorption effect. However, even for the electronic component it is difficult to say what would be the magnitude of the $-S$ variation produced purely by pressure changes. The effect on electrons arising from a primary electronic component could probably be estimated fairly well from the cascade theory, but the effect on the remaining electrons which arise from mesons and which probably form about $\frac{2}{3}$ of the electrons at sea level, is extremely difficult to assess. It is likely that about equal numbers of these electrons arise by knock-on processes and by decay, and as their production is spread over various strata of the lower atmosphere, individual electrons may be influenced by different pressure changes in reaching sea level. In addition the point of origin of the mesons which produce the electrons is affected by pressure changes, again in a way depending upon altitude. In fact the position is so complicated that it seems almost impossible to calculate the resultant effect (which is known to be small) with any certainty.

An alternative approach is from the experimental measurements of the day-to-day variation of intensity and the corresponding pressure variation, i.e. determination of what is usually called the barometric coefficient. Here again no definite conclusion may be reached, for as already mentioned, it is uncertain how much of the observed barometric effect is a true mass-absorption effect and how much is produced by other factors, such as movement of meson-producing layers, which may be differently related to semi-diurnal and to day-to-day pressure changes. Duperier finds a barometric coefficient of 0·35% per mm. Hg and deduces that about 60% of this is a mass absorption effect and that the remainder is caused by movement of meson-producing layers; this result is dependent upon mesons being created at about 16 km. which may not be the case. It does appear fairly certain, however, that the $-S$ effect observed by Duperier with no absorber is too large to arise purely as a mass-absorption effect from pressure changes.

Although the explanation of the $-S$ effect is not clear, the suggestion made by Duperier (1945) that the main factor responsible is the atmospheric oscillation predicted by Pekeris is untenable when the magnitude of this oscillation is considered. A negative S effect can only be produced by the Pekeris oscillation if mesons arise below 30 km. but the maximum displacement of isobars below 30 km. is only about 3 metres at latitude 50° and this movement is insufficient to produce an observable cosmic-ray effect. Duperier appears to be considering the vertical movement of individual particles, which indeed may be as large as 20 metres, as he states, but which is irrelevant in a consideration of the height of meson production, where the important quantity is the vertical movement of isobaric level.

Further confusion on this point has arisen from recent publications by two workers in Ceylon, which apparently confirm Duperier's conclusion that the $-S$ variation can be accounted for by the Pekeris theory (Mailvaganam 1946, Kidnapillai and Mailvaganam 1946). It has already been mentioned (§ 3.1) that the results obtained by these workers for the movement of isobars are incorrect. Apart from this, their final result of 0·14% for the amplitude of the $-S$ effect seems to apply at $\lambda = 0$, whereas Duperier's value of 0·18%, with which they compare it, applies at $\lambda = 50°$ and if produced by pressure oscillations would be four times as large at $\lambda = 0$.

§ 5. THE DIURNAL VARIATION

From § 2.1 it will be seen that although the D variation at high latitudes, recorded by different observers using similar apparatus, usually has an amplitude

about 0·2% the phase varies appreciably even at stations having the same latitude. For example, the results of Hess and Graziadei (1936) and of Forbush (1937), which both appear to be well established show a discrepancy of several hours in phase when allowance is made for the fact that with no external temperature correction the maximum observed by Hess and Graziadei would probably occur about four hours earlier. Duperier (1941) observes a maximum as late as 17^h, but here the discrepancy may arise partly from the difference in thickness of absorber used. Doan (1936) whose results are fairly convincing, places the maximum at 9^h. In fact all that can be concluded in general about the time of maximum intensity seems to be that it occurs during the daytime rather than during the night.

It is possible that the recordings made with ionization chambers, even when shielded with 10 cm. Pb, are affected by fluctuations in the gamma-ray content of the atmosphere. The latter, in some localities at least, appears to show a daily variation with maximum about noon. Forbush (1937) estimates that this factor might cause as much as one third of the D variation recorded by his apparatus and suggests that it might produce quite different distortion of the true cosmic-ray D variation in experiments performed in different localities. However, it appears very unlikely that the wide phase variation recorded in the experiments mentioned above can be entirely due to this effect. The results of Alfvén and Malmfors (1943) recorded in Stockholm with Geiger counter apparatus and supported by those of Kolhorster (1941) in Berlin, indicate that the D effect is appreciably different in different directions with the same zenith angle, and in view of this it does not seem improbable that the true D variation at a particular zenith angle will be different in different localities.

The variation in character of the experimentally observed D effect has been ignored by most workers seeking an explanation of the effect; following the early results of Hess they usually assume that the maximum occurs at midday and try to account for this. For instance, Vallarta and Godart (1939) suggest that such a variation can be accounted for at high latitudes by a heliomagnetic field and at low latitudes by fluctuations in the geomagnetic field. It is clear, however, that the D effect indicated by a wider survey of experimental data could not be mainly produced by either a heliomagnetic field or by geomagnetic fluctuations since it appears to show an appreciable variation in phase at different stations at the same latitude. Malmfors (1945) shows that such explanations are also incompatible with the results found by Alfvén and himself (1943) in Stockholm. These results are particularly interesting as they also eliminate meteorological changes as the main cause of the D variation. Malmfors suggests that occasional small disturbances of the isotropy of the primary radiation in remote space may be responsible for the Stockholm results.

Before the cause of the D effect can be considered further, more experiments at various latitudes and longitudes are needed to establish the variation of the phase of the effect under a given absorber with geographical situation and also the variation at a given station of phase and amplitude with thickness of absorber and with angle θ.

ACKNOWLEDGMENTS

The authors wish to acknowledge their indebtedness to Mr. K. Weekes and Dr. M. V. Wilkes of Cambridge University, for furnishing the data quoted in table 3 and also for many helpful discussions on the subject of atmospheric oscillations. In addition they would like to thank Professor P. M. S. Blackett and

Dr. L. Jánossy of Manchester University for stimulating discussions on the cosmic-ray aspect of the problem.

REFERENCES

ALFVÉN and MALMFORS, 1943, *Ark. Mat. Astr. Fys.*, **29**, No. 24.
BARNOTHY and FORRO, 1936, *Z. Phys.*, **100**, 742 ; 1937, *Ibid.*, **104**, 534 ; 1939, *Phys. Rev.*, **55**, 868.
BUDDEN, RATCLIFFE and WILKES, 1939, *Proc. Roy. Soc.* A, **171**, 188.
CHAPMAN, 1919, *Philos. Trans.*, **218**, 1 ; 1924, *Quart. J.R. Met. Soc.*, **50**, 165.
DOAN, 1936, *Phys. Rev.*, **49**, 107.
DUPERIER, 1944, *Terr. Magn. Atmos. Elect.*, **49**, 1 ; 1945, *Proc. Phys. Soc.*, **57**, 468.
EHMERT, 1940, *Naturwissenschaften*, **28**, 28.
EULER and HEISENBERG, 1938, *Erbegn. Exakt. Naturw.*, **17**, 1.
FORBUSH, 1937, *Terr. Magn. Atmos. Elect.*, **42**, 1.
HESS and GRAZIADEI, 1936, *Terr. Magn. Atmos. Elect.*, **41**, 9.
HOYLE, 1947, *Roy. Ast. Soc.* (in press).
KIDNAPILLAI and MAILVAGANAM, 1946, *Phys. Rev.*, **70**, 94.
KOLHORSTER, 1941, *Phys. Z.*, **42**, 55.
MAILVAGANAM, 1946, *Proc. Phys. Soc.*, **58**, 468.
MALMFORS, 1945, *Ark. Mat. Astr. Fys.*, **32 A**, No. 8.
PEKERIS, 1937, *Proc. Roy. Soc.* A, **158**, 650 ; 1939, *Ibid.*, **171**, 634.
RAU, 1939, *Z. Phys.*, **114**, 265 ; 1940, *Ibid.*, **116**, 105.
REGENER and RAU, 1939, *Naturwissenschaften*, **27**, 803.
SARABHAI, 1945, *Proc. Indian Acad. Sci., Bangalore*, A, **21**, 66.
SARABHAI and NICOLSON, 1947, *Phys. Soc. Intern. Conf.: I—Fundamental Particles*, 68.
SCHONLAND, DELATISKY and GASKELL, 1937, *Terr. Magn. Atmos. Elect.*, **42**, 137.
STEINMAURER, 1935, *Beitr. Geophys.*, **45**, 148.
TAYLOR, 1929, *Proc. Roy. Soc.* A, **126**, 169 ; 1932, *Mem. R. Met. Soc.*, **4**, No. 35 ; 1936, *Proc. Roy. Soc.* A, **156**, 318.
THOMPSON, 1938, *Phys. Rev.*, **54**, 93.
WHIPPLE, 1934, *Quart. J.R. Met. Soc.*, **60**, 51 ; 1935, *Ibid.*, **61**, 285.
VALLARTA and GODART, 1939, *Rev. Mod. Phys.*, **11**, 180.

The Neutrons Emitted in the Disintegration of Nitrogen by Deuterons

BY W. M. GIBSON AND D. L. LIVESEY
Cavendish Laboratory, Cambridge

MS. received 18 *December* 1947

ABSTRACT. The photographic plate method has been used in a study of the neutrons produced in the disintegration of nitrogen by deuterons.

A single group of neutrons, corresponding to an energy release of (5·15±0·10) MEV., was detected, but the existence of the low-energy neutron group reported by Stephens, Djanab and Bonner (1937) was not confirmed. The new results show that, if this group does exist, its intensity is not more than 15% of that of the principal neutron group, and that no excited levels of the ^{15}O nucleus less than 5 MEV. above the ground state are effective in this reaction.

The neutron flux from the N+D reaction was compared with that of D+D neutrons produced by disintegration of deuterium present in the surface layers of the target employed. The data obtained were used in determinations of the angular distributions of the D+D and N+D neutron fluxes, and in tests of the reliability of the photographic plate method for relative flux measurements.

§1. INTRODUCTION

THE neutrons produced in the disintegration of nitrogen by deuterons according to the scheme :

$$^{14}_{7}\mathrm{N} + ^{2}_{1}\mathrm{D} \rightarrow ^{15}_{8}\mathrm{O} + ^{1}_{0}\mathrm{n}$$

have been investigated by Stephens, Djanab and Bonner (1937), who used an expansion chamber and detected three groups of neutrons emitted from nitrogen targets bombarded by deuterons. They attributed two of the groups to the above reaction, and the effective Q values were found to be $(1{\cdot}1 \pm 0{\cdot}2)$ MEV. and $(5{\cdot}1 \pm 0{\cdot}2)$ MEV. respectively. The third group was ascribed to the disintegration by deuterons of deuterium present in the surface layers of the targets employed, and the Q value of this group (3·3 MEV.) was in agreement with the known energy release of the D + D reaction.

Further investigation of the N + D reaction is desirable in order to confirm the existence of an excited level in the $^{15}_{8}\mathrm{O}$ nucleus, which is indicated by the presence of the low-energy group in the N + D neutron spectrum. In addition, the 5 MEV. neutron group may be useful in experiments where a neutron source of this energy is required, and for this purpose the characteristics of the neutron spectrum must be determined at various angles to the direction of the deuteron beam.

The use of photographic plates in the determination of neutron energies has been described by Powell (1940, 1942) and Richards (1941 a), who have studied the distributions in energy of the neutrons emitted in the bombardment of a number of light elements by deuterons. Their results were in general agreement with those obtained by the expansion chamber method. The photographic plate technique has the advantage that plates may be exposed simultaneously at different angles to the direction of the primary beam, so that information may be obtained concerning the angular distribution of the neutron yield (Richards 1941 b, Livesey and Wilkinson 1948). The photographic technique has been improved considerably as a result of the introduction by Ilford Ltd. of concentrated emulsions (Powell, Occhialini, Livesey and Chilton 1946), with which greatly increased accuracy of track measurements is attainable, and at present it is the most convenient and precise method for the determination of neutron spectra. This method was therefore adopted for a more detailed investigation of the neutrons emitted in the disintegration of nitrogen by deuterons.

§2. EXPERIMENTAL METHOD

A thick target of aluminium nitride was bombarded with a beam of deuterons accelerated through 930 kilovolts by the Cavendish Laboratory high tension equipment.

Four light-tight boxes containing photographic plates of the Ilford C.2 type with emulsions 100 microns thick were set up around the target so that the plates recorded neutrons emitted at 0°, 30°, 90° and 150° respectively.

In order to obtain reasonably good geometrical conditions with the relatively large neutron source, the plates were placed 15 cm. from it and were irradiated for 3 hours with an average beam current of 80 μa. This arrangement gave a maximum spread of $\pm 3°$ in the directions of the neutrons incident upon the plates. A stop could not usefully be employed to reduce the size of the N + D neutron source, as the stop itself acted as a source of D + D neutrons.

A second series of plates was irradiated with neutrons emitted from a pure aluminium target bombarded with deuterons, in order to estimate the contribution of the aluminium to the spectrum of neutrons from the aluminium nitride target. The conditions of exposure were the same as for the nitride target, except that the target surface was cooled less efficiently and was therefore maintained at a higher temperature by the beam.

After the plates had been processed, detailed microscope measurements were carried out on the proton tracks occurring in the plates by two observers, using a Leitz microscope fitted with a 1/12 inch oil-immersion objective which, in conjunction with twin eyepieces of power $\times 10$, gave an overall magnification of $\times 1200$. Traverses were made across each plate in a direction parallel to that of the incident neutrons, and all proton tracks were recorded which originated in the area covered by the traverse, which were completely contained within the emulsion, and which made angles of less than 20° with the neutron direction. Between 300 and 500 tracks were recorded in each plate. The area examined was calculated from the total length of the traverse; it was approximately 20 mm² in all cases.

For each selected track the total length a projected on the focal plane of the microscope was measured, and the initial direction of the proton was derived from measurements of the angle of scattering projected on the focal plane α and the initial angle of dip ψ. In order to obtain ψ it was necessary to correct the distances measured in the vertical plane for the effects of shrinkage of the emulsion caused by fixation. The correction consisted in multiplying all vertical distances by a factor s, which was assumed to be equal to the ratio of the initial to the final thickness of the emulsion. A series of experimental determinations of the shrinkage factor indicated $s = 2{\cdot}0 \pm 0{\cdot}2$, and this value was used in all calculations of the angle ψ. The actual angle of scattering γ for each proton track was calculated, to the nearest degree, from the relation $\sec\gamma = \sec\alpha \sec\psi$.

The proton range R was calculated from the equation $R = a \sec\psi$. This formula applies strictly only to tracks which are straight; in fact, some of the tracks were deflected from straight lines by nuclear collisions, but these deflections did not produce appreciable errors in the estimates of R and γ. The proton energy E_p was derived from the range–energy relation obtained for the B. 1 type of emulsion by Lattes, Fowler and Cuer (1947). A comparison of the properties of the B. 1 and C. 2 emulsions has shown that the stopping-powers of the two types for α-particles are very nearly identical over a wide range of energies. It is therefore reasonable to assume that the stopping-powers for protons are the same. The neutron energy E_n is related to the proton energy E_p by the formula $E_n = E_p \sec^2\gamma$. The quantity E_n was calculated for each individual track recorded.

§ 3. NEUTRON SPECTRA

The energy distributions of the neutrons emitted from the aluminium nitride target at the four angles of observation ($\phi = 0°$, 30°, 90° and 150°), and from the aluminium target at $\phi = 0°$, were derived from the numbers of tracks recorded in successive intervals of 0·1 MeV. in energy E_n. The data were divided, according to the magnitude of the scattering angle γ, into three groups defined by the conditions :

(i) $0° \leqslant \gamma \leqslant 9°$; (ii) $10° \leqslant \gamma \leqslant 14°$; (iii) $15° \leqslant \gamma \leqslant 19°$.

A typical track distribution is shown in figure 1, which refers to tracks measured in the 150° nitride plate.

It was found that, in the energy distributions obtained for $15° \leqslant \gamma \leqslant 19°$, the D+D and N+D neutron groups were broader than those occurring in the distributions obtained for low values of γ. This effect was due to small errors in definition of the directions of the incident neutrons, caused by the use of a comparatively large neutron source. This "angular straggling" is always more pronounced in the case of protons scattered at large angles, and measurements on these tracks are less reliable for the determination of neutron energies. Despite the straggling effects the principal neutron groups were clearly resolved in the distributions obtained for $\gamma < 20°$, and no difficulty was experienced in estimating the number of proton tracks which fell within each group. The data for $0° \leqslant \gamma \leqslant 9°$ were used in all energy determinations, since the effects of angular straggling were very small in these cases.

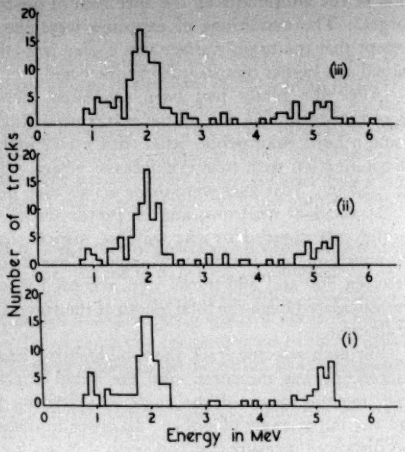

Figure 1. Number of tracks plotted against neutron energy for 150° plate :
(i) $0 \leqslant \gamma \leqslant 9°$; (ii) $10° \leqslant \gamma \leqslant 14°$; (iii) $15° \leqslant \gamma \leqslant 19°$.

Since the total number of tracks measured in each plate was comparatively small, statistical variations in the number of tracks at each energy were considerable. The observed distributions were therefore smoothed by the addition to each ordinate on the energy scale of the mean of the two neighbouring ordinates. In order to obtain the actual neutron energy distributions, the smoothed experimental distributions were corrected, firstly for the variation of the total neutron–proton scattering cross-section with energy, the formulae of Kittel and Breit (1939) being used, and secondly for the escape of protons from the emulsions. The correction for the latter effect was calculated geometrically on the assumption that the proton range varies with energy according to the Geiger rule, which, for a fixed neutron energy E_n, yields the following relation between the proton range R and the scattering angle γ : $R = R_0 \cos^3\gamma$ where R_0 is the range of a proton with energy E_n. The fraction f of the total number of protons, scattered in the range $\gamma_1 \leqslant \gamma \leqslant \gamma_2$, which is recorded in an emulsion of thickness $2d$, is given by

$$f = 1 - \frac{R_0}{8\pi d} \frac{\{(\gamma_2 - \gamma_1) + \frac{1}{4}(\sin 2\gamma_2 - \sin 2\gamma_1) - \frac{1}{4}(\sin 4\gamma_2 - \sin 4\gamma_1) - \frac{1}{12}(\sin 6\gamma_2 - \sin 6\gamma_1)\}}{(\sin^2\gamma_2 - \sin^2\gamma_1)},$$

provided that $R_0 \cos^3\gamma_2 \sin\gamma_2 \leqslant 2d$. Although the Geiger rule does not accurately represent the range–energy relation for protons, the correction factor is not

appreciably affected by the departures from it which actually occur. The calculated factor is plotted as a function of the neutron energy in figure 2 for the three ranges of γ used in the experiment.

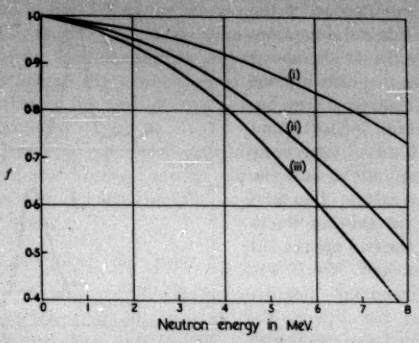

Figure 2. Escape fraction f as a function of neutron energy: (i) $0 \leqslant \gamma \leqslant 9°$; (ii) $10° \leqslant \gamma \leqslant 14°$; (iii) $15° \leqslant \gamma \leqslant 19°$.

The corrected neutron spectra for the aluminium nitride target at four angles of observation and for the aluminium target at $\phi = 0°$, are shown in figure 3. The four nitride spectra show two principal neutron groups, the mean energy of the one varying between 1·9 MeV. at 150° and 3·5 MeV. at 0°, and that of the other lying between 5 MeV. and 6 MeV. at all angles. In addition, a third group below 1 MeV. was detected in the 0° spectrum, the investigation of which was extended to lower energies than in the other cases. This group is ascribed to the disintegration of carbon present on the target surface, according to the reaction :

$$^{12}_{6}\mathrm{C} + ^{2}_{1}\mathrm{D} \rightarrow ^{1}_{0}\mathrm{n} + ^{13}_{7}\mathrm{N} - 0{\cdot}27 \text{ MeV}.$$

A similar group was found in the 0° aluminium spectrum. The occurrence of the $^{12}C + D$ neutron group indicates that high-energy neutrons were emitted also as a result of the disintegration of the isotope ^{13}C :

$$^{13}_{6}\mathrm{C} + ^{2}_{1}\mathrm{D} \rightarrow ^{1}_{0}\mathrm{n} + ^{14}_{7}\mathrm{N} + 5{\cdot}5 \text{ MeV}.$$

It has been shown by Bonner and Brubaker (1936) that the abundance of the $^{13}C + D$ neutron group is only 1% of that of the $^{12}C + D$ group. It is clear, therefore, that the $^{13}C + D$ reaction cannot account for more than a small proportion of the 5–6 MeV. neutrons occurring in the nitride spectra, and these may be identified with the N + D neutron group investigated by Stephens, Djanab and Bonner (1937). Nevertheless, a small neutron component was found near 6 MeV. in the 0° aluminium spectrum, and this may be ascribed to the $^{13}C + D$ reaction.

The remaining principal group in the nitride spectra was produced by the disintegration of deuterium present in the surface layers of the target, as may be seen by comparison with the D + D neutron spectra obtained by Livesey and Wilkinson (1948), who deduced a value of $3{\cdot}23 \pm 0{\cdot}02$ MeV. for the energy release of the reaction. The shape of the D + D neutron group in the 0° aluminium spectrum is different from that of the D + D group in the 0° nitride spectrum, and this is probably due to the high temperature at which the aluminium target was maintained : under these conditions the material closest to the surface of the target retained only a very small amount of deuterium, and so the yield of neutrons of maximum energy was low.

Between 0·8 MeV. and 2·0 MeV. no clearly defined group was detected in the nitride spectra; this result disagrees with those of Stephens, Djanab and Bonner.

A comparison of the nitride and aluminium spectra at 0° shows that the distributions of neutron energy between 0·8 Mev. and 2·0 Mev. are very nearly the same in the two cases. The ratio of the neutron fluxes in the two spectra (Al flux/AlN flux) was determined directly, and the values obtained for the energy ranges 1·0–1·5 Mev. and 1·5–2·0 Mev. were $1·6 \pm 0·2$ and $1·4 \pm 0·2$ respectively.

The fact that the aluminium target produced more neutrons in the energy range 1·0–2·0 Mev. than the aluminium nitride target shows that nitrogen did not contribute appreciably to this group of neutrons. It is known that the carbon isotope ^{13}C emits neutrons of this energy when bombarded with deuterons, but the abundance of the $^{13}C + D$ group, as calculated from the results of Bennett, Bonner, Hudspeth, Richards and Watt (1941), is too small to account for the observed effect. It is possible that the aluminium present in both targets produced most of the neutrons in this energy range. If this hypothesis is correct, the ratio of neutron fluxes, as calculated from the chemical compositions of the targets, should be 1·5, which is in agreement with the experimental value. An upper limit may therefore be set to the abundanee of the low-energy N + D group reported by Stephens, Djanab and Bonner (1937). On the assumption that the maximum variation in the neutron flux ratio is three times the probable

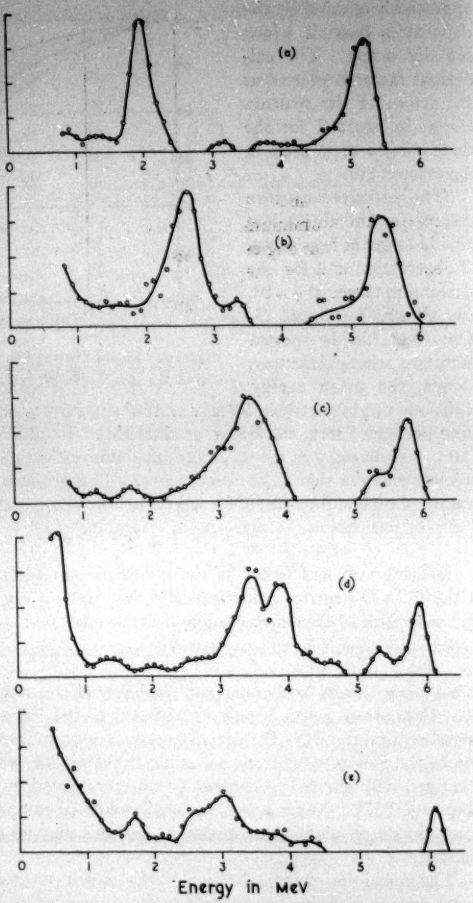

Figure 3. Corrected neutron spectra, with ordinates in arbitrary units: (a) AlN target at 150°, (b) AlN target at 90°, (c) AlN target at 30°, (d) AlN target at 0°, (e) Al target at 0°.

error, this upper limit is found to be 15% of the abundance of the high-energy N+D group at the same angle, namely 0°. This same conclusion is valid for all four angles of observation, and it disagrees entirely with the results of Stephens, Djanab and Bonner, who estimated the abundance of the low-energy group to be 150% compared with that of the high-energy group, at an angle of 90° to the direction of the deuteron beam.

The high-energy N+D neutron group is well-defined and is clearly resolved from other components in all the neutron spectra investigated. The mean thick-target energy varies between 5·1 MEV. at 150° and 5·7 MEV. at 0° when the bombarding energy is 0·93 MEV.

§4. THE ENERGY RELEASE OF THE N+D REACTION

In order to obtain the energy release of the N+D reaction, it was necessary to extract, from the observed thick-target spectrum for each of the four angles of observation, the corresponding thin-target energy. A careful examination of the spectra of figure 3 showed that the effects of both angular straggling and range straggling of the proton tracks could be represented analytically by the superposition of a generalized Gaussian error function on the actual thick-target neutron spectrum. A method described by Livesey and Wilkinson (1948) was therefore employed to derive the thin-target energy for each spectrum. The N+D spectrum at each angle was re-plotted, with the same corrections and smoothing procedure as those previously described, but with the neutron energy specified at 0·05 MEV. intervals, and the integrated spectrum was constructed in each case. The correction required for estimating the thin-target energy (E_0) from the value given by extrapolation of the straight part of the integrated spectrum was obtained by comparing the shape of the experimental spectrum with those of a set of theoretical curves calculated for different values of the Gaussian straggling parameter. The extrapolated energies, the derived thin-target energies, and the corresponding values for the energy release Q are included in table 1.

Table 1. Extrapolated energies, thin-target energies and calculated Q values in MEV.

Angle ϕ°	0	30	90	150
Extrapolated energy	6·00	5·94	5·82	5·39
Correction	−0·08	−0·10	−0·13	−0·10
Thin-target energy, E_0	5·92	5·84	5·69	5·29
Q value	5·07	5·05	5·27	5·20

These figures were checked by independent determinations of E_0 from the spectra corresponding to angles of scattering γ between 10° and 14°, and no discrepancies were found. If the four estimates of the Q value are of equal weight, the mean value is 5·15 MEV., and the probable error, derived from the above results only, is ±0·06 MEV. The uncertainties in the range-energy relation of Lattes, Fowler and Cuer (1947) must also be taken into account; the probable error in their data for energies between 5 MEV. and 6 MEV. is ±0·07 MEV. In addition, the error of ±10% in the shrinkage factor of the emulsions leads to a probable error of ±0·03 MEV. in the final Q value. These errors in combination give a total probable error of ±0·10 MEV., and the energy release is therefore quoted as $Q = 5{\cdot}15 \pm 0{\cdot}10$ MEV.

This result agrees with the value of $5{\cdot}1 \pm 0{\cdot}2$ MEV. derived by Stephens, Djanab and Bonner (1937), and it may also be checked by calculation of the maximum energy of the positrons emitted by the oxygen isotope, ^{15}O. The (d, p) reaction in nitrogen has been studied by Cockcroft and Lewis (1936) and by Holloway and Moore (1940), and the most accurate results give a value of $8{\cdot}55 \pm 0{\cdot}08$ MEV. for the energy release. Comparison of the two reactions:

$$^{14}_{7}N + {}^{2}_{1}D \rightarrow {}^{1}_{1}H + {}^{15}_{7}N + 8{\cdot}55 \pm 0{\cdot}08 \text{ MEV.}$$

$$^{14}_{7}N + {}^{2}_{1}D \rightarrow {}^{1}_{0}n + {}^{15}_{8}O + 5{\cdot}15 \pm 0{\cdot}10 \text{ MEV.}$$

yields the relation $^{15}_{8}O - {}^{15}_{7}N = -({}^{1}_{0}n - {}^{1}_{1}H) + 3{\cdot}40 \pm 0{\cdot}13$ MEV. The neutron–hydrogen mass difference is equivalent to 0·76 MEV., according to Mattauch (1942) and Stephens (1947), hence the difference in the masses of $^{15}_{8}O$ and $^{15}_{7}N$ is equivalent to $2{\cdot}64 \pm 0{\cdot}13$ MEV. This exceeds the maximum positron energy from ^{15}O by an amount equivalent to the mass of two electrons, that is, 1·02 MEV., provided that the mass of the neutrino is negligible. The maximum positron energy is therefore $1{\cdot}62 \pm 0{\cdot}13$ MEV., and this result agrees with the experimental value of 1·72 MEV. deduced from the data of Konopinski (1943).

The results shown in figure 3 did not confirm the existence of the excited state of ^{15}O which was indicated by the results of Stephens, Djanab and Bonner (1937). A detailed examination of the nitride spectra, and especially of the 150° spectrum, leads to the conclusion that the energy release of the N + D reaction is single-valued and that no excited levels of the ^{15}O nucleus less than 5 MEV. above the ground state are operative in this reaction.

§ 5. ANGULAR DISTRIBUTIONS OF NEUTRON YIELD

In making relative measurements of neutron flux by the photographic plate method, it is assumed that the number of proton tracks occurring per unit area within a defined solid angle, is, after correction for the escape effect, proportional to the product of the neutron flux and the total neutron–proton scattering cross-section. This assumption is valid if the angular distribution of neutron–proton scattering is independent of the neutron energy in the range investigated, and if the concentration of hydrogen in the emulsion is constant. That the latter condition was satisfied in this experiment was shown by the fact that no abnormally large variations in the abundance of proton tracks were detected in examining different parts of the plates. The angular distribution of neutron–proton scattering has been determined experimentally by Dee and Gilbert (1937), by Bonner (1937) and by Champion and Powell (1944) for neutron energies below 10 MEV., and it is generally accepted that the distribution in the centre-of-mass coordinate system is effectively isotropic within this energy range.

The reliability of the method of observation and of the escape correction used in this experiment may be checked by comparison of the observed angular distribution of proton tracks with that corresponding to isotropic scattering in the centre-of-mass coordinates. Provided that the effects of angular straggling may be neglected, the number of proton tracks recorded in the range of angles defined by $\gamma_1 \leqslant \gamma \leqslant \gamma_2$ should be proportional to the integral

$$\int_{\gamma_1}^{\gamma_2} 2 \cos\gamma \sin\gamma \, d\gamma = (\sin^2\gamma_2 - \sin^2\gamma_1).$$

The experimental data were tested by dividing the total numbers of proton tracks in the D + D and N + D groups, corrected for escape, by the function

$(\sin^2\gamma_2 - \sin^2\gamma_1)$, to see whether the same quantity was obtained for the different angular ranges. The results are shown in table 2.

Table 2. Ratio of experimental and theoretical proton abundances, in arbitrary units

Spectrum	$0° \leqslant \gamma \leqslant 9°$	$10° \leqslant \gamma \leqslant 14°$	$15° \leqslant \gamma \leqslant 19°$
0°	35±3	41±3	31±3
30°	33±3	24±2	22±2
90°	18±2	21±2	17±2
150°	24±2	28±2	25±2

The 0°, 90° and 150° results are internally consistent, but the 30° figures show possible deviations from isotropic scattering. These deviations are probably not significant, but they may be regarded as an indication that the 30° results are less reliable than the others.

In the four neutron spectra obtained with the nitride target, the N + D and D + D neutron groups were everywhere resolved, and the number of neutrons detected in each group was readily estimated. In order to test more stringently the accuracy of the escape correction at the higher neutron energies, and also to detect whether there was any tendency on the part of the observers to count too many long tracks at high scattering angles, the ratio of the D + D flux to the N + D flux was determined for the three ranges of the scattering angle γ. In the calculation of this ratio, the mean scattering cross-sections for the two neutron groups were derived from the data of Kittel and Breit (1939). The results are shown in table 3.

Table 3. Ratio of D + D and N + D neutron fluxes

Spectrum	$0° \leqslant \gamma \leqslant 9°$	$10° \leqslant \gamma \leqslant 14°$	$15° \leqslant \gamma \leqslant 19°$	Mean Ratio
0°	4·1±0·9	4·8±0·8	4·4±0·8	4·4 ±0·5
30°	3·4±0·6	4·3±1·0	5·9±1·3	4·4 ±0·5
90°	1·7±0·3	1·8±0·3	1·3±0·2	1·50±0·13
150°	1·8±0·2	2·5±0·3	2·5±0·3	2·12±0·18

The internal consistency of these results shows that the method of observation and of correction for escape did not give rise to serious errors.

The consistency tests already described indicate that any errors occurring when the photographic plate method is used for comparing neutron fluxes can be reduced to low values by the methods used in this experiment. The data were used to determine the angular distribution of the D + D neutron flux in order to compare the results obtained with those of Allen, Livesey and Wilkinson (1948), who determined the angular distribution of neutrons emitted from a thick deuterium target bombarded by deuterons of energy 0·93 MeV. The angular distribution was obtained by estimating the neutron flux at each angle relative to that at 0°, and the results are shown in table 4.

Table 4. Angular distribution of D + D neutron flux

Angle ϕ°	$0° \leqslant \gamma \leqslant 9°$	$10° \leqslant \gamma \leqslant 14°$	$15° \leqslant \gamma \leqslant 19°$	$0° \leqslant \gamma \leqslant 19°$
0	1·00±0·08	1·00±0·07	1·00±0·07	1·00±0·05
30	1·15±0·12	0·76±0·07	0·90±0·09	0·90±0·05
90	0·29±0·04	0·28±0·03	0·26±0·03	0·27±0·02
150	0·62±0·06	0·45±0·06	0·54±0·06	0·52±0·04

The results for the angle range $0° \leqslant \gamma \leqslant 19°$ may be compared with the experimental curve of Allen, Livesey and Wilkinson in figure 4.

In general the agreement between the two sets of results is close.

The above results show that it is possible to make reliable determinations of angular distributions of neutron flux by the photographic plate method. The angular distribution of the N + D neutron flux was calculated from the data referring to the entire range of scattering angles between 0° and 19°; for ϕ equal to 0°, 30°, 90°, 150° the values obtained were $1{\cdot}00 \pm 0{\cdot}10$, $0{\cdot}91 \pm 0{\cdot}10$, $0{\cdot}90 \pm 0{\cdot}08$, $1{\cdot}37 \pm 0{\cdot}15$ respectively.

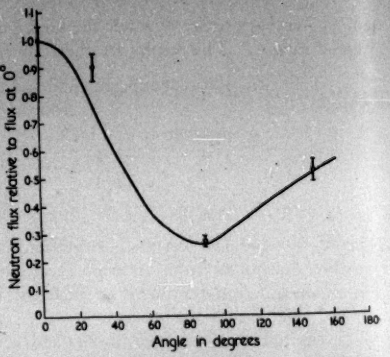

Figure 4. Angular distribution of D + D neutron flux from thick target:

Experimental curve of Allen, Livesey and Wilkinson, with 3 photographic plate results for the angle range $0 \leqslant \gamma \leqslant 19°$.

The 150° figure is somewhat higher than the others, but the statistical accuracy is lower than that in the D + D distribution, and the deviation from an isotropic distribution of the neutron yield is hardly significant.

ACKNOWLEDGMENT

The authors wish to express their indebtedness to Dr. W. E. Burcham for helpful criticism and advice, and to the Department of Scientific and Industrial Research for financial assistance.

REFERENCES

Allen, K. W., Livesey, D. L., and Wilkinson, D. H., 1948, in course of preparation.
Bennett, W. E., Bonner, T. W., Hudspeth, E., Richards, H. T., and Watt, B. E., 1941, *Phys. Rev.*, **59**, 781.
Bonner, T. W., 1937, *Phys. Rev.*, **52**, 685.
Bonner, T. W., and Brubaker, W. M., 1936, *Phys. Rev.*, **50**, 308.
Champion, F. C., and Powell, C. F., 1944, *Proc. Roy. Soc.* A, **183**, 64.
Cockcroft, J. D., and Lewis, W. B., 1936, *Proc. Roy. Soc.* A, **154**, 261.
Dee, P. I., and Gilbert, C. W., 1937, *Proc. Roy. Soc.* A, **163**, 265.
Holloway, M. G., and Moore, B. L., 1940, *Phys. Rev.*, **58**, 847.
Kittel, C., and Breit, G., 1939, *Phys. Rev.*, **56**, 744.
Konopinski, E. J., 1943, *Rev. Mod. Phys.*, **15**, 209.
Lattes, C. M. G., Fowler, P. H., and Cuer, P., 1947, *Nature, Lond.*, **159**, 301.
Livesey, D. L., and Wilkinson, D. H., 1948, in course of preparation.
Mattauch, J, 1942, *Kernphysikalische Tabellen* (Berlin : J. Springer).
Powell, C. F., 1940, *Nature, Lond.*, **145**, 155; 1942, *Proc. Roy. Soc.* A, **181**, 344.
Powell, C. F., Occhialini, G. P. S., Livesey, D. L., and Chilton, L. V., 1946, *J. Sci. Instrum.*, **23**, 102.
Richards, H. T., 1941 a, *Phys. Rev.*, **59**, 796; 1941 b, *Ibid.*, **60**, 167.
Stephens, W. E., 1947, *Rev. Mod. Phys.*, **19**, 19.
Stephens, W. E., Djanab, K., and Bonner, T. W., 1937, *Phys. Rev.*, **52**, 1079.

Dissociation Energy of the NO Molecule*

By L. Gerö and R. Schmid
Budapest

MS. communicated by J. G. Valatin after the deaths of both authors ; received 25 *June* 1947

ABSTRACT. During a new investigation of the NO band spectrum many bands of the β and γ system were photographed and analysed, and the rotational constants evaluated. Intensity drops and perturbations were found and two predissociation limits at 53800 and 50500 cm^{-1} were established. In this way the dissociation energy of NO is fixed at 4·29 ev. The $x^2\Pi$ ground state of NO dissociates in the $N(^2D)+O(^3P)$ atomic term combination. The new dissociation scheme is strongly supported by the results of photochemical experiments.

In the course of a new investigation of the band spectrum of the NO molecule, many bands of the β, γ and ϵ system were photographed with great intensity and resolving power. The rotational analysis of the ϵ system was given in a preceding paper (Gerö, Schmid and Szily 1944); after remeasuring the whole of the NO spectrum between 1950 and 2700 A. some new data for the β and γ bands can also be given.

Light source, spectroscope and experimental details were described in the paper mentioned above. The rotational analysis of the following γ bands ($A^2\Sigma - X^2\Pi$) was carried out up to quite large rotational quantum numbers: (0,0), (0,1), (0,2), (0,3), (0,4), (0,5), (1,0), (1,1), (1,3), (1,4), (1,5), (1,6), (2,0), (2,2), (2,3), (2,7), (3,1), (3,4), (3,5). Wave numbers of the (1,0), (2,0) and (3,1) bands are given in the tables 1–3. Some bands of the β-system ($B^2\Pi - X^2\Pi$) were also present between the much stronger γ-bands; the (1,5), (1,6), (2,3), (2,4) and (4,2) β-bands were analysed up to $K \simeq 35$–40, i.e. rather high rotational quantum numbers. When photographed in active nitrogen, which is especially favourable for exciting the β-bands, they are observable only up to $K \simeq 25$–30 (Jenkins, Barton and Mulliken 1927).

Averages of the upper-state combination differences of all bands with common initial states were evaluated. The rotational constants have been determined by the usual graphical method, which yields the B_v constants given in table 4. The data are not accurate enough to determine the variation of the D_v constants with v'; $D' = 6{\cdot}0 \cdot 10^{-6}$ cm^{-1} was therefore used throughout.

The vibrational terms included in table 4 are the heights of the first rotational levels with $J = \frac{1}{2}$ of the different rotational term series above the $x^2\Pi_{\frac{1}{2}}$ ($v = 0, J = \frac{1}{2}$) ground level, determined graphically using all bands and branches. The rotational constant and the height of the first rotational level of the $D^2\Sigma$, $v = 0$ state, evaluated from the $v' = 0$, ϵ-bands, are also given in table 4. As can be seen, the B_0' of the ϵ-bands is greater than each of the B'-values of the γ-bands;

* This paper was written by L. Gerö in 1943. In early 1945, during the period after the siege of Budapest, the first copy of the manuscript went astray, and figures 1 and 2 had to be reconstructed. In figure 2 we were able to mark only schematically the places where the accidental predissociation effect was observed.—J. G. Valatin.

Table 1

$A^2\Sigma - X^2\Pi_{\frac{1}{2}}$; 1,0 band

J	$^SR_{21}$	R_1	Q_1	P_1
$\frac{1}{2}$	46552·28	46544·61	46540·51	
$1\frac{1}{2}$	558·89	547·66	539·28	46535·57
$2\frac{1}{2}$	566·48	551·09	538·73	531·18
$3\frac{1}{2}$	574·70	554·97	538·73	527·39
$4\frac{1}{2}$	583·36	559·61	539·28	524·27
$5\frac{1}{2}$	592·20	564·85	541·10	521·58
$6\frac{1}{2}$	602·34	570·91	543·13	519·40
$7\frac{1}{2}$	612·57	577·11	545·50	517·84
$8\frac{1}{2}$	623·42	584·21	548·57	517·08
$9\frac{1}{2}$	634·88	591·52	552·28	517·08
$10\frac{1}{2}$	646·85	599·84	556·44	517·08
$11\frac{1}{2}$	659·67	608·51	561·45	517·84
$12\frac{1}{2}$	673·24	617·92	566·48	519·40
$13\frac{1}{2}$	686·40	627·87	572·56	521·58
$14\frac{1}{2}$	700·99	638·34	579·19	524·27
$15\frac{1}{2}$	716·11	649·35	586·44	527·39
$16\frac{1}{2}$	731·31	660·87	594·04	531·18
$17\frac{1}{2}$	747·65	673·24	602·34	535·57
$18\frac{1}{2}$	764·47	686·07	611·05	540·51
$19\frac{1}{2}$	781·62	699·27	620·53	546·02
$20\frac{1}{2}$	799·31	713·23	630·66	552·28
$21\frac{1}{2}$	817·79	727·71	641·19	558·89
$22\frac{1}{2}$	836·76	743·06	652·35	566·43
$23\frac{1}{2}$	856·39	758·50	664·16	573·99
$24\frac{1}{2}$	876·47	774·71	676·68	582·34
$25\frac{1}{2}$	897·11	791·50	689·26	591·52
$26\frac{1}{2}$	918·24	808·76	702·67	600·75
$27\frac{1}{2}$	939·74	826·74	716·55	611·05
$28\frac{1}{2}$	962·12	845·01	731·31	621·64
$29\frac{1}{2}$	985·18	864·09	746·32	633·07
$30\frac{1}{2}$	47008·58	883·59	761·97	644·67
$31\frac{1}{2}$	032·46	903·87	778·21	657·32
$32\frac{1}{2}$	057·01	924·56	795·11	670·21
$33\frac{1}{2}$	082·05	945·58	812·44	683·68
$34\frac{1}{2}$	107·87	967·26	830·40	697·63
$35\frac{1}{2}$	133·96	989·66	848·90	712·07
$36\frac{1}{2}$		47012·55	867·92	727·71
$37\frac{1}{2}$		035·93	887·52	743·06
$38\frac{1}{2}$		059·84	907·67	759·44
$39\frac{1}{2}$		084·53	928·37	776·39
$40\frac{1}{2}$		109·46	949·50	793·88
$41\frac{1}{2}$		135·18	971·27	811·65
$42\frac{1}{2}$		161·27	993·57	830·40
$43\frac{1}{2}$		187·93	47016·49	849·60
$44\frac{1}{2}$		215·34	040·09	868·99
$45\frac{1}{2}$		243·07	063·94	889·35
$46\frac{1}{2}$		271·35	088·47	910·14
$47\frac{1}{2}$		300·20	113·59	931·59
$48\frac{1}{2}$		329·47	139·39	953·10
$49\frac{1}{2}$		359·64	165·49	975·51
$50\frac{1}{2}$		390·10	192·23	998·03
$51\frac{1}{2}$		421·32	219·58	47022·48
$52\frac{1}{2}$		452·83	247·36	046·07
$53\frac{1}{2}$		485·00	275·69	070·78
$54\frac{1}{2}$		517·63	304·65	095·97
$55\frac{1}{2}$		550·85	334·12	121·77
$56\frac{1}{2}$		584·48	364·17	148·08
$57\frac{1}{2}$		618·93	394·78	174·82
$58\frac{1}{2}$		653·45	425·89	202·01
$59\frac{1}{2}$		689·02	457·43	230·20
$60\frac{1}{2}$		724·90	489·62	258·46
$61\frac{1}{2}$		760·94	522·46	287·60
$62\frac{1}{2}$		798·25	555·62	317·19
$63\frac{1}{2}$		835·75	589·44	347·49
$64\frac{1}{2}$		873·78	623·69	378·74
$65\frac{1}{2}$		912·34	658·95	409·50
$66\frac{1}{2}$		951·20	694·07	440·88
$67\frac{1}{2}$			729·98	473·14
$68\frac{1}{2}$				505·60

$A^2\Sigma - X^2\Pi_{\frac{3}{2}}$; 1,0 band

J	R_2	Q_2	P_2	$^OP_{12}$
$1\frac{1}{2}$	46439·04	46427·87	46419·77	46415·95
$2\frac{1}{2}$	446·70	431·12	419·08	411·21
$3\frac{1}{2}$	454·34	434·81	419·08	407·16
$4\frac{1}{2}$	462·26	439·04	419·08	403·31
$5\frac{1}{2}$	470·97	443·83	419·77	400·31
$6\frac{1}{2}$	480·04	448·97	421·06	397·60
$7\frac{1}{2}$	490·00	454·34	422·91	395·42
$8\frac{1}{2}$	500·19	460·71	425·13	393·87
$9\frac{1}{2}$	510·46	467·19	427·87	392·45
$10\frac{1}{2}$	521·58	474·36	431·12	391·87
$11\frac{1}{2}$	533·10	482·01	434·81	391·87
$12\frac{1}{2}$	545·50	490·00	439·04	391·87
$13\frac{1}{2}$	557·81	498·91	443·83	392·45
$14\frac{1}{2}$	570·91	508·00	448·97	393·87
$15\frac{1}{2}$	584·21	517·84	454·88	395·81
$16\frac{1}{2}$	598·62	528·02	461·23	398·25
$17\frac{1}{2}$	613·55	538·73	467·92	401·22
$18\frac{1}{2}$	628·35	549·83	475·22	404·58
$19\frac{1}{2}$	643·97	561·45	483·06	408·54
$20\frac{1}{2}$	659·67	573·99	491·26	413·00
$21\frac{1}{2}$	676·68	586·44	500·19	418·00
$22\frac{1}{2}$	694·01	599·84	509·55	422·91
$23\frac{1}{2}$	711·66	613·55	519·40	429·21
$24\frac{1}{2}$	729·87	627·87	529·68	435·50
$25\frac{1}{2}$	748·40	642·82	540·51	442·90
$26\frac{1}{2}$	767·64	658·01	552·28	450·11
$27\frac{1}{2}$	787·47	674·13	564·14	458·40
$28\frac{1}{2}$	807·64	690·30	576·63	467·19
$29\frac{1}{2}$	828·36	707·05	589·46	
$30\frac{1}{2}$	849·60	724·54	602·92	485·53
$31\frac{1}{2}$	871·39	742·36	617·16	495·58
$32\frac{1}{2}$	893·72	760·84	631·36	506·40
$33\frac{1}{2}$	916·57	779·80	646·85	517·84
$34\frac{1}{2}$	939·74	799·31	662·17	529·68
$35\frac{1}{2}$	963·51	819·35	678·60	
$36\frac{1}{2}$	987·72	839·77	695·08	554·97
$37\frac{1}{2}$	47012·55	860·87	712·07	567·91
$38\frac{1}{2}$	038·08	882·31	729·87	581·65
$39\frac{1}{2}$	063·94	904·48	748·40	595·98
$40\frac{1}{2}$	090·34	927·25	767·01	611·05
$41\frac{1}{2}$	117·33	950·12	786·35	626·59
$42\frac{1}{2}$	144·74	973·83	806·15	642·82
$43\frac{1}{2}$	172·70	998·03	826·74	659·67
$44\frac{1}{2}$	201·27	47022·48	847·56	676·68
$45\frac{1}{2}$	230·20	047·93	868·99	694·01
$46\frac{1}{2}$	259·73	073·73	890·82	
$47\frac{1}{2}$	290·00	099·99	913·28	
$48\frac{1}{2}$	320·37	126·83	936·39	
$49\frac{1}{2}$	351·48	154·21	959·80	
$50\frac{1}{2}$	383·12	182·01	983·81	
$51\frac{1}{2}$	415·32	210·39	47008·58	
$52\frac{1}{2}$	447·99	239·37	033·79	
$53\frac{1}{2}$	481·14	268·80	059·84	
$54\frac{1}{2}$	514·78	298·66	085·79	
$55\frac{1}{2}$	549·29	329·47	112·55	
$56\frac{1}{2}$	583·78	360·36	139·39	
$57\frac{1}{2}$	618·93	391·86	167·76	
$58\frac{1}{2}$	654·90	424·11	196·04	
$59\frac{1}{2}$	691·20	456·71	224·97	
$60\frac{1}{2}$	728·20	489·62	254·37	
$61\frac{1}{2}$	765·44	523·59	284·65	
$62\frac{1}{2}$	803·37	557·82	314·93	
$63\frac{1}{2}$	841·30	592·66	346·05	
$64\frac{1}{2}$	880·47	627·70	377·66	
$65\frac{1}{2}$	919·90	663·65	409·50	
$66\frac{1}{2}$		669·62	442·39	
$67\frac{1}{2}$			475·55	

Table 2

$A^2\Sigma - x^2\Pi_1$; 2,0 band

J	${}^SR_{21}$	R_1	Q_1	P_1
½	48861·73	48854·14	48850·11	
1½	868·28	856·62	849·08	48844·83
2½	875·42	860·16	848·29	839·85
3½	883·30	863·88	848·29	836·10
4½	391·89	868·28	849·08	832·78
5½	900·71	873·82	850·11	830·33
6½	910·23	879·70	851·92	828·06
7½	920·38	885·05	854·14	826·39
8½	930·65	891·89	856·62	825·08
9½	941·81	898·97	860·16	824·03
10½	953·43	907·00	863·88	824·03
11½	965·54	915·21	868·28	825·08
12½	978·40	923·83	873·08	826·39
13½	991·93	933·09	878·77	828·06
14½	49005·38	943·06	884·67	830·33
15½	019·58	953·43	891·10	832·78
16½	034·56	964·58	898·08	836·10
17½	049·88	975·97	905·85	839·85
18½	065·75	988·14	914·09	844·14
19½	082·25	49000·79	922·85	849·08
20½	099·36	013·84	932·04	854·14
21½	117·04	027·49	941·81	860·16
22½		041·99	952·24	866·77
23½		056·48	963·10	873·82
24½		071·86	974·25	881·32
25½		087·55	986·20	889·28
26½		103·55	998·85	898·08
27½		120·71	49011·58	907·00
28½		137·99	025·28	916·86
29½		155·56	039·30	926·87
30½		174·31	053·80	937·67
31½		193·09	068·87	949·05
32½		212·61	084·56	960·75
33½		232·31	100·39	972·86
34½		252·63	117·04	986·20
35½		273·65	134·15	998·85
36½		295·18	152·12	49012·71
37½		317·13	170·20	027·49
38½		339·13	188·78	041·99
39½		362·66	207·57	057·66
40½		385·88	227·80	073·26
41½		410·36	248·00	090·13
42½		434·71	268·96	106·98
43½		459·95	290·00	124·52
44½		485·14	311·69	142·24
45½		511·26	334·12	161·14
46½		537·63	356·74	180·12
47½		564·89	380·17	199·82
48½		592·94	404·01	219·68
49½		621·05	428·19	240·62
50½		649·14	452·98	261·03
51½		678·99	478·38	282·42
52½			504·47	303·66
53½				325·65

$A^2\Sigma - x^2\Pi_1$; 2,0 band

J	R_2	Q_2	P_2	${}^OP_{12}$
1½		48737·33	48729·52	
2½		739·90	728·59	
3½	48763·05	743·46	727·90	48716·22
4½	771·40	747·43	727·90	712·35
5½	779·30	752·00	728·59	709·08
6½	788·39	756·89	729·52	706·28
7½	797·35	762·27	731·08	703·67
8½	807·06	768·12	733·01	701·53
9½	817·50	774·52	735·31	700·75
10½	828·05	781·23	738·33	699·16
11½	839·23	788·39	741·68	698·87
12½	850·51	796·20	745·43	698·87
13½	863·09	804·42	749·76	699·16
14½	875·42	812·97	754·42	700·75
15½	888·09	822·06	759·70	701·53
16½	901·60	831·54	765·33	702·93
17½	915·21	841·61	771·40	705·07
18½	929·91	851·92	778·21	708·06
19½	944·66	863·09	785·23	711·33
20½	960·07	874·54	792·70	714·91
21½	975·97	886·34	800·75	719·19
22½	991·93	898·97	809·21	723·63
23½	49008·67	911·76	818·34	728·59
24½	025·73	924·98	828·06	734·69
25½	043·63	938·87	837·65	
26½	061·63	953·43	848·29	
27½	080·39	967·89	859·25	
28½	099·36	983·15	870·50	
29½	119·09	998·85	882·32	
30½	138·98	49015·02	894·78	
31½	159·35	031·79	907·58	
32½	180·12	048·94	920·93	
33½	201·76	066·56	934·82	
34½	223·75	084·56	949·05	
35½	246·30	103·55	963·91	
36½	269·72	122·54	979·21	
37½		142·24	995·01	
38½	316·40		49011·58	
39½	340·45	182·71		
40½	365·27	203·96	045·36	
41½	390·54	225·37	063·07	
42½	416·51	247·51	081·21	
43½	442·58	269·72	099·36	
44½	469·74	292·77	119·09	
45½	497·27	316·30	138·98	
46½	525·91	340·45	159·35	
47½	553·52	365·27	180·12	
48½	582·74	390·54	201·22	
49½	612·31	416·51	222·93	
50½	642·36	442·58	244·94	
51½	673·32	469·74	267·63	
52½		497·27		

this is a strong argument against the hypothesis that the γ and ϵ bands belong to the same band system. It must also be determined whether there are homogeneous perturbations in one or in another of these bands which deform the rotational constants. From figure 1 it is seen that the $B'-B''$ curves (Gerö 1935 a) for the bands γ (0,2), (1,0), (2,0) and (3,1) and ϵ (0,3) are nearly horizontal straight lines which means that no considerable perturbations are present in these bands.

Predissociation phenomena were found in the upper state of the γ-bands. The rotational term series show sudden intensity falls at $v=0$, $K=74$; $v=1$,

Table 3

$A^2\Sigma - X^2\Pi_{\frac{1}{2}}$; 3,1 band				$A^2\Sigma - X^2\Pi_{\frac{3}{2}}$; 3,1 band			
J	R_1	Q_1	P_1	J	R_2	Q_2	P_2
$\frac{1}{2}$	49254·40						
$1\frac{1}{2}$	257·02	49249·43		$1\frac{1}{2}$		49137·99	49130·29
$2\frac{1}{2}$	260·52	249·43		$2\frac{1}{2}$		140·48	129·01
$3\frac{1}{2}$	264·21	249·43		$3\frac{1}{2}$		144·22	129·01
$4\frac{1}{2}$	268·96	249·43		$4\frac{1}{2}$		147·99	129·01
$5\frac{1}{2}$	273·65	250·23	49231·53	$5\frac{1}{2}$		152·12	129·01
$6\frac{1}{2}$	278·90	252·12	228·91	$6\frac{1}{2}$		157·49	130·29
$7\frac{1}{2}$	284·87	254·40	227·80	$7\frac{1}{2}$		162·95	131·98
$8\frac{1}{2}$	291·43	257·02	226·05	$8\frac{1}{2}$		168·61	133·09
$9\frac{1}{2}$	298·46	260·52	225·37	$9\frac{1}{2}$		174·82	135·99
$10\frac{1}{2}$	306·34	264·21	225·37	$10\frac{1}{2}$		181·60	138·98
$11\frac{1}{2}$	314·75	268·96	226·05	$11\frac{1}{2}$		188·78	142·24
$12\frac{1}{2}$	323·60	273·65	227·80	$12\frac{1}{2}$		196·36	146·23
$13\frac{1}{2}$	332·80	278·90	228·91	$13\frac{1}{2}$		203·96	150·41
$14\frac{1}{2}$	342·66	284·87	231·53	$14\frac{1}{2}$		212·61	155·56
$15\frac{1}{2}$	353·04	291·43	233·71	$15\frac{1}{2}$	49287·60	222·05	160·44
$16\frac{1}{2}$	363·74	298·46	236·91	$16\frac{1}{2}$	300·74	231·53	166·09
$17\frac{1}{2}$	375·34	305·95	240·62	$17\frac{1}{2}$	314·75	241·45	172·23
$18\frac{1}{2}$	387·19	314·14	244·94	$18\frac{1}{2}$	328·89	252·12	179·01
$19\frac{1}{2}$	399·76	322·73	249·43	$19\frac{1}{2}$	343·66	262·61	185·90
$20\frac{1}{2}$	412·99	331·93	255·13	$20\frac{1}{2}$	358·67	274·16	193·09
$21\frac{1}{2}$	426·45	341·49	261·03	$21\frac{1}{2}$	373·98	285·92	201·22
$22\frac{1}{2}$	440·77	352·14	267·63	$22\frac{1}{2}$	390·54	298·46	209·70
$23\frac{1}{2}$	454·86	362·66	274·16	$23\frac{1}{2}$	407·11	310·98	218·81
$24\frac{1}{2}$	469·74	373·98	281·98	$24\frac{1}{2}$	424·50	324·29	228·91
$25\frac{1}{2}$	485·14	385·88	290·00	$25\frac{1}{2}$	441·68	338·09	238·15
$26\frac{1}{2}$	501·75	397·91	298·46	$26\frac{1}{2}$	459·95	352·14	248·00
$27\frac{1}{2}$	518·74	410·99	307·58	$27\frac{1}{2}$	478·38	366·88	259·38
$28\frac{1}{2}$	535·99	424·50	317·13	$28\frac{1}{2}$	497·27	382·15	270·62
$29\frac{1}{2}$	553·52	438·28	327·50	$29\frac{1}{2}$	516·56	397·91	282·42
$30\frac{1}{2}$	572·12	452·98	338·09	$30\frac{1}{2}$		413·77	295·18
$31\frac{1}{2}$	590·71	467·22	348·97	$31\frac{1}{2}$		430·31	307·58
$32\frac{1}{2}$	609·77	483·03	360·67	$32\frac{1}{2}$		447·21	320·73
$33\frac{1}{2}$	629·99	498·84	373·03	$33\frac{1}{2}$		464·62	334·12
$34\frac{1}{2}$	650·01	515·90	385·88	$34\frac{1}{2}$		483·03	348·97
$35\frac{1}{2}$	670·63	532·78	398·96	$35\frac{1}{2}$		501·75	363·74
$36\frac{1}{2}$	692·03	550·25	412·99	$36\frac{1}{2}$			380·17
$37\frac{1}{2}$		568·31	427·50				
$38\frac{1}{2}$			441·68				

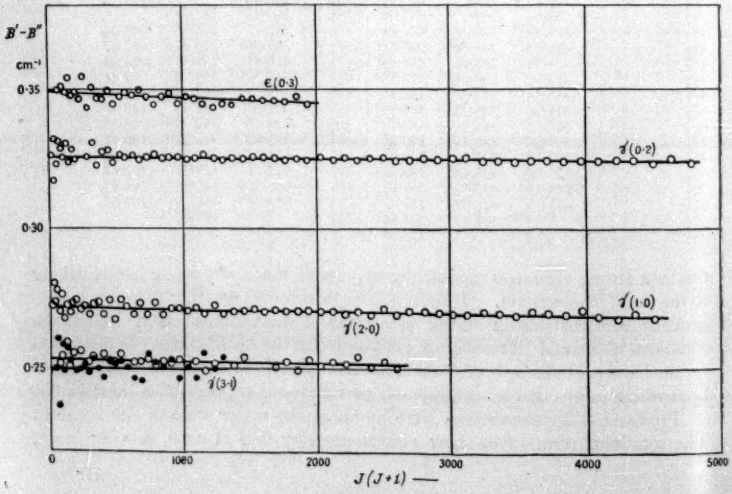

Figure 1.

Table 4

			Vibrational terms			B_v
	$v=0$	44199·2				1·9870
			2341·4			
	1	46540·6		31·5		1·9688
			2309·9		1·7	
$A^2\Sigma$	2	48850·5		33·2		1·9498
			2276·7			
	3	51127·2				1·9290
$D^2\Sigma$	$v=0$	53291·9				1·9917

$K=64$; $v=2$, $K=52$; $v=3$, $K=38$; joining these points in figure 2, a limiting curve of predissociation can be drawn, which intersects the ordinate axis at a value of about 53 800 cm^{-1}. An N + O atomic term combination must lie at this energy, which gives rise to the predissociation phenomena observed.

The upper-state rotational term series of the β-bands intersect in many places the much steeper upper term series of the γ-bands. In the neighbourhood of the intersections perturbation phenomena should be discovered. Tables 5 and 6 contain parts of the corresponding branches of the $(4,2)\beta$–$(2,2)\gamma$ and $(2,4)\beta$–$(1,4)\gamma$ bands respectively, which belong to common lower states. At the intersection points of the upper states the differences of corresponding wave numbers change their signs; these places in the tables are marked with arrows.

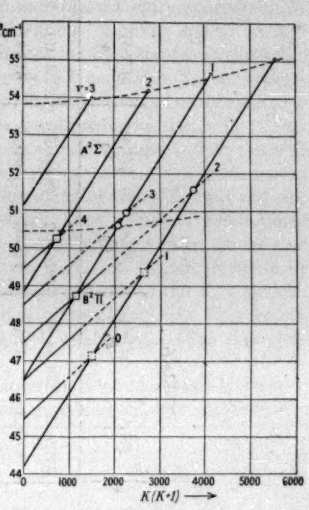

Figure 2.

Table 5

J	$\beta(4,2)$ R_1	$\gamma(2,2)$ R_1	$\beta(4,2)$ P_1	$\gamma(2,2)$ P_1	$\beta(4,2)$ R_2	$\gamma(2,2)$ R_2
21½	45519·76	45320·10	45428·05	45153·05	45440·58	45269·54
22½	495·79	335·97	399·50	161·19	416·22	287·42
23½	469·47	352·28	369·32	169·72	390·21	305·87
24½	442·75	369·32	338·31	178·49	364·38	324·56
25½	414·45	386·66	305·87	188·60	336·77	⟷
26½	384·74	⟷	272·49	199·12	307·58	364·38
27½	354·48	423·63	237·61	210·06	277·62	384·74
28½	323·17	442·75	202·43	⟷	246·49	405·79
29½	290·44	462·84	165·15	233·76		
30½		483·19	127·00	246·49		

No irregularity of any kind could be detected in the wave numbers or intensities in either of the branches.

The $R_1(32\frac{1}{2})$ and $P_1(34\frac{1}{2})$ lines of the $(2,4)\beta$ and $(1,4)\gamma$ bands respectively have the same wave numbers; thus the upper rotational terms $F_1(33\frac{1}{2})$ of both

Table 6

J	$\gamma(1,4)$ $^3R_{21}$	$\beta(2,4)$ R_1	$\gamma(1,4)$ R_1	$\beta(2,4)$ P_1	$\gamma(1,4)$ P_1	$\beta(2,4)$ R_2	$\gamma(1,4)$ R_2	$\beta(2,4)$ P_2	$\gamma(1,4)$ P_2
$26\frac{1}{2}$	39632·27	39841·66	39522·52	39726·52	39314·99	39763·22	39484·56	39644·29	39269·28
$27\frac{1}{2}$	657·40	814·48	544·28	695·15	329·11	736·06	508·24	612·92	285·03
$28\frac{1}{2}$	683·82	786·20	566·69	662·55	343·21	707·74	532·53	580·19	301·59
$29\frac{1}{2}$	710·85	756·76	589·74	628·92	359·05	678·48	557·58	546·47	318·93
$30\frac{1}{2}$	738·54	726·52	613·60	594·53	374·97	647·97	583·19	511·90	336·78
$31\frac{1}{2}$	767·05	695·15	638·00	558·75	391·65	616·45	609·48	476·03	355·35
$32\frac{1}{2}$	796·00	663·26	663·26	522·07	409·13	583·84	636·37	439·48	374·57
$33\frac{1}{2}$	826·04	629·96	689·33	484·56	427·27	550·11	663·82	401·41	394·40
$34\frac{1}{2}$	856·61	595·71	715·91	445·99	445·99	515·35	692·15	362·24	415·02
$35\frac{1}{2}$	887·14	559·58	743·07	405·96	465·37	479·57	721·14	322·52	436·23

bands have almost equal energies. As neither line broadening, nor anomalous intensity are observable (the intensity of the common lines being approximately the sum of the intensities of the two coinciding lines), the interaction of the two electronic states $B^2\Pi$ and $A^2\Sigma$ must be extraordinarily small.

The points at which the expected perturbations could not be detected are

marked with squares in figure 2, full lines show where both intersecting term series were observed, and broken lines, where only the upper series of the γ-bands were observed. There are, however, three points where intensity anomalies were observed in the branches of the γ-bands; these points are marked with circles. Two circles lying close together in a term series mean that as a result of intersection with Π-states, the F_1 and F_2 perturbations of the $A^2\Sigma$ term series do not take place at the same J-values. These points also lie near the γ–β upper-term intersections, but at higher energies than those intersections at which no effect could be detected. Between the circles and squares a limiting curve (similar to the limiting curve of predissociation at 53 800 cm^{-1}) can be drawn. Above this limiting curve, intensity diminutions are present, but no shifts of rotational level; below the curve no such effects are observed. As the (4,2) band of the β system comes to an end with a sudden intensity drop just at this limiting curve and no β-bands with $v'>4$ were found, the limit at 50 500 cm^{-1} is a real predissociation limit. This limit corresponds to a continuum, which is in strong interaction with the $B^2\Pi$ state. At the intersection points above the limiting curve, the eigenfunctions of the $B^2\Pi$ state are mixed with the eigenfunctions of the $A^2\Sigma$ state and this mediates the intensity-weakening for the γ-band lines. Such a combination of predissociation and perturbation effects was called by Coster, Brons and van der Ziel (1933) "accidental predissociation" and was treated theoretically by Ittmann (1934) in the case of the Second Positive bands of the N_2 molecule; but neither the perturbing states, nor the cause of predissociation were known in the N_2 spectrum, while in NO both are well established. (See also Gerö 1935 b, and Gerö and Schmid 1940.)

The energy difference of the two predissociation limits found is about 3300 cm^{-1}. Now in the energy scheme of N + O atomic term combinations, only one difference comes near to this value, namely the difference $N(^2D)+O(^3P)-N(^4S)+O(^1D)=3355$ cm^{-1}; all other differences are much larger. Relating these two combinations to the limiting curves, the term scheme of figure 3 is obtained. According to this scheme, the dissociation energy of the NO molecule is 34 600 $cm^{-1}=4{\cdot}29$ ev. The $x^2\Pi$ ground state dissociates *not* into the $N(^4S)+O(^3P)$ ground atomic term combination, but into the $N(^2D)+O(^3P)$ combination, with a dissociation energy of 53 800 cm^{-1}. (The extrapolated value, which in most cases is 10–25 % greater than the real one, is $\omega_e^2/(4\omega_e x_e)=62\,500$ cm^{-1}, and, therefore, a dissociation energy of 34 600 cm^{-1} for the ground state would be too small.)

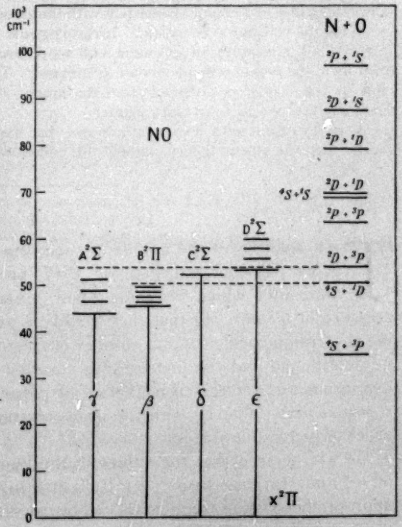

Figure 3.

The above dissociation scheme of NO is strongly supported by the photochemical experiments of Flory and Johnston (1935). They irradiated NO with the 1832 A. line of mercury and found considerable photochemical decomposition. The energy of this mercury line, 54 567 cm^{-1}, is slightly greater than the dissociation limit of the NO ground state at 53 800 cm^{-1}; hence the efficiency of this wavelength.

REFERENCES

Coster, D., Brons, F., and van der Ziel, A., 1933, *Z. Phys.*, **84**, 304.
Flory, P. J., and Johnston, H. L., 1935, *J. Amer. Chem. Soc.*, **57**, 2641.
Gerö, L., 1935 a, *Z. Phys.*, **93**, 669; 1935 b, *Ibid.*, **96**, 669.
Gerö, L., and Schmid R., 1940, *Z. Phys.*, **116**, 246.
Gerö, L., Schmid, R., and von Szily, F. K., 1944, *Physica*, **11**, 144.
Ittmann, G. P., 1934, *Naturwissenschaften*, **22**, 118.
Jenkins, F. A., Barton, H. A., and Mulliken, R. S., 1927, *Phys. Rev.*, **30**, 150, 175.

Collision Broadening of the Inversion Spectrum of Ammonia: III. The Collision Cross-sections for Self-broadening and for Mixtures with Non-polar Gases

By B. Bleaney and R. P. Penrose
Clarendon Laboratory, Oxford

ABSTRACT. The widths of the lines of the inversion spectrum of pure ammonia near 1 cm^{-1} previously determined experimentally (Bleaney and Penrose 1947) are shown to vary from line to line in a manner consistent with the assumption of a simple dipole–dipole interaction for the collision mechanism. Measurements of the line breadth constant for the line $(J,K)=(3,3)$ in mixtures of ammonia with six different non-polar gases are described, and from them the collision diameters are calculated. They are found to be approximately the same as the diameters obtained from the kinetic theory, whereas in pure ammonia the diameters are two to four times greater.

A survey of microwave spectra indicates that the collision diameter is only significantly greater than the kinetic theory diameter for encounters between permanent electric dipoles.

§1. Introduction

The analysis of the ammonia spectrum has been described in an earlier paper (Bleaney and Penrose 1947, hereafter called "A"). Of twenty-nine lines which were identified, seventeen were so well resolved at a pressure of 0·5 mm. Hg that they could be examined in detail. By measuring the absorption coefficient at a number of frequencies the shape of each line could be determined and the line breadth constant calculated. The results of these measurements were given in table 4 of paper A; for convenience, this table is repeated here (table 1), with the order rearranged so that the lines are given in order of increasing breadth.

It will be seen that the values of the line breadth constant at the pressure of 0·5 mm. Hg vary from $1{\cdot}8\times10^{-4}$ cm^{-1} to $4{\cdot}7\times10^{-4}$ cm^{-1}. From them the appropriate collision frequencies can be calculated since the collision frequency f is associated with a line breadth constant $\Delta\bar{\nu}=f/2\pi c$. This collision frequency,

which is the number of times per second that the absorption of radiation by one molecule is interrupted by the approach of another molecule, varies from $3{\cdot}4\times10^7$ to $8{\cdot}9\times10^7$ per second. The collision frequency at 0·5 mm. pressure deduced from viscosity measurements by means of the kinetic theory is only $4{\cdot}0\times10^6$ per second, which is considerably smaller. It follows that the interruption of absorption of centimetre-wave radiation occurs when another molecule approaches to a distance which is considerably greater than that required for an appreciable transfer of momentum from one molecule to the other. The relative distances can be found by calculating the collision diameters (σ) of the ammonia molecule from the formula $f=\sqrt{2}v\pi\sigma^2N$, where N is the number of molecules per cm^3 and v is the average velocity of the molecules. The values of σ range from 8·7 A. for the narrowest lines to 14·2 A. for the broadest, whereas the kinetic theory diameter is only 4·4 A.

Table 1

Line (J,K)	$\Delta\bar{\nu}$ at $p=0{\cdot}5$ mm. Hg $\times10^{-4}$ cm^{-1}	γ_0 (db/km.)	I_{exp} db/mol	I_{theor} db/mol
5,1	1·8	7	3·3	3·5
3,1	2·4	29	14·5	14
2,1	2·6	51	25	27
5,2	2·6	20	13	15
11,9	2·9	8·5	5·7	6·4
6,3	3·1	44	35·5	34
3,2	3·2	100	62·5	59
5,3	3·3	96	71	73·5
6,4	3·6	42	35	34·5
7,6	3·9	132	100	95·5
7,5	4·1	28	27	27
8,7	4·1	44	34	32·5
10,9	4·2	35	25·5	23
3,3	4·5	360	289	289
4,4	4·5	190	149	151
5,5	4·7	186	148	137
6,6	4·7	276	198	210

$\Delta\bar{\nu}$ is measured value of the line breadth constant (cm^{-1}).
γ_0 is measured value of absorption at centre of line (db/km.).

I is integrated intensity $=\int_0^\infty \frac{\gamma}{\bar{\nu}^2}\,d\bar{\nu}$ reduced to a length of path containing one mol of gas per unit cross-section.

I_{exp} is calculated from the relation $I_{exp}=\bar{\nu}_0^{-2}\pi\gamma_0\Delta\bar{\nu}(10^{-5}V_0)$, where V_0=molar volume at a pressure of 0·5 mm. Hg.

I_{theor} is calculated from the relation $I_{theor}=\dfrac{4\pi^3N_{JK}V_0|\mu_{JK}|^2}{3kT}$.

N_{JK}=number of ammonia molecules per cm^3 in rotational level (J,K).
$|\mu_{JK}|^2$=square of dipole moment associated with the line (J,K).

These large values for the collision cross-section may be attributed to the effect of the large electric field of the ammonia dipole, which will produce a considerable perturbation of the energy levels of an approaching molecule at distance of the order of 10^{-7} cm. This assumption is supported by consideration of the large variation in the widths of the different lines. This is at first sight surprising, since each line arises from an exactly similar transition between the levels of the inversion doublet. The significant difference arises, however, from the fact

that each line is due to molecules in a particular rotational energy level, and the line widths vary with the state of rotation of the molecule in the same way as does the Stark splitting due to an external electric field. In the following section of this paper the variation of line width is discussed, and it is shown that it can be explained by the simple hypothesis that a collision occurs when the electrical forces between the molecules due to their strong dipoles cause the energy of interaction to reach a certain value. The magnitude of the interaction energy required to produce a collision is evaluated from the observed line widths by averaging over the various settings of the dipoles with respect to the line of centres at a collision.

§2. THE COLLISION CROSS-SECTION FOR SELF-BROADENING

The magnitude of the splitting or perturbation of the energy levels of a molecule possessing a permanent electrical dipole moment when subjected to a constant electric field is determined by the steady component of the dipole moment. In the general state of rotation of a symmetrical top molecule, the dipole moment will be precessing about the axis of total angular momentum of the molecule, and the steady component is determined by the projection of the moment on that axis. The frequency of precession is of the same order as the rotational frequency, and one may therefore expect that the perturbation due to a transient electric field is still determined by the steady component of the dipole moment if the duration of the transient is long compared to the period of rotation. Since the experimental collision diameter is about 10^{-7} cm. for ammonia, the duration of a collision is of the order of 10^{-11} sec., while the rotational periods are less than 10^{-12} sec. Thus it is reasonable to assume that the interaction between the electric field of one molecule and the dipole moment of an absorbing molecule is determined by the steady component of the latter. In ammonia this varies as $K/(J^2+J)^{\frac{1}{2}}$, where J, K are the rotational quantum numbers of a symmetrical top. The interaction should therefore be largest when $K=J$, and smallest when K is small compared with J. Inspection of table 1 shows that the line widths increase steadily as K/J approaches unity.

The variation of the line breadth constant with the rotational state of the molecule may be given a quantitative aspect by assuming that a collision occurs when two molecules approach to a distance such that the energy of interaction between them reaches a certain value W. For the molecules in a particular rotational state defined by the quantum numbers (J, K), the average distance at which a collision takes place will then be determined by the relation $W \propto \bar{\mu}/r^3$. The variation in the line breadth constants depends only on the variation in the collision cross-section. Since the latter is proportional to r^2, the line breadths should vary, on this hypothesis, as $(\bar{\mu}/W)^{\frac{1}{2}}$. Hence, assuming that W is independent of the rotational state of the molecule, $\Delta\bar{\nu}$ should vary as $(K^2/(J^2+J))^{\frac{1}{2}}$ for the lines of this inversion spectrum. In figure 1 the widths

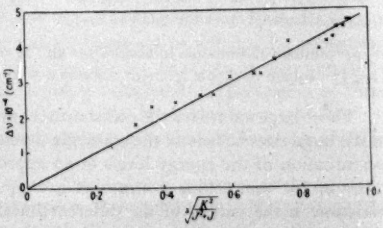

Figure 1. Widths of lines in ammonia inversion spectrum near 1 cm^{-1}.

($\Delta\bar{\nu}$) of the seventeen lines measured at 0·5 mm. Hg pressure are plotted against $(K^2/(J^2+J))^{\frac{1}{2}}$. Within the experimental error (about 5% in $\Delta\bar{\nu}$) the points fall on a straight line, thus confirming that the interruption of the absorption is due to dipole–dipole interaction.

The success of this simple theory encourages a more exact calculation of the magnitude of the interaction energy between two ammonia molecules required to produce a collision. This requires an averaging process in order to take account of the variation of the interaction energy between two dipoles with the angles at which they lie with respect to the line through their centres. A simple method of obtaining the average cross-section for collision is given in the Appendix to this paper. It is found that the average cross-sectional area for collisions of this type is

$$S_{11}=2{\cdot}45(\mu_1^2\overline{\mu_2^2}/W^2)^{\frac{1}{2}}, \qquad \ldots\ldots(1)$$

where $\mu_1^2=\mu^2\{K^2/(J^2+J)\}$ is the squared dipole moment of an ammonia molecule in the rotational state (J, K), $\overline{\mu_2^2}$ = the mean square of the dipole moment of all the ammonia molecules, and W = interaction energy required to produce a collision.

Hence the line breadth constant $\Delta\bar{\nu}$ is

$$\Delta\nu=\frac{2NS_{11}}{\pi\boldsymbol{c}}\sqrt{\left(\frac{\boldsymbol{R}T}{M}\right)}, \qquad \ldots\ldots(2)$$

where N is number of molecules per cm^3, M is molecular weight, T absolute temperature, and $\boldsymbol{c}$ and $\boldsymbol{R}$ have their usual meanings.

At room temperature, computation of the average value of $\{K^2/(J^2+J)\}$ over all rotational states of ammonia gives $\overline{\mu_2^2}=0{\cdot}40\,\mu^2$. Inserting the expression for S_{11}, and taking $\mu=1{\cdot}44\times10^{-18}$ E.S.U., we obtain

$$\Delta\bar{\nu}=4{\cdot}5\times10^{-14}p_{\text{mm}}W^{-\frac{1}{2}}(K^2/(J^2+J))^{\frac{1}{2}} \quad (\text{cm}^{-1}), \qquad \ldots\ldots(3\,a)$$

where p_{mm} is the pressure of ammonia in mm. Hg.

The experimental value of $\Delta\bar{\nu}$ at a pressure of 0·5 mm. Hg, obtained from figure 1, is

$$\Delta\bar{\nu}=0{\cdot}50\times10^{-3}(K^2/(J^2+J))^{\frac{1}{2}} \quad (\text{cm}^{-1}). \qquad \ldots\ldots(3\,b)$$

Hence the interaction energy W is $3{\cdot}0\times10^{-16}$ ergs, or $W/\boldsymbol{hc}=1{\cdot}5\,\text{cm}^{-1}$, which is approximately equal to twice the separation of the two energy levels of the inversion doublet, between which transitions are taking place. It is thus hardly surprising that the absorption or emission of radiation is interrupted.

The mechanism of this collision process is rather different from that assumed in the simple theory of collision broadening of spectral lines in the optical region. For such lines the periodic time (10^{-15} sec.) of the radiation is much shorter than the duration of a collision between two molecules (10^{-13} to 10^{-11} sec.). The "classical picture" of a collision is that of a small change in the natural frequency of the molecule due to the influence of an approaching molecule, which causes the oscillating molecule gradually to get out of phase with the exciting radiation. This effect persists over some hundreds of oscillations throughout the duration of a collision, and the integrated effect causes such a large phase shift that the absorption or emission of radiation is interrupted. The perturbation of the energy levels caused by the approaching molecule is, however, small compared with the separation of the two levels between which transitions are being induced. This is very different from the situation in the ammonia inversion spectrum. Here a collision is caused by a large perturbation of the energy levels acting for less than one period of the radiation.

§ 3. THE CROSS-SECTION FOR COLLISIONS WITH NON-POLAR MOLECULES

Since the abnormally large collision diameters in pure ammonia are ascribed to the effects of dipole–dipole interaction, it would be expected that the cross-section for collisions between an absorbing ammonia molecule and a non-polar molecule would be considerably smaller. Measurements were therefore undertaken of the line breadth constant of the strongest line in the inversion spectrum of ammonia ($J,K=3,3$) for admixtures of six non-polar gases. Since none of the gases used had appreciable absorption at centimetre wavelengths, the effect of diluting the ammonia with one of them is to increase the collision frequency for the same partial pressure of ammonia and thus to broaden the line. Although it was possible to determine the line breadth constant for the mixture by the method already described (Bleaney and Penrose 1947) for the inversion lines of pure ammonia, the close agreement with the theoretical intensity obtained in the previous measurements on this line made it possible to use a different technique which was not only simpler but rather more accurate. Instead of measuring the absorption coefficient at a number of frequencies in order to delineate the line, the absorption coefficient was measured only at the centre of the line. For a mixture with a non-absorbing gas the absorption there is smaller than in pure ammonia, varying inversely as the line breadth constant at pressures where the absorption due to tails of neighbouring lines is negligible. The formula for the absorption coefficient at the centre of a line is

$$\alpha=\frac{4\pi^2|\mu_{JK}^3|\bar{\nu}_0^2 N_{JK}}{3\boldsymbol{k}T\Delta\bar{\nu}} \quad \text{per cm.} \qquad \ldots\ldots(4)$$

where $|\mu_{JK}|^2$, N_{JK} and $\Delta\bar{\nu}$ are as already defined and $\bar{\nu}_0$ is the wave number of the line in cm^{-1}.

The line breadth constant $\Delta\bar{\nu}=f/2\pi\boldsymbol{c}$, where f is the collision frequency. For a given mixture both f and N_{JK} vary directly as the pressure, and the absorption coefficient at the centre of a line is therefore independent of the pressure. The addition of a non-absorbing gas to a certain concentration of ammonia increases f from the value for pure ammonia, f_{11}, to $f_{11}+f_{12}$, where f_{12} is the frequency of collisions between an ammonia molecule in the state (3,3) and molecules of the foreign gas. The absorption is therefore reduced in the ratio

$$\alpha_2/\alpha_1=f_{11}/(f_{11}+f_{12}),$$

where α_1 is the absorption coefficient for pure ammonia and α_2 that for the mixture.

Hence $f_{12}/f_{11}=(\alpha_1/\alpha_2)-1$.

If S_{12} and S_{11} are respectively the cross-sections for ammonia–foreign gas collisions and for ammonia–ammonia collisions, the expressions for f_{12} and for f_{11} are

$$f_{12}=2N_2S_{12}(2\boldsymbol{R}T/\pi)^{\frac{1}{2}}(M_1^{-1}+M_2^{-1})^{\frac{1}{2}},$$

$$f_{11}=4N_1S_{11}(\boldsymbol{R}T/\pi M_1)^{\frac{1}{2}},$$

where N_1, N_2 are the numbers of ammonia and foreign gas molecules per cm^3 respectively, and M_1, M_2 the molecular weights of ammonia and of the foreign gas.

Hence the ratio of the cross-sections is

$$\frac{S_{12}}{S_{11}}=\frac{N_1}{N_2}\frac{f_{12}}{f_{11}}(\tfrac{1}{2}(1+M_1/M_2))^{-\frac{1}{2}}=\frac{N_1}{N_2}\left(\frac{\alpha_1}{\alpha_2}-1\right)(\tfrac{1}{2}(1+M_1/M_2))^{-\frac{1}{2}}. \qquad \ldots\ldots(5)$$

§4. EXPERIMENTAL

The six non-polar gases used in the mixtures were helium, hydrogen, nitrogen, oxygen, argon and carbon disulphide. The ratios in which the mixtures were made up were chosen so that the line breadth constant for the mixture would be approximately double that for the same partial pressure of pure ammonia. Two slightly different techniques were used to prepare the mixtures, the choice depending on whether the non-polar gas would condense in liquid air or not.

The mixtures were prepared in a bulb of about one litre volume which had a small side tube which could be immersed in liquid air. In cases where the foreign gas would not condense at liquid air temperature, the bulb was first filled with ammonia at a known pressure. After the bulb has been isolated, the ammonia was frozen out in the side tube (the vapour pressure of ammonia at 90° K. is about 10^{-6} mm. Hg). Then a suitable pressure of the foreign gas was admitted to the bulb, after which the bulb was again isolated. Finally the liquid air bath was removed, and the ammonia in the side tube allowed to evaporate and mix with the other gas, several days usually being allowed to elapse to ensure proper mixing. Since the volume of the side tube was negligible in comparison with that of the bulb, the error due to its different temperature was negligible.

When the foreign gas would condense at liquid air temperature, the following procedure was adopted. A second bulb was filled to a known pressure with the foreign gas, which was then transferred to the first bulb by freezing it into the side tube by means of a liquid air bath. This operation was repeated with ammonia. The first bulb was then isolated, and the gases allowed to evaporate and mix as before.

In each of these methods a given volume was filled to a known pressure with each of the constituents of the mixture. The ratio (N_2/N_1) of the numbers of molecules per cm^3 of the two gases was therefore accurately known.

The intensity of absorption of the mixture of gases was determined by observing the reduction in power transmitted through a cavity resonator of known Q, when the gas was admitted. A full account of this technique has already been given in paper A. In terms of the detector readings δ_0 and δ_1 before and after admitting the mixture, the absorption coefficient is given by the expression $\alpha=(2\pi/\lambda Q_0)((\delta_0/\delta_1)^{\frac{1}{2}}-1)$. The absorption was measured for a number of pressures such that the partial pressure of ammonia lay in the range 0·2 mm. to 3 mm. Figure 2 shows the absorption–pressure curve for an ammonia–oxygen mixture in the proportion $N_1/N_2=0{\cdot}107$. The falling-off in the absorption at low pressures is due to the disturbance of thermal equilibrium (Bleaney and Penrose 1948), while the rise at high pressures is attributable to

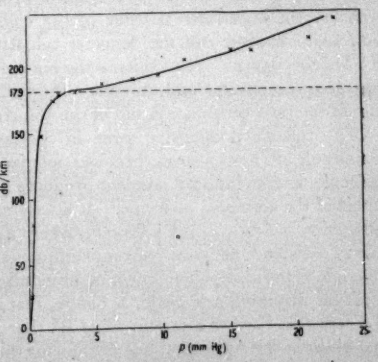

Figure 2. Absorption in ammonia-oxygen mixture at 0·7964 cm^{-1}.

the contributions from other lines in the spectrum. The shape of the full curve includes an allowance for this rise, and provides a means for smoothing the points. The dotted line represents the corrected value (179 db/km.) for the line (3,3) in this mixture. The absorption coefficient for the centre of this line in pure ammonia is 360 db/km. (see A, or table 1 of this paper). From the ratio of these two absorptions, the ratio of the collision cross-sections for ammonia–oxygen and ammonia–ammonia can be calculated by means of equation (5). Since the latter is known accurately from previous measurements by the authors, the collision diameter (σ_{12}) for ammonia–oxygen can be evaluated from the formula $\sigma_{12}=\sqrt{(S_{12}/\pi)}$.

From similar measurements and calculations for the other mixtures, the value of the collision diameter in each case was determined.

§ 5. RESULTS AND DISCUSSION

The results of these measurements are shown in table 2.

Table 2

(1)	(2)	(3)	(4)	(5)	(6)	(7)	(8)
Helium	4·0	0·21	0·0295	17·6	2·35	3·20	3·6
Hydrogen	2·0	0·78	0·064	38·2	3·50	3·58	4·5
Nitrogen	28·0	1·72	0·205	122	6·4	4·09	5·0
Oxygen	32·0	1·51	0·123	73·5	4·85	4·02	4·9
Argon	39·9	1·74	0·111	66·3	4·6	4·04	4·0
Carbon disulphide	76·1	8·6	0·296	177	7·5	—	6·9
Ammonia	17·0	—	—	597	13·8	4·4	—

(1) Gas mixed with NH_3; (2) molecular weight; (3) polarizability (in $cm^3\times10^{-24}$); (4) S_{12}/S_{11} measured; (5) S_{12} measured (in $cm^3\times10^{-16}$); (6), (7), (8) collision diameters in A.; (6) measured; (7) according to kinetic theory; (8) calculated.

In the first three columns are shown the non-polar gas, its molecular weight and its polarizability. The experimental value of the ratio of the collision cross-section to that for the line (3,3) in pure ammonia is given in column (4), and the actual cross-section in column (5). The last three columns contain respectively the experimental value of the collision diameter, the kinetic theory molecular diameter and the diameter calculated by an extension of the theory of § 2 of this paper. The values of the kinetic theory diameter are not, of course, measured directly for each mixture; the figure given is obtained by taking the sum of the radii of ammonia and of the admixed gas (Kennard 1938).

The calculated diameter given in the last column is obtained as follows. A molecule of a non-polar gas becomes polarized in the electric field of an ammonia molecule, and its induced moment produces a field which acts on the permanent dipole of the ammonia molecule. It is easy to show that the energy of the latter interaction is $r^{-6}a|\mu_{JK}|^2(1+3\cos^2\theta)$, where a = polarizability of non-polar molecule; r = distance between centres of ammonia molecule and non-polar molecule; θ = angle between dipole moment of ammonia molecule and radius vector.

If the assumption is made, as before, that a collision occurs when the energy of interaction reaches a certain value W, then by an averaging process similar to that given in the Appendix, one obtains for the collision cross-section

$$S_{12}=3\cdot90(\mu_1^2a/W)^{\frac{1}{2}}.$$

If the value of W necessary for a collision is assumed to be the same as that found for an ammonia–ammonia collision, i.e. $3{\cdot}0 \times 10^{-16}$ ergs, the value of S_{12}, and hence the collision diameter, may be calculated.

Inspection of table 2 shows that the experimental values of the collision diameter are of the same order as the kinetic theory values, as, also, are the values calculated on the basis of the theory outlined in the preceding paragraph. The latter means that at the distance between the molecules required by the purely electrical interaction for a collision, other forces come into play, and that the collision mechanism suggested is superseded by more powerful interactions. It is satisfactory, however, that the theory does not give values of the collision diameter which are much bigger than those observed.

The collision cross-section for ammonia–nitrogen appears to be exceptionally large in comparison with those for ammonia–oxygen and ammonia–argon. This was unexpected, since the polarizability and the kinetic theory diameter of each of these molecules is very nearly the same. The first measurements were made with commercial nitrogen, and gave a collision cross-section of 128×10^{-16} cm^2. The experiment was then repeated with a mixture made from specially pure and dry nitrogen, for which the value shown in table 2 was obtained. The two values agree, within the experimental error, and the abnormally high value seems, therefore, to be correct. There appears, however, to be no obvious explanation.

In the rotational state (3,3) the dipole moment precesses about the axis of total angular momentum at a fairly small angle, and its projection on that axis is large. Its effect in producing interactions that may cause collisions is therefore almost a maximum, corresponding to the fact that the line (3,3) in pure ammonia is one of the broadest in the inversion spectrum. The collision diameter is 14·2 A., whereas the line (5,1) gives a collision diameter of only 8·7 A. in pure ammonia. This wide variation between the different lines seems unlikely to occur for collisions between ammonia and non-polar molecules, since the collision diameters are approximately the same as those given by the kinetic theory. For the same reason it is unlikely that there will be any significant difference between collisions which broaden the line and those which produce thermal relaxation (Bleaney and Penrose 1948), since a kinetic theory collision must surely be effective in producing thermal relaxation.

§ 6. COMPARISON WITH OTHER CENTIMETRE WAVE SPECTRA

There are as yet few data on the widths of lines in centimetre wave spectra of molecules other than ammonia. Accurate measurements have been made on the water-vapour line at 0·742 cm^{-1} for mixtures of water vapour and air by Autler and Becker (1946), and for pure water vapour by Townes and Merritt (1946). At a temperature of 45° C. the former workers find $\Delta\bar{\nu} = 0{\cdot}087 \pm 0{\cdot}001$ cm^{-1} for zero concentration of water vapour in the atmosphere, rising to $0{\cdot}107 \pm 0{\cdot}001$ cm^{-1} at a concentration of 50 gm/m^3. From these figures the value of the collision diameter for water-air is 5·4 A., which lies between the values for ammonia–oxygen and ammonia–nitrogen given in table 2. The diameter for water–water collisions is found to be 10·2 A., while the value calculated from a direct measurement by Townes and Merritt on pure water vapour at a pressure of 0·103 mm. Hg is 10·0 A. These values are comparable with those for the narrower lines in pure ammonia; this is satisfactory, since the water molecule

is an asymmetrical top, and the dipole moment will have a fairly small steady component in the two rotational levels between which the centimetre wave transition takes place.

The measurements of Beringer (1946) on the oxygen spectrum at $2\,cm^{-1}$ show that the line breadth constant at atmospheric pressure must lie between $0{\cdot}02$ and $0{\cdot}05\,cm^{-1}$. This gives for the collision diameter $2{\cdot}8$ to $4{\cdot}5$ A., whereas the kinetic theory diameter is $3{\cdot}6$ A. The collision diameter for oxygen–nitrogen was the same.

The main conclusion to be drawn from these results is that the collision diameter is only significantly greater than the kinetic theory diameter for encounters between permanent dipoles. For collisions between permanent dipoles and non-polar molecules the diameter is approximately the same as the kinetic theory diameter, and the measurements on the oxygen spectrum suggest that this is also true (as would be expected) for collisions between two non-electrically polar molecules.

APPENDIX

Calculation of the collision cross-section

Let $\mu_1=\mu(K^2/(J^2+J))^{\frac{1}{2}}$ be the mean dipole moment averaged over the rotation of the molecule absorbing radiation, and let μ_2 similarly be the mean dipole moment of an approaching molecule which causes an interruption of the absorption. Then the latter produces at a point whose coordinates are (r,θ) with respect to the direction of its mean dipole moment an electric field E whose magnitude is

$$|E|=\mu_2 r^{-3}(1+3\cos^2\theta)^{\frac{1}{2}}.$$

If the dipole μ_1 makes an angle ϕ with this field, the interaction energy is

$$\mu_1 E\cos\phi=\mu_1\mu_2 r^{-3}\cos\phi(1+3\cos^2\theta)^{\frac{1}{2}}.$$

The assumption is made that a "collision" occurs when this energy reaches a certain value W. Then the dipole μ_2 can be imagined as surrounded by a surface at which the interaction with the dipole μ_1 reaches the required value for a collision. Owing to the directional nature of the dipole this surface is not spherical, but has the form of a prolate spheroid whose major axis is twice as long as the two minor axes. To find the mean cross-section of the molecule it is sufficiently accurate to find the volume of this spheroid, and to use the cross-section of a sphere of equal volume. Since the interaction energy varies as $1/r^3$, this leads to a very simple mathematical procedure.

The equation for the surface of the spheroid is

$$r^3=\mu_1\mu_2\cos\phi(1+3\cos^2\theta)^{\frac{1}{2}}/W.$$

Hence its volume V is

$$\frac{4\pi}{3}\int_0^{\pi/2} r^3\sin\theta\,d\theta=\frac{4\pi}{3}\frac{\mu_1\mu_2\cos\phi}{W}\int_0^{\pi/2}(1+3\cos^2\theta)^{\frac{1}{2}}\sin\theta\,d\theta=\frac{4\pi}{3}.1{\cdot}38.\frac{\mu_1\mu_2\cos\phi}{W}$$

since the value of the integral is $1+(\ln(2+\sqrt{3}))/2\sqrt{3}=1{\cdot}38$.

This expression for the effective volume of an approaching molecule requires to be averaged over the mean dipole moments of all approaching molecules, and over the angle ϕ which the absorbing dipole μ_1 makes with the field of the

approaching dipole. The former averaging requires simply that μ_2 be replaced by $\overline{\mu_2}$, the average of the mean dipole moments of all the molecules present; the second averaging gives simply a factor of one-half. Hence

$$\overline{V} = \frac{2\pi}{3} \cdot 1{\cdot}38\,\mu_1\overline{\mu_2}/W.$$

Equating this volume to that of the equivalent sphere, one finds for the mean cross-section area of the approaching molecules

$$S_{12} = \pi(3\overline{V}/4\pi)^{\frac{2}{3}} = \pi(0{\cdot}69\mu_1\overline{\mu_2}/W)^{\frac{2}{3}} = 2{\cdot}45(\mu_1^2\overline{\mu_2^2}/W^2)^{\frac{1}{6}}.$$

ACKNOWLEDGMENTS

The authors are indebted to the Director of Physical Research, Admiralty, on whose behalf part of this work was carried out, for permission to publish. They also desire to express their acknowledgments to the Royal Commissioners for the Exhibition of 1851, whose award to one of them (R. P. Penrose) made the continuation of the work possible.

REFERENCES

Autler, S. H., and Becker, G. E., 1946, *Phys. Rev.*, **70**, 300.
Beringer, R., 1946, *Phys. Rev.*, **70**, 53.
Bleaney, B., and Penrose, R. P., 1947, *Proc. Roy. Soc.* A, **189**, 358; 1948, *Proc. Phys. Soc.*, **60**, 83.
Kennard, E. H., 1938, *The Kinetic Theory of Gases* (New York and London: McGraw-Hill Book Co.), p. 149.
Townes, C. H., and Merritt, F. R., 1946, *Phys. Rev.*, **70**, 558.

Efficiency of Counting Systems

By M. Blackman and J. L. Michiels
Imperial College, London

MS. received 10 *September* 1947; *read* 6 *February* 1948

ABSTRACT. A review is made of the derivation of formulae for the efficiency of counting systems, comprising in the general case a counter and amplifier, a scaling circuit and a recorder. In the case of recorders of constant resolving time no complete formula has been found in the literature, and this has been derived. A number of existing formulae are shown to be valid only for a particular type of variable recorder. A discussion is given of the use of the formulae in practical counting experiments.

§ 1

In various branches of nuclear and atomic physics it is necessary to measure the intensity of some kind of incoming radiation, the measurement taking the form of a count of the number of particles or photons arriving within a given time. For this some form of counting system is employed. In nuclear physics a counting system normally consists of a counter and amplifier feeding a scaling circuit (hereafter termed a "scaler") which in turn actuates a recorder. The counter may be an ionization chamber, Geiger-Müller tube etc., depending upon the type of

radiation to be detected. In all cases its function is to produce an electrical impulse upon the passage through it of a particle or photon of the incoming radiation. These impulses are then fed into the remainder of the system. In such a counting system the various components have finite resolving times. That is, after they have been actuated, a certain recovery time must elapse before they can again be actuated. Because of this, a certain fraction of the incoming radiation which arrives during the recovery time will not be detected. A large number of theoretical and semi-theoretical discussions occur in the literature in which the efficiency of counting systems is treated. In the simplest of all cases, in which the counting system consists of a counter, amplifier and a simple recorder, it is usual to assume an infinitely small resolving time for all parts of the system except the recorder which has a constant resolving time τ. The efficiency E of this system is then defined as the ratio of the counts recorded in a given time to the number of particles arriving in that time. It is rather astonishing to find, even in this simple case, that there are at least three different expressions for this efficiency E to be found in the literature, namely :—

$$(a)\quad E=1/(1+\mu\tau) \text{ (Ruark and Brammer 1937),} \qquad \ldots\ldots(1)$$

$$(b)\quad E=\exp(-\mu\tau) \text{ (Volz 1935, Schiff 1936),} \qquad \ldots\ldots(2)$$

$$(c)\quad E=\{1-\exp(-\mu\tau)\}/\mu\tau \text{ (Locher 1933).} \qquad \ldots\ldots(3)$$

In these formulae, μ is the average number of particles arriving per second, the distribution of particles being supposed to be a random one. There are also generalizations of (*a*) and (*b*) due to Ruark and Brammer (1937) and Alaoglu and Smith (1938) for cases where the finite resolving time of the counter is taken into account and where a scaler is introduced. In view of the different versions which are current, it seems worth while to examine the problem afresh in order to find which formula is correct, and how it should be generalized. *

§ 2

In discussing the efficiency of counting systems, it is essential to adopt a clear terminology for the impulses in various parts of the systems. In this paper, the incoming radiation will be said to consist of a stream of 'particles'. The electrical impulses produced by the counter will be referred to as 'pulses' and an event which actuates the recorder will be termed a 'count'. The efficiency E of the counting system is defined as the ratio of the number of particles counted in a given interval of time to the number of particles arriving at the counter within this time. In this connection it should be remarked that it is possible for some of the incoming particles not to actuate the counter for reasons other than that it is recovering from the effect of a previous particle. In a Geiger-Müller tube, irradiated by X rays, for example, only a certain fraction of the incoming photons will eject an electron from the wall of the counter and so be capable of producing a discharge within it. This cause of inefficiency is not dealt with in these calculations which are concerned solely with the effect of finite resolving times within the system. The incoming particles are assumed to be distributed at random and arriving at an average rate μ.

§ 3

Consider first a system in which no scaling circuit is employed. The recorder is assumed to have a constant resolving time τ and the counter and amplifier to have

* Results essentially in agreement with those of the present paper have recently been derived by Jost (1947) by a very elegant method. Jost's paper, however, emphasizes the mathematical rather than the physical aspect of the problem.

a resolving time negligibly small compared with this. Suppose that N counts occur in a certain experiment of duration T. After each count the recorder is inactive for a period τ. Let p be the average number of particles which occur within a period τ after a given particle. Then, on average, this number of particles is lost at each count. Hence the total number of particles arriving during the experiment is $N+pN$ and the efficiency of the system is

$$E=N/(N+pN)=1/(1+p). \qquad \ldots\ldots(4)$$

It is now necessary to calculate p. It is well known that for particles distributed at random, the probability $W(m,t)$ of m particles arriving in an interval t is

$$W(m,t)=e^{-\mu\tau}(\mu\tau)^m/m! \qquad \ldots\ldots(5)$$

Consider a time interval τ commencing immediately after the arrival of a particle. The above formula is still valid since there is no correlation between the time of arrival of particles. Hence the probability of m further particles following the first particle within the resolving time τ is $W(m,\tau)$. In such a case the number of particles lost is m. Hence p the average number lost in time τ is

$$p=\sum_{m=1}^{\infty} mW(m,\tau)$$

$$=e^{-\mu\tau}.\,\mu\tau\sum_{1}^{\infty}(\mu\tau)^{m-1}/(m-1)!=\mu\tau. \qquad \ldots\ldots(6)$$

The efficiency is therefore given by

$$E=1/(1+\mu\tau). \qquad \ldots\ldots(7)$$

This formula is one of three quoted in the introduction and has been derived in various ways in the literature, for example by Ruark and Brammer (1937). The formula (2) has been derived by Schiff (1936) who employs the following argument for a recorder with a constant resolving time. The probability of no particle arriving within a time τ after a given particle is $e^{-\mu\tau}$ (see equation (5) for $m=0$). This is then put equal to the probability of counting the next particle which in turn is put equal to the efficiency. This expression gives the probability that no loss will occur, but it is not immediately related to the magnitude of the probable loss which does occur. At very small counting rates, the number of particles which arrive in an interval τ will be either 0 or 1 to a very good approximation, and in this limit the efficiency $(1-\mu\tau)$ is correct. In all other cases it bears no relation to the true efficiency. It will be seen later, however, that this formula is correct for another type of recorder in which the resolving time is not constant. Formula (3) has been given by Locher (1933). He finds

$$p=\mu\tau-1+e^{-\mu\tau}. \qquad \ldots\ldots(8)$$

He takes a series of intervals of duration τ at random, and assumes that if there is only one particle within such an interval it is counted. If there are two, one is lost and so on. With this assumption

$$p=\sum_{m=2}^{\infty}(m-1)\,W(m,\tau),$$

which can readily be seen to lead to (8) if τ is identified with the resolving time of the recorder. He then considers an "experiment" of duration τ in which the average number of particles arriving is $\mu\tau$ and hence deduces the average fraction lost and

the efficiency, obtaining equation (3). This result differs from the correct result given by (7), particularly for very low counting rates in which region the loss given by (3) is half that given by the correct formula. The error in Locher's argument is that he has ignored the fact that the intervals τ, having been defined as times during which the recorder is inactive, start only after a particle has been recorded. Consequently if, as in Locher's calculation, such periods are chosen at random, the first particle, which actuates the recorder, will not always occur at the beginning of the period and hence the effective resolving time assumed in the calculation is in general less than τ. Evidently, if the counting rate is very low, the probability of the first particle occurring anywhere within a period τ will be constant and the effective resolving time assumed will be $\tau/2$. If the counting rate is very high, the probability of the first particle occurring very near the beginning of the period will increase and Locher's formula should then tend to the correct one, which in fact it does.

§ 4

Consider now a counting system in which a scaler of scale-factor n is used. The scaler and all components of the system previous to the recorder are again assumed to have resolving times negligibly small compared with that of the recorder which has the constant value τ. As before, an experiment is considered in which N counts are obtained in an interval T. Let p again be the average number of particles lost during an interval τ after a count. The number of particles recorded is nN and the total number arriving is $nN+pN$. The efficiency is therefore given by

$$E=nN/(nN+pN)=n/(n+p)=1/(1+p/n). \qquad \ldots\ldots(9)$$

In this procedure the number of pulses ($<n$) left in the scaler at the end of the experiment has been ignored. This is a sufficiently good approximation when N is very large compared with n. In this connection it should be noted that the formula derived for the efficiency will in any case be valid only if the number of counts is large. This follows from the fact that the number of particles lost after a count is obtained by taking a statistical average over the possible cases which can occur in a large number of counts. If only a small number of counts are taken, the loss will show fluctuations about its mean value p which may be quite large. In experimental work, it is usual to count a number of particles sufficiently large for the statistical fluctuation in this number to be small. If, however, a scaler of large scale-factor is employed, the number of counts may not be sufficiently large for the fluctuation in p, the average number of pulses lost per count to be small. In applying the expressions for the efficiency of the system, it is therefore necessary to consider both the value of p and its fluctuations.

It is now necessary to calculate p in this case. Suppose that m particles arrive at the system within a time τ after a count. If m is less than n, these are stored in the scaler and none are lost. If m is equal to or greater than n but less than $2n$, then n are lost. In general, if $qn>m\geqslant(q-1)n$, then $(q-1)n$ are lost. Hence the expression for p is

$$\begin{aligned} p=n\{&W(n,\tau)+W(n+1,\tau)+\ldots+W(2n-1,\tau)\} \\ &+2n\{W(2n,\tau)+W(2n+1,\tau)+\ldots+W(3n-1,\tau)\} \\ &+\ldots. \end{aligned}$$

A function $L(n, \tau)$ can be defined by

$$L(n,\tau) = \{W(n,\tau) + W(n+1,\tau) + \ldots \text{ to } \infty\}$$
$$= e^{-\mu\tau}\{(\mu\tau)^n/n! + (\mu\tau)^{n+1}/(n+1)! + \ldots\}. \qquad \ldots\ldots(10)$$

In terms of this function

$$p = n\{L(n,\tau) - L(2n,\tau)\} + 2n\{L(2n,\tau) - L(3n,\tau)\} + \ldots$$
$$= n\{L(n,\tau) + L(2n,\tau) + \ldots\}. \qquad \ldots\ldots(11)$$

The function $L(n, \tau)$ can be expressed in terms of tabulated functions (Molina 1942).

It is evident that if $\mu\tau/n$ is small compared with unity, the series $L(n, \tau)$ will converge very rapidly. In the case where $\mu\tau/n$ is very small, an approximate expression can be obtained from (11),

$$p = ne^{-\mu\tau}\{(\mu\tau)^n/n!\}$$

and
$$E = 1 - e^{-\mu\tau}\{(\mu\tau)^n/n!\} \qquad \mu\tau/n \ll 1. \qquad \ldots\ldots(12)$$

The expression (11) does not, as far as we know, appear to have been given in the literature. Lewis (1937) has given an expression for the loss in the above type of system in the region of small losses. His formula gives the fractional loss in the form of an expression which is equivalent to the function $L(n, \tau)$ instead of $p/(p+n)$. This is a valid approximation. A somewhat similar expression has been given by Alaoglu and Smith (1938) who introduced the function $L(n, \tau)$. They use it in conjunction with a different formation of the efficiency of the system. They calculate the probability that the time t in which a group of n particles follow a given particle (that is, after a count) is less than τ. This probability they find to be the function $L(n, \tau)$. The probability $G(n, \tau) = 1 - L(n, \tau)$ of the time t being greater than τ, they call the efficiency of the system. This is not a satisfactory definition of efficiency for a recorder of constant resolving time, but the formal result applies to a certain type of recorder of variable resolving time. This type of recorder is discussed in § 6.

§ 5

The system considered can now be further generalized to include the case in which the counter and amplifier have a constant resolving time σ. The recorder has a constant resolving time τ. It is assumed that the resolving time of the first stage of the scaler, if not negligible, can be incorporated in that of the counter and amplifier and that those of the succeeding stages of the scaler can be neglected. In such a system, not all the particles arriving at the counter will produce pulses which are fed into the scaler and thence to the recorder. Owing to the effect of the recovery time of the counter, the pulses which reach the recorder are no longer randomly distributed in time. Alaoglu and Smith (1938) have introduced a probability function $L^*(m, t, \sigma)$ giving the probability that the time of arrival of a group of m pulses, after a given pulse, is less than a specified time t. This function can be calculated in the following way. It is first necessary to obtain the probability that a pulse will occur at a time between t and $t + dt$ after a given pulse, there being no intervening pulses. The probability that no particle will arrive within an interval t is, for a random distribution, equal to $e^{-\mu t}$. Now the probability that no pulse will occur in a period t following a pulse is the same as the probability that no particle will arrive in the interval between σ and t, since no pulse can occur

between 0 and σ, and for any time after σ an incoming particle will produce a pulse. That is, the probability that no pulse will occur in the interval t is $e^{-\mu(t-\sigma)}$. But the probability of a particle arriving in the subsequent interval dt is μdt. Hence the probability $Q^*(t,\sigma)\,dt$ of a pulse occurring in the interval between t and $t+dt$ after a given pulse, with no intervening pulse is

$$\left.\begin{aligned} Q^*(t,\sigma)\,dt &= e^{-\mu(t-\sigma)}\mu dt, \quad t \geqslant \sigma \\ &= 0 \qquad\qquad\quad t < \sigma \end{aligned}\right\}. \qquad \ldots\ldots(13)$$

The function $L^*(1,t,\sigma)$ which expresses the probability that the time interval between a pulse and its successor is less than t is therefore given by

$$L^*(1,t,\sigma) = \int_0^t Q^*(t,\sigma)\,dt. \qquad \ldots\ldots(14)$$

In order to calculate $L^*(m+1,t,\sigma)$ from $L^*(m,t,\sigma)$, one can proceed as follows (Alaoglu and Smith 1938). Consider a pulse occurring at a time between x and $x+dx$ after a given pulse ($x<t$), there being no intervening pulses. The probability of obtaining m pulses in a time less than $(t-x)$ is by definition $L^*(m,t-x,\sigma)$. Hence the probability of a pulse occurring at x followed by m pulses within the succeeding interval $(t-x)$ is

$$Q^*(x,\sigma)\,dx\,L^*(m,t-x,\sigma).$$

Therefore $$L^*(m+1,t,\sigma) = \int_0^{t-m\sigma} Q^*(x,\sigma)\,L^*(m,t-x,\sigma)\,dx.$$

The upper limit in the integral is determined by the fact that it must be possible to fit at least m pulses of duration σ in the interval $(t-x)$; alternatively this can be stated in the form

$$L^*(m,t,\sigma) = 0 \text{ if } t < m\sigma.$$

It has been shown by Alaoglu and Smith, using a proof by induction, that the function L^* is given by

$$\begin{aligned} L^*(m,t,\sigma) &= \Gamma\{\mu(t-m\sigma), m\}/(m-1)! \\ &= e^{-\mu(t-m\sigma)}\left\{\frac{[\mu(t-m\sigma)]^m}{m!} + \frac{[\mu(t-m\sigma)]^{m+1}}{(m+1)!} + \ldots\right\}. \end{aligned} \qquad \ldots\ldots(15)$$

Here, as before, $\Gamma(x,m)$ is the incomplete gamma function.

Now $L^*(m,t,\sigma)$ can also be considered as the probability of m or more than m pulses occurring within the interval t following a pulse. There is, however, an upper limit M to the number of pulses which can possibly occur within a given interval owing to the finite recovery time σ following each pulse. This limit is given by $t = M\sigma + f$, $f < \sigma$. When this limit is exceeded, $L^*(m,t,\sigma)$ is zero.

Let $W^*(m,t,\sigma)$ be the probability that exactly m pulses occur in an interval t following a given pulse. Then $L^*(m,t,\sigma)$ can be written as

$$L^*(m,t,\sigma) = W^*(m,t,\sigma) + W^*(m+1,t,\sigma) + \ldots + W^*(M,t,\sigma).$$

That is, the probability of m or more pulses occurring within an interval t is the sum of the probabilities of exactly m, $m+1$ etc. pulses arriving within the interval t. Hence

$$W^*(m,t,\sigma) = L^*(m,t,\sigma) - L^*(m+1,t,\sigma). \qquad \ldots\ldots(16)$$

If m is greater than M, $L^*(m,t,\sigma)$, and thus $W^*(m,t,\sigma)$ is zero.

Let p^* be the average number of pulses lost by the recorder in an interval τ following a count. Then

$$p^* = n\{W^*(n,\tau,\sigma) + W^*(n+1,\tau,\sigma) + \ldots + W^*(2n-1,\tau,\sigma)\} + 2n\{W^*(2n,\tau,\sigma) + W^*(2n+1,\tau,\rho) + \ldots + W^*(3n-1,\tau,\sigma)\} + \ldots$$

This can be written

$$p^* = n\{L^*(n,\tau,\sigma) - L^*(2n,\tau,\sigma)\} + 2n\{L^*(2n,\tau,\sigma) - L^*(3n,\tau,\sigma)\} + \ldots$$

that is
$$p^* = n\{L^*(n,\tau,\sigma) + L^*(2n,\tau,\sigma) + \ldots + L^*(qn,\tau,\sigma)\}, \quad \ldots\ldots(17)$$

where $qn < M < (q+1)n$.

If, as before, N counts are recorded, the number of pulses leaving the amplifier is $nN + p^*N$. From (6) the average number of particles arriving during a pulse is $(1+\mu\sigma)$. Hence the number of particles arriving during the experiment is $N(n+p^*)(1+\mu\sigma)$. The efficiency of the counting system is therefore given by

$$E = nN/N(n+p^*)(1+\mu\sigma) = 1/(1+p^*/n)(1+\mu\sigma). \quad \ldots\ldots(18)$$

This formula is seen to reduce to those given for the simpler cases if first σ is put equal to zero (cf. (10) and (15)) and then n is put equal to unity. Also if τ is less than $n\sigma$, p^* is zero and the only loss is that due to the counter and amplifier. This should be so, since in this case the recorder has already recovered before another group of n pulses can have arrived from the amplifier. If $\mu(\tau - n\sigma)/n$ is much smaller than one, the expression for the efficiency can be reduced to the approximate form

$$E = (1 - e^{-\mu(\tau - n\sigma)}[\mu(\tau - n\sigma)]^n/n!)/(1+\mu\sigma). \quad \ldots\ldots(19)$$

In figure (1), the fraction of pulses counted $1/(1+p^*/n)$ has been plotted as a function of $\mu(\tau - n\sigma)/n$ for various scale-factors. In computing values of p^*, use has been made of tables by Molina (1942). If σ is zero, these curves give the efficiency of the system directly. In the general case, the value obtained from the curves must be divided by $(1+\mu\sigma)$ to give the efficiency.

Feather (1943, 1945) has also, by a different method, derived expressions for the statistical distribution in time of pulses from a counter, the results being generalized to include the case when the incident stream of particles has a non-random distribution. He has applied his formulae to the calculation of the

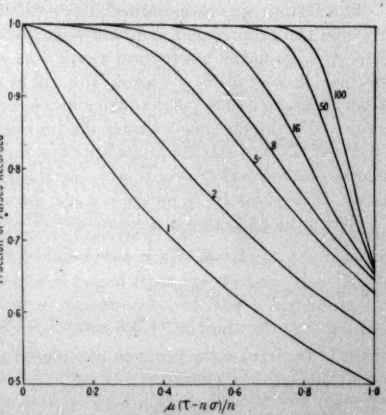

Figure 1. Fraction of pulses recorded as a function of the product of $((\tau - n\sigma)/n)$, the effective resolving time, and μ the average rate of entry of particles into the counting system, for various values of n, the scale factor of the system.

losses in a system consisting of a counter and recorder, but has not, however, extended them to take into account the effect of a scaler.

§ 6

It remains to consider the situation which arises when the resolving time of the recorder is not constant. The efficiency must then depend upon the way in which the resolving time varies, that is, upon the mechanism of the recorder. One case which arises in practice is that in which the arrival of a pulse within the resolving time re-excites the recorder without, however, recording that pulse. That is, the recovery time begins again after any such pulse. This type of recorder is termed by Ruark and Brammer (1937) a type I recorder and that with a constant resolving time a type II recorder. This is a convenient form of nomenclature. A common example of a type I recorder is the so-called Cenco counter.

Consider now a simple counting system consisting of a counter and amplifier feeding directly a type I recorder of natural resolving time τ. The resolving time of the counter and amplifier are assumed negligibly small.

Consider a stream of pulses entering the recorder. If the interval between two successive pulses is less than τ, the recorder is re-excited and the pulse lost. If the interval is greater than τ, the pulse is recorded whether the previous one has been recorded or not. Hence the probability of recording a pulse is equal to the probability, $e^{-\mu\tau}$, that the interval between two successive pulses is greater than τ. This will be equal to the fraction of pulses recorded and consequently the efficiency is

$$E = e^{-\mu\tau}. \qquad \ldots\ldots(20)$$

This argument is due to Ruark and Brammer (1937) who attribute it to Volz (1935) and Schiff (1936).

The argument can be immediately extended to the general counting system in which the counter and amplifier have a constant resolving time σ and feed a scaler of scale-factor n actuating a type I recorder. Here the recorder registers only groups of n pulses. A group of n will be recorded only if the last pulse of the group occurs in a time greater than τ measured from the last pulse of the previous group. This is the case whether the previous group has been recorded or not. That is, if $G^*(n, \tau, \sigma)$ is the probability that the group of n pulses after a given pulse occupies an interval greater than τ, the fraction of pulses recorded is $G^*(n, \tau, \sigma)$. As before, every pulse is, on the average, associated with $(1+\mu\sigma)$ particles.

Hence the efficiency is

$$E = nG^*(n, \tau, \sigma)/n(1+\mu\sigma) = G^*(n, \tau, \sigma)/(1+\mu\sigma). \qquad \ldots\ldots(21)$$

The function G^* is given by

$$G^*(n, \tau, \sigma) = 1 - L^*(n, \tau, \sigma),$$

where $L^*(n, -\tau, \sigma)$ is the function considered above. That is

$$G^*(n, \tau, \sigma) = e^{-\mu(\tau - n\sigma)}\{1 + \mu(\tau - n\sigma) + \ldots + [\mu(\tau - n\sigma)]^{n-1}/(n-1)!\}. \qquad \ldots\ldots(22)$$

Equation (21) applies equally well in the case where σ is zero.

The above formula for E was given by Ruark and Brammer (1937) for $n = 1$, and by Alaoglu and Smith (1938) in the general case. Ruark and Brammer explicitly derive their formula for a recorder of constant resolving time, that is, a

type II recorder, for which it certainly does not apply. Alaoglu and Smith refer to a "recorder which will not respond unless the interval between the count and its predecessor is greater than τ". This statement applies equally well to type I and type II recorders. Their calculated efficiency, however, is valid only for a type I recorder.

§ 7

An experimental verification of the expression given by Ruark and Brammer has been published by Lifschutz and Duffendack (1938). This expression is

$$E = e^{-\mu(\tau-\sigma)}/(1+\mu\sigma).$$

What was actually done experimentally, however, was to verify the formula in a case for which it was not derived. In view of the confusion which seems to exist, it is as well to quote the remarks of Ruark and Brammer (1937, p. 324) : "If τ_r is greater than τ_i and the recorder of a kind which cannot be re-excited while it is in action (type II), the efficiency of the apparatus is $f'/f = (\exp[-f(\tau_r - \tau_i)])/(1+f\tau_i)$". Here f'/f is our E, $\tau_r \equiv \tau$, $\tau_i \equiv \sigma$ and $f \equiv \mu$.

In the experimental paper, the formula was interpreted as being applicable to recorders which are re-excited during recovery (type I). This is shown by the following quotation (p. 717) : "In order to test the theory, the circuits used must satisfy the assumptions made in deriving the formulae. In referring to equation 1 (*a*) it is clear that with $\tau > \sigma$ and $\sigma \to 0$ equation 1 (*a*) becomes $n_1 = n_0 \exp(-n_0\tau)$. In other words the recorder circuit used to test equation 1 (*a*) must be a type I recorder". Equation 1 (*a*) referred to is Ruark and Brammer's formula given above. A slightly different notation is used : $n_1/n_0 \equiv E$ and $n_0 \equiv \mu$.

The experimental work was carried out employing a type I recorder (a Cenco counter) and very satisfactory agreement was obtained with the theoretical formula. As shown above, the formula in fact should apply only to a type I recorder.

§ 8

In practice, experimental conditions are usually adjusted so that the counting rate is sufficiently low for losses to be small. In these circumstances the efficiencies of both type I and type II recorders are the same. In figure 2 the region of low counting losses is plotted in some detail. The ordinates in this diagram are values of $100p^*/(p^*+n)$, that is, the percentage loss of pulses in the recorder. The abscissae are rates of entry of particles into the system. Logarithmic scales are used on both axes. Curves are drawn for various combinations of selected values of the scale-factor n and the effective resolving time $(\tau - n\sigma)$.

It can be seen that for a given value of n, the curves for different values of $(\tau - n\sigma)$ are similar in shape, and can be obtained from one another by a simple displacement in abscissae. This is a consequence of the employment of logarithmic scales and the fact that the losses are functions of the product $\mu(\tau - n\sigma)$.

The losses due to the counter and amplifier can be obtained from the formula (18) for $x = 0$. The total loss is the sum of those due to counter and recorder separately in the region of small losses. Inspection of figure 2 shows that the curves are all very nearly straight lines whose slopes increase with the scale-factor. The logarithmic plot emphasizes this effect rather strongly. The steepness of the curves for moderately large scale-factors does, however, indicate that where there is uncertainty in the value of $(\tau - n\sigma)$, any attempt to make a correction

for appreciable counting losses would fail. Further, any fluctuation in the rate of entry of particles will tend to introduce large errors into any such correction. For large scale-factors therefore, it would appear to be desirable to arrange working conditions so as to make recorder losses negligible (e.g. less than 0·1%). That is, the maximum counting rate employed should be less than that corresponding to the point on figure 2 at which the relevant curve cuts the axis. These precautions are not essential for scale-factors of 1 or 2, and here it may be possible to make small corrections if the parameters of the system are sufficiently accurately known.

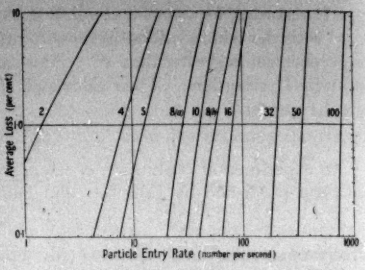

Figure 2. Logarithmic plot of the percentage loss of pulses as a function of the average rate of entry of particles into the counting system. The curves are drawn for various scale factors indicated in the diagram, with a value of 0·1 sec. for $(\tau - n\sigma)$, the effective recording time of the recorder. The two curves 8 (*a*), 8 (*b*), with values of $(\tau - n\sigma)$ equal to 0·1 and 0·05 sec. respectively, and scale factor 8, show that a change in $(\tau - n\sigma)$ results in a parallel displacement of the curve.

In addition to fixing a safe counting rate, it is also necessary to fix a minimum total counting time. This must be sufficiently large to ensure both a small fluctuation in the total number of particles entering the system and a sufficient number of counts.

APPENDIX

The two tables given below summarize, in a form suitable for practical application, the data concerning the performance of various kinds of counting-devices. The authors are greatly indebted to Dr. C. E. Wynn-Williams for suggesting the form in which these tables should be compiled.

Table 1

The table gives critical mean rates of entry of particles per second for scalers of various scale factors associated with recorders of various resolving times. For entry rates less than these, the losses due to finite resolving time of the recorder are less than 0·1% and can usually be ignored in comparison with the losses due to the counter or other device at the input of the counting system and the statistical fluctuations. As the particle entry-rate is increased above these values, the fraction lost increases so rapidly, particularly for high scale factors, that it is unwise to attempt to apply a loss-correction. The working rate should therefore be kept well below the critical rate. The critical entry-rate for other values of the scale factor can be determined sufficiently accurately by interpolation on a graph of the values given in the table. Note that the critical rates are inversely proportional to the resolving times.

Recorder resolving time (seconds)	Scale factor							
	2	4	8	10	16	32	64	100
1/5	0·25	2	10	15	32	86	210	360
1/10	0·50	4	20	30	64	172	420	710
1/25	1·2	10	50	75	160	430	1000	1800
1/50	2·3	21	100	150	320	860	2100	3600
1/75	3·5	32	150	225	480	1300	3200	5300
1/100	4·5	42	200	300	640	1700	4200	7100

Table 2

The table gives maximum permissible mean rates of entry of particles per second into a scale-of-one device for different values of the mean fraction of particles lost and for various resolving times of the device. In brackets are also given the minimum time of counting (in seconds) at these maximum rates for the statistical fluctuation in the count not to exceed the instrumental losses. The table shows that it is difficult to work to an accuracy much better than about 0·5% unless long counting times are employed.

Type of device	Resolving time (sec.)	Percentage of count lost by scale-of-one device						
		0·1	0·2	0·5	1	2	5	10
Input stage of hard valve scalers limit about 10^{-7} sec.	10^{-6}	1000 (1000)	2000 (125)	5000 (8)	10,000 (1)	At higher entry-rates an adequate count is secured in less than 1 sec. but special timing devices are required.		
	2×10^{-6}		1000 (250)	2500 (16)	5000 (2)			
	5×10^{-6}		400 (625)	1000 (40)	2000 (5)			
Input stage of thyratron scalers limit about 10^{-5} sec.	10^{-5}			500 (80)	1000 (10)	2000 (2)		
	2×10^{-5}			250 (160)	500 (20)	1000 (3)		
Geiger-Müller counters limit about 5×10^{-5} sec.	5×10^{-5}			100 (400)	200 (50)	400 (7)		
	10^{-4}			50 (800)	100 (100)	200 (13)		
	2×10^{-4}	At lower entry-rates counting time must exceed 1000 sec. (about 16 min.) otherwise statistical fluctuations may exceed instrumental losses.			50 (200)	100 (26)	260 (2)	
	5×10^{-4}				20 (500)	40 (64)	100 (4)	
	10^{-3}				10 (1000)	20 (130)	50 (8)	
	2×10^{-3}					10 (260)	25 (17)	55 (2)
Modified ratchet uniselectors limit about $1\cdot3\times10^{-2}$ sec.	5×10^{-3}					4 (640)	10 (40)	22 (5)
	10^{-2}						5 (80)	11 (10)
	2×10^{-2}						2·5 (160)	5 (20)
Modified telephone call counters limit about 4×10^{-2} sec.	5×10^{-2}						1 (400)	2 (50)
	10^{-1}						0·5 (800)	1 (100)
		10^6	$2\cdot5\times10^5$	4×10^4	10^4	$2\cdot5\times10^3$	4×10^2	10^2
		Minimum desirable count.						

REFERENCES

ALAOGLU, L., and SMITH, N. M., Jr., 1938, *Phys. Rev.*, **53**, 832.

FEATHER, N., 1943, *Proc. Camb. Phil. Soc.*, **39**, 84 ; 1945, *Atomic Energy declassified report*, Br. 555.

JOST, R., 1947, *Helv. Phys. Acta*, **20**, 173.

LEWIS, W. B., 1937, *Proc. Camb. Phil. Soc.*, **33**, 549.

LIFSCHUTZ, H., and DUFFENDACK, O. S., 1938, *Phys. Rev.*, **54**, 714.

LOCHER, G. L., 1933, *J. Franklin Inst.*, **216**, 553.

MOLINA, E. C., 1942, *Tables of Poisson's Exponential Limits* (New York : Van Nostrand).

RUARK, A., and BRAMMER, F. E., 1937, *Phys. Rev.*, **52**, 322.

SCHIFF, L. I., 1936, *Phys. Rev.*, **50**, 88.

VOLZ, H., 1935, *Z. Phys.*, **93**, 539.

DISCUSSION

Dr. Denis Taylor. The computation of counting losses is important both from the point of view of arranging the conditions of the experiment so that the losses may be reasonably small and also so that the true counting rate may be calculated from the observed counting rate. The analysis given by the authors allows this computation to be made for most of the practical cases which arise in nuclear physics. One case which is of some importance, and which seems to have escaped mention, is the case when the resolving time of the scaler itself must be allowed for. In the simple case when only the resolving time of the input stage of the scaler is important, it is presumed that the analysis given by the authors applies, but that σ, the resolving time of the detector (ion-chamber or Geiger-Müller counter), must now include the resolving time of the input stage of the scaler. Other cases can arise which are more complicated. A typical example is a pulse analyser which has been designed recently at T.R.E. This consists of a pre-sorting stage, a " scale of two ", a " ring of five " and an electro-mechanical register. The resolving time of the input circuit was 100 μsec., that of the second stage (i.e. after the " scale of two ") was 2 msec., and that of the electro-mechanical register was 0·1 sec. The second stage had a high resolving time because cold cathode valves were used for the " ring of five " to economize in power supplies (30 such chains are used in the complete equipment). In a case like this, the finite resolving time of the second stage of the scaler must be allowed for. Have the authors considered extending their analysis to cover this case ? We have made some vain efforts to do this at T.R.E., but eventually obtained the information we required by connecting a Geiger-Müller counter to two counting chains, one of the type described above and a second one in which the resolving time of the second stage of the scaler was sufficiently small to have a negligible effect on the counting rate. The counting losses for the second chain could be computed and, therefore, a comparison of the observed counting rates for the two chains allowed the counting losses for the former to be determined.

Another case of considerable importance is the computation of counting losses in the counting of particles from pulsed sources. The use of particle accelerators which give short pulses of particles, usually of a few seconds' duration, repeated from a few to a few hundred times a second, as, for example, with a synchrotron, frequency modulated cyclotron, etc., is likely to increase very much during the next few years, and the importance of being able to compute the counting losses in such cases cannot be overestimated. Have the authors given any attention to this problem ?

Finally, I should like to call the authors' attention to a further paper on the computation of counting losses which may have escaped their attention. This is Hole, *Arkiv Mat. Astr. Fys.*, 1946, **33 A**, No. 11.

Dr. G. Burniston Brown. I should like to ask whether any experimental confirmation of the formula arrived at by the authors has been attempted ? Physicists must not be prevented, by the fact that amplifiers etc. were mentioned, from noticing that this is a mathematical paper whose conclusion is nothing more than the consequence of assumptions made at the start and during its progress. The result would have been just as correct for elephants as for amplifiers, provided we assume that if n stimuli are given to an elephant, a fraction p of them produce a " kick ", etc. Anyone making use of the theory of probability should bear in mind that it is the most obscure of all theories, and that Leibniz, the late Lord Keynes, and Dr. Harold Jeffreys all agree in admitting that they cannot define the concept of probability.

Why should modern physicists be excused from the venerable custom of *calibrating* their instruments ? Arguments from the theory of probability can never take the place of experiment.

Authors' reply. In reply to Dr. Taylor, we have not so far considered the extension of our calculations to the case where the second (and further) stages of the scaler have appreciable resolving times, but we think it probable that the methods used are capable of this extension. The problem of counting losses from pulsed sources is of a different type. It is, for instance, obvious that when the resolving time of the counting system is longer than the duration of a pulse only one particle can be counted per pulse. It is therefore necessary to modify even the most elementary formulae for counting losses. We are considering this

calculation in view of its general interest and are indebted to Dr. Taylor for calling our attention to this case.

With regard to the point raised by Dr. Brown, we have drawn attention in our paper to an experimental verification of one of the formulae discussed, namely the work of Lifschutz and Duffendack. It would be possible in principle to calibrate a counting system empirically if standard sources of suitable types were available in every laboratory. In some cases, however, this calibration would involve considerable difficulties, e.g. the efficiency of a Geiger counter for γ rays varies with the energy of the γ ray, and a whole range of standard γ-ray sources would be necessary.

Certain Aspects of the Mechanism of Spark Discharge

By L. B. LOEB
University of California, Berkeley, California, U.S.A.

MS. received 12 *November* 1947 ; *read* 23 *April* 1947

Sparks are a class of transient occurrence in which a given existing conduction current in a gas suddenly and irreversibly changes to a current of higher magnitude, operating more efficiently by different mechanisms under conditions which rendered the previous lower current unstable (Loeb 1939, p. 408).

Certain general features of the threshold for spark breakdown, common to all mechanisms but differing in detail for the different processes, will first be presented. The more complete equation for sparks in one regime will then be used to describe the *general* properties which may be expected.

Spark breakdown in general requires fields of sufficient intensity to ensure that two processes, a primary and a secondary, are activated. The primary process is one which causes electron multiplication in the field by electron impact to reach such values that after traversing the gap of length δ the $\exp(\alpha\delta)$, or $\exp\left(\int_0^{\delta} \alpha\, dx\right)$, electrons created by one initiating electron are adequate. This is the *primary*, and predominating, process, with α, Townsend's first coefficient, representing the number of new electrons created per centimetre of path in the field direction by an electron (Loeb 1939, Chapter VIII and p. 369). Alone this process leads to field intensified currents which are proportional to the initial ionization present. The progeny of $\exp(\alpha\delta)$ electrons produced by one electron in crossing a gap is called an *electron avalanche*. The average distance traversed in the field direction to produce an ionizing act is then $1/\alpha$. The function of the secondary process is to furnish secondary electrons to replace the initiating electrons and to maintain or build up a discharge. It can take one of two possible forms (Loeb 1939, Chapter IX, pp. 377 and 403):

(*a*) A secondary process *at the cathode* leading to Townsend's type of breakdown, (i) by impact on the cathode of positive ions that liberate electrons; (ii) by photoelectric effect on the cathode of photons excited in avalanche formation; (iii) by action of metastable atoms on the cathode (limited to certain gases).

(*b*) A secondary process *in the gas* that leads to sparks by the streamer mechanism, i.e. photo-ionization.

To explain the behaviour observed, the liberation of electrons at the cathode by positive ion impact on the cathode is indicated as the most likely process. As Townsend has shown, this leads to a current

$$i = i_0[e^{\alpha\delta}/(1-\gamma e^{\alpha\delta})], \qquad \ldots\ldots(1)$$

when expressed in a simplified form (Thomson 1911, Townsend 1915).

When $\gamma e^{\alpha\delta}=1$ this expression becomes indeterminate mathematically. However, as Holst and Oosterhuis (1923) long ago indicated, $\gamma e^{\alpha\delta}=1$ has another interpretation. This becomes clear if one reasons as follows :—

(*a*) For $\gamma e^{\alpha\delta}<1$ the discharge follows equation (1) and the current is not self-sustaining; i.e. it depends on i_0 and ceases with i_0. It yields merely a field intensification of i_0.

(*b*) For $\gamma e^{\alpha\delta}=1$, on the average, each avalanche of $e^{\alpha\delta}$ electrons by the primary process is multiplied by a value of γ large enough to give one new secondary electron when the $e^{\alpha\delta}$ positive ions return to the cathode. Thus one initiating electron at the cathode is able to maintain its succession indefinitely. This is then the *threshold* for a self-sustaining discharge independent of i_0. It marks the sparking threshold.

(*c*) For $\gamma e^{\alpha\delta}>1$ the ionization of successive avalanches is cumulative and more ions are created than start. As electrons have a mobility 100 times that of positive ions, positive space charges accumulate in the gap near the cathode. These produce a very efficient secondary mechanism that allows of the discharge continuing as glow or arc at a higher current. The space charge will grow and the spark will materialize the faster the greater the amount by which $\gamma e^{\alpha\delta}$ exceeds unity.

The mechanism of such a spark then proceeds as follows. An avalanche crosses a gap of length δ at a speed of the order of 10^7 cm/sec. in sparking fields at atmospheric pressure in a time T_e. Arrived at the anode the $e^{\alpha\delta}$ electrons are absorbed and the positive ions, of which 50% are created within the last $1/\alpha$ cm., start back to the cathode. Arrived there in a time T_+, roughly 100 times as great as T_e, these ions yield $\gamma e^{\alpha\delta}$ electrons which start a new chain of avalanches, again taking a time T_e and T_+. At this time $\gamma^2 e^{2\alpha\delta}$ electrons begin a third sequence. When, as a result of η trips, the positive ion space-charge of $\gamma^{\eta-1}e^{\eta\alpha\delta}$ positive ions produces a self-sustaining field for a glow, the spark is complete. Its time of formation, or *formative time* lag is

$$T_f = (T_+ + T_e)\eta. \qquad \ldots\ldots(2)$$

If the secondary mechanism had involved photoelectric action at the cathode, the time T_f would not have involved T_+, for the photons reach the cathode without delay. Thus T_f would be merely ηT_e. What evidence there is, however, indicates that photoelectric emission at the cathode is largely ineffective because of the wide geometrical dispersion of photons, for it will be rare indeed that a photon is liberated near the origin of the initial avalanche. Thus, in general, the γ mechanism is responsible for sparks and the value of T_f is given by equation (2).

The question has been studied by Schade (1937) using equation (2) with Townsend's mechanism active at lower pressures and has been verified as being in accord with observation. For gaps in Ne and H_2, T_f has a value of 10^{-1} to 5×10^{-5}, and has been shown to depend on T_+ and η.

Near sparking in air at atmospheric pressure the quantity $\alpha\delta$ has the relatively small value of about 17. Furthermore, ionization is a chance phenomenon and

it is not certain that every electron will ionize each time that it has traversed $1/\alpha$ cm. There is also nothing to prevent electrons by accident from ionizing twice in a distance $1/\alpha$, even though on the average it does so only once. Thus the individual avalanches will yield an electron multiplication which fluctuates above and below $e^{\alpha\delta}$ in a purely random fashion, i.e. if $\alpha\delta$ varies by ± 1 the avalanche may vary by a factor of e or $1/e$. Again electron liberation by positive ion impact is purely a chance phenomenon with an *average* value γ under any set of conditions. Thus the quantity $(\gamma e^{\alpha\delta})_1$, as yielded by *individual* avalanches will fluctuate about the *average* value $\gamma e^{\alpha\delta}$ in considerable measure.

Accordingly even though the potentials are chosen so that the average $\gamma e^{\alpha\delta} = 1$, individual avalanches occurring will yield other values of the product. Thus if V_s is the potential corresponding to $\gamma e^{\alpha\delta} = 1$, an occasional fortunate avalanche will build up a spark at a potential V less than V_s, and at a potential V greater than V_s an occasional unlucky avalanche will not give the necessary perpetuating electrons and there will be no spark. It is clear then that in individual avalanches sparks occur at values of V below and fail at values above the value of V fixed by $\gamma e^{\alpha\delta} = 1$, through the relations of α/p to X/p.

If now there be applied to a gap a potential V with initial value less than V_s and the fraction of P_s initiating electrons which give avalanches resulting in the formation of a spark be plotted against V, the curve A of figure 1 would be observed. This curve is the integral from $V=0$ to $V=V$ of the fluctuations of the value of $(\gamma e^{\alpha\delta})_1$ for individual electrons about the average value for which $\gamma e^{\alpha\delta} = 1$ and $V = V_s$. Thus differentiation of the curve A of figure 1 gives the chance of a variation of $(\gamma e^{\alpha\delta})_1$ in a sequence of avalanches about the mean value as expressed in terms of V. The differential curve is shown in figure 1, curve B. If the derivative gives a symmetrical distribution, V_s will be the maximum value, and in the integrated curve it will represent the point of inflection at $P_s = 0{\cdot}5$. With values of $\alpha\delta \sim 20$ this is nearly true.

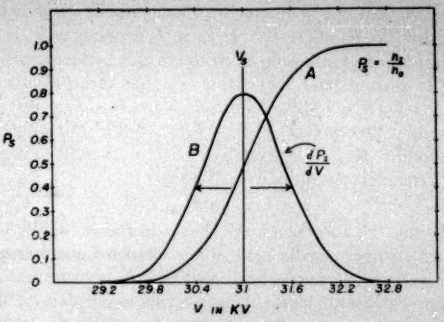

Figure 1.

(*A*) Probability of sparking P_s plotted against applied potential in kilovolts.

(*B*) Derivative of sparking probability against voltage indicating the distribution of sparking events about the threshold plotted in terms of voltage.

Curves of the type of curve A in figure 1 will be obtained if the fraction of individual avalanches leading to a spark are observed and plotted against V. By measuring time lags using varying but known ultraviolet illumination of the cathode and different potentials V, Wilson (1936) obtained curves analogous to figure 1 curve A and used these to evaluate V_s. The width of curve B of figure 1 depends on the magnitude of the fluctuations in γ and $e^{\alpha\delta}$ and on the number of sequences η to build up the space charge. While any one of the steps in the sequence of η successive events could interrupt the spark, it is probably only the

early ones where not many positive ions are present that are most critical. Thus at V_s where η is large the curve may be somewhat broader than at higher values of V. The width of curves calculated for Schade's data by Hertz (1937) using fluctuations of γ only lie around 1%. Actual widths may be much larger as fluctuations in $e^{\alpha\delta}$ are larger than in γ. No experiments using individual electrons have been made.

Whether the distribution be wide or narrow, it is important to know that this distribution is always present and that sparks will sometimes occur below a potential V_s based on *average* values and will sometimes fail above. The value of V_s, unless the curves are very distorted, will be that at which $P_s = 0{\cdot}5$. Thus, to be certain of the sparking threshold experimentally, a $(P_s - V)$ curve must be obtained from individual avalanches and V_s chosen as above. It should further be noted that T_f varies with V about V_s and that properly to interpret formative time lag studies these lags must be established relative to V_s.

When a potential V is applied, as in sparking potential measurements, it is observed that even at V_s, or above, the spark does not occur at once. The time between applications of V and the appearance of the spark is called the *time lag of sparking*. We shall call it the *observational* time lag, T_0. In 1925 Laue and Zuber showed it to be composed of a statistical time element T_s, depending on the chance of arrival of an initiating electron and the chance that this electron caused a spark, and of a formative time element, T_f which is the time taken for the spark to grow, i.e. $T_0 = T_s + T_f$. In turn, T_s depends on $T_a = 1/n_0$, the average time between liberation of initiating electrons, which is the reciprocal of the number of electrons per second, and the chance P_s that these events will give a spark. That is, $T_s = T_a/P_s = 1/n_0 P_s$. Thus $T_0 = 1/n_0 P_s + T_f$. But by equation (2) T_f on Townsend's theory is $T_f = (T_+ + T_e)\eta$. With gap length δ, field strength X, and ion mobility K_+, T_+ is given by $T_+ = \delta/K_+X$, and T_e is given by $T_e = \delta/K_eX$, where K_e is the electron mobility. Thus

$$T_f = (\delta/K_+X + \delta/K_eX)\eta. \qquad \ldots\ldots(3)$$

It must be also recognized that η decreases rapidly with increase of V above V_s as α/p changes rapidly with X/p. Thus for overvoltages $(V - V_s)/V_s$ which are not very large η approaches unity and T_f approaches $T_f = \delta/K_+X + \delta/K_eX$. Hence for Townsend sparks we can write

$$T_0 = 1/n_0 P_s + (\delta/K_+X + \delta/K_eX)\eta. \qquad \ldots\ldots(4)$$

If now $T_a = 1/n_0$ be made small by large n_0, and if P_s and η be made unity by using a sufficiently large overvoltage $(V - V_s)/V_s$, then T_0 becomes sensibly

$$T_0 = \delta/K_+X, \qquad \ldots\ldots(5)$$

since $K_e \gg K_+$. For rare sparks below V_s observed with large n_0, the value of T_f will be slightly larger than that of equation (3) due to the decrease in XK_+. The conditions given by equation (5) are those under which most experimental studies of both V_s and T_0 have been made—except those whose purpose it was to study T_s. This means that true values of V_s have rarely been observed, but with large n_0 and the narrow statistical range of V about V_s the values are not seriously wrong. It also means that by using large values of $(V - V_s)/V_s$ the quantity T_0 observed has been the *characteristic* value of $T_f = \delta/K_+X$ for the Townsend mechanism. Observations of T_0 near V_s would give exceptionally long and non-informative values of T_f. It may be noted here, however, that values of n_0 must not be too high, since various workers (see Loeb 1939, pp. 386, 448–9 Loeb and Meek 1941,

pp. 32, 172) have shown that a heavy n_0 with much field intensification can cause a space charge distortion that lowers the sparking potential or of itself leads to a spark.

It may also be noted that n_0 can be determined, even at breakdown fields, by measuring the value of the photoelectric current at two potentials below cumulative ionization and evaluating the constants in J. J. Thomson's equation for photo-ionization currents in gases (Loeb 1939, Chapter VII, Sect. 3, p. 310 and equation, p. 313; Johnson 1948). This enables the value of the current from the cathode, n_0, to be calculated for purposes of study.

It must finally be concluded that to evaluate V_s one must observe T_0 under the following conditions : T_f must be kept much less than T_s and T_s is increased by a controlled n_0 which must be sufficiently small. Then sensibly $T_0 = 1/n_0 P_s$ and by observing T_0 for different values of V about V_s, P_s can be evaluated as a function of V and by differentiation the peak value will locate V_s.

Practically all studies except Schade's have so far been made on sparks passing by the streamer mechanism and not by the Townsend mechanism. It is thus essential to see how the considerations above apply to the streamer.

The streamer starts with an avalanche of $e^{\alpha x}$ electrons where x is nearly equal to the gap length δ at V_s. If $e^{\alpha x}$ is great enough, electrons of the avalanche passing to the anode leave behind an adequate positive space charge to initiate a streamer. Meek (1940) and Raether (1941) independently assessed this as occurring when the space charge tip field X' equalled the imposed field X. The density is determined by $e^{\alpha x}$ and the radius of the avalanche head ρ produced by diffusion of charges during advance. The diffusion is restricted in scope so that $e^{\alpha x}$ and the pressure primarily determine the density of charge. To enable a streamer to advance, the space charge tip field plus the imposed sparking field must be great enough over an adequate small volume element $\Delta x'$ deep and solid angular aperture $\pi/2$, so that a photoelectron produced in this volume in advancing to the tip can extend the space charge by making $\exp\left(\int_{\Delta x'}^{0} \alpha' \, dx\right) = \exp\left(\int_{0}^{x} \alpha \, dx\right)$. Here α is the value in the undistorted field X where the electron avalanche travels a distance x to start a streamer and α' is the much higher value in the vector field $X+X'$ between $\Delta x'$ and ρ. If several photoelectrons can be produced in $\Delta x'$ the volume can be smaller or X' less. The production of photoelectrons in a distance $\Delta x'$ depends on the density of photon production in the avalanche tip and on the absorption coefficient μ of the gas for wavelengths which produce photo-ionization, as well as on $\Delta x'$. Photon production varies directly with the number of electrons $e^{\alpha x}$ and can be set as $fe^{\alpha x}$, where f is a nearly constant multiplier which may be greater or less than unity, but probably less. It should be noted in passing that the density of the molecules in these mechanisms will play a very critical rôle since ρ and μ are pressure dependent, so that pressure will be an important parameter, apart from the rôle of X/p.

It is now clear that while the avalanche formation is common to both Townsend and streamer mechanisms so that only one initiating electron is needed in both, the probability γ of the Townsend mechanism is replaced by the chance of photo-ionization in restricted volumes $\Delta x'$ in the streamer mechanism which might be lumped in a factor ϵ. Thus streamer progress likewise depends on $fe^{\alpha x}$ for photon production, multiplied by a probability factor ϵ akin to γ, which is now complex and involves μ, $\Delta x'$ and the criterion of Meek and Raether. Thus one may set the

sparking threshold by streamer mechanism as $\epsilon f e^{\alpha x}=1$ for streamer propagation. It is at once clear that with streamers the statistical time lag T_s will, by its dependence upon n_0 and P_s, play the same rôle as with Townsend's mechanism except that now P_s will depend on other factors lumped in ϵ such as μ, $\Delta x'$, and pressure. T_f will show differences with streamer formation. As, however, the condition $\epsilon f e^{\alpha x}=1$ is radically different from $\gamma e^{\alpha\delta}=1$, the analogy is largely formal.

It was the early discovery, 1923–27, that the value of T_f for higher pressure sparks is much less than is possible on Townsend's picture (Loeb 1939, pp. 32–33, Loeb and Meek 1941, p. 449) that, together with the help of corona studies (Loeb 1939, pp. 433, 440–450) and cloud track pictures (Raether 1935, Flegler and Raether, 1936, 1938, 1940), led to the streamer theory. In this case, the time scales indicated that T_f depended primarily on the time of electron crossing, T_e. For once the electron travels a distance x, to near the anode, the streamer forms and progresses back to the cathode with a velocity several times that of the electron. This high speed of the streamer advance results from two conditions. The enhanced tip fields of positive and negative space charges in the streamer increase electron velocities, and photo-ionization in advance of both space charges leads to an increased velocity, because photons move with the velocity of light. These increases are of the order of the ratio of the square roots of the enhanced tip fields X' to the applied field X, from $\sqrt{2}$ to $\sqrt{10}$ according to Raether's computations (Raether 1940), and of the order of the ratio $(\Delta x'+\rho)/\Delta x'$, where ρ is the radius of the avalanche tip and $\Delta x'$ the width of the sensitive part. These factors can increase the velocity of the streamer by a possible factor of 2 to 10 fold above that of the avalanche advance. They depend critically on pressure and on applied field strength. Accordingly for streamer advance $T_f=x/XK_e+x/bXK_e$, where b is the multiplication factor $\sqrt{(X'/X)}\,.\,(\Delta x'+\rho)/\Delta x'$. The final stage of spark breakdown after the streamer has crossed the gap is very short, for it is determined by the velocity of re-ionization of an ionized streamer channel by the steep potential wave proceeding up the streamer channel from the instant of junction of streamer head and cathode. The velocities, as shown by Snoddy, Dietrich and Beams (1937), by Allibone and Meek (1938 a, b), and by Schonland *et al.* (1934, 1935, 1937) are of the order of 10^{10} cm/sec. The time lag of the return stroke is T_p. Thus for a streamer,

$$T_f=x/XK_e+x/bXK_e+T_p. \qquad \ldots\ldots(6)$$

Since $b>1$ and T_p is very small, one has sensibly $T_f=x/XK_e$. Here again with increased potential, i.e. overvoltages, b is greatly increased. Furthermore, with overvoltages streamers form in mid-gap at a distance x from the cathode much less than δ as α increases rapidly with V. Such streamers have been observed with Kerr cell shutters by Dunnington (1931) and White (1934) in overcharged gaps. Hence, T_f will decrease with $(V-V_s)/V_s$ very rapidly and continuously in the proportion x/δ.

Thus with the streamer mechanism statistical and formative time lags appear. There is, however, one difference apart from the fact that the value of T_f for streamers is much less than that for Townsend's discharge $(\delta/X_sK_e \ll \delta/X_sK_+)$. This is that T_f has a fairly sharply defined *upper* limit, $\delta/XK_e+\delta/bXK_e+T_p$ for streamers, and *decreases* rapidly with V above V_s; in a Townsend discharge on the other hand T_f is *indefinitely great at* V_s and, for slight increases in V above V_s, decreases rapidly towards a *minimum* value δ/XK_+, the characteristic value.

In a further development of the streamer theory of spark discharge, one of the critical data yet to be determined is the condition for the change over from a Townsend to a streamer mechanism (Loeb and Meek 1941, pp. 49, 71, 76). From a knowledge of this much information on streamer propagation could be derived; it is hoped that some of this lacking information may be provided by the researches now being carried out by Meek and Craggs. It is indispensable for sparking theory, however, that the transition be observed as a function of pressure and gap length. The only way in which this can be done today is by means of a careful study of time lag, thus establishing the value of P_s and the position of V_s from a knowledge of T_0 and n_0. Then by increasing n_0 so that $1/n_0 P_s \ll T_f$ one can observe T_0 when $T_0 = T_f$, and so determine T_f as a function of $(V - V_s)/V_s$. Then from the value of T_f observed in relation to δ/XK_+ and δ/XK_e the operative mechanism is clear. This must be done with δ constant for different pressures p and with p constant with different gap lengths δ.

That such transitions will not occur at a single value of the product $p\delta$ for a given gas is indicated by the fact that unlike the Townsend mechanism, neither the streamer mechanism nor a pure space charge breakdown follow Paschen's law (Loeb 1939, p. 410, Loeb and Meek 1941, pp. 8, 46, 72, 81, Varney *et al.* 1935) which states that $V_s = f(p\delta)$. Physically interpreted, the failure of Paschen's law and the principle of similitude with streamers follows from the fact that a Paschen's law breakdown depends on the *number of ions created in the gap*, while the streamer mechanism depends on *ion concentrations*. The failure of Paschen's law has not been observed at ordinary pressures, as the present day accuracy of measurements of V_s with the peculiar mathematical character of the sparking equations, either Townsend or streamer, are not adequate. Thus characteristic data in the transition region are urgently called for. It is essential, however, at this point to study the character of the departure from Paschen's law in streamer formation as shown by Meek's theory alone in order to proceed further.* Meek's equation may be written as

$$f\left(\frac{V_s}{p\delta}\right)(p\delta) + \ln f\left(\frac{V_s}{p\delta}\right) = 14{\cdot}46 \ln \frac{V_s}{p\delta} - \ln p\delta + \ln \delta, \qquad \ldots\ldots(7)$$

where $V_s = X_s'\delta$ for a uniform gap. Here it is seen that V_s is a function of $p\delta$ as Paschen's law predicts up to the last term $\ln \delta$. The Meek equation again takes the form,

$$\alpha\delta + \ln \alpha/p = 14{\cdot}46 + \ln X/p + \tfrac{1}{2} \ln \delta/p \qquad \ldots\ldots(8)$$

with

$$\frac{\alpha}{p} = f\left(\frac{X}{p}\right) = f\left(\frac{X\delta}{p\delta}\right) = f\left(\frac{V}{p\delta}\right). \qquad \ldots\ldots(9)$$

The form of the function $f(X/p)$ for lower values of X/p in the streamer region is either

$$\alpha/p = A \exp(BX/p), \quad \text{or} \quad \alpha/p = A((X/p) + B)^2, \qquad \ldots\ldots(10)$$

the latter holding for the higher range of X/p. What is done in solution of Meek's equation for V_s by trial and error is as follows: For a given p and δ a value of X/p is chosen and the corresponding value of α/p obtained from the curve for $\alpha/p = f(X/p)$. The values are then inserted into equation (8) and the relative

* It must be noted, however, that apart from the concentration effects in Meek's equation the value of μ is also independently pressure dependent so that the pressure dependence may be much greater than calculated above.

magnitudes of the two sides of the equation observed. A value of X/p is next chosen to make the other side of the equation larger. Thus by successive approximations, or by the use of Simpson's rule, a value of X/p can be obtained to satisfy the equation. This value at X/p is X_s/p and yields V_s from $X_s\delta = V_s$. It is at once seen from equation (8) that if one calculates V_s for δ constant and p varying or for p constant and δ varying, different values of V_s will be obtained for the same product $p\delta$. This is, of course, because if δ is increased and p decreased, $\ln(\delta/p)$ increases, while for the same $p\delta$ if p is increased and δ decreased, $\ln(\delta/p)$ decreases. The changes however, are small because of the logarithmic function. Therefore, for any one value of $p\delta$ there will be two values of X_s/p and hence of V_s depending on whether the value $p\delta$ is reached by decreasing δ and increasing p or vice versa. The difference between the two values will be the greater the greater the range of variation in δ and p, but it will be relatively small in its effect on V_s, for V_s depends on α (equations (9) and (10)) which varies rapidly with X_s, while compensating changes in δ/p in equation (8) would have to be very great since they alter the left-hand side by only $\ln\delta/p$. Experimentally, therefore, it would be only for larger ranges of variation that deviations from Paschen's law would be detected experimentally.

Failure to recognize this fact has in the past led to misunderstanding. When Meek first studied his equation he put it to test by calculating V_s as a function of $p\delta$, using the value of δ at 760 mm. Hg initially and decreasing p. In consequence, he obtained a V_s curve in which $\ln(\delta/p)$ increased as p decreased. This required a larger value on the right-hand side of the equation with the result that he plotted a (V_s, $p\delta$) curve which was high. He noted a marked departure of the (V_s, $p\delta$) curve from the experimentally observed values of Whitehead, at $p\sim200$ and *assumed* that this was the point at which Townsend's mechanism changed to streamer mechanism (Meek 1940, Loeb and Meek 1940, 1941, p. 49). Roughly Dunnington's spark photographs with Kerr cell shutter also indicated a similar value as the point of appearance of mid-gap streamers in an overcharged gap (Dunnington 1931). Actually the appearance of mid-gap streamers depends not on the product $p\delta$ alone but also on p and/or δ. Later L. H. Fisher (1946) computed V_s as a function of $p\delta$ from Meek's equation using constant p and varying δ. He thus found a curve which started at the same δ as Meek's curve for atmospheric pressure $p=760$, but which began to fall below Meek's curve as $p\delta$ decreased. This curve appeared not to depart seriously from the observed

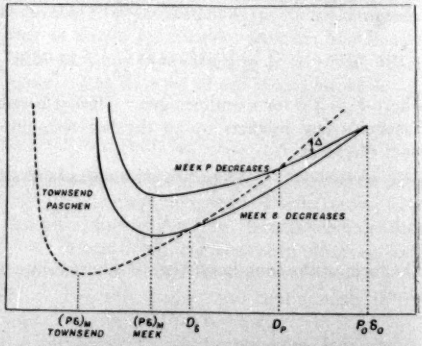

Figure 2. Represents the sparking potential plotted against product $p\delta$ for Townsend's equation and Meek's equation. Note, that starting from a value $p_0\delta_0$, Meek's equation has two values, depending on whether δ is kept constant and p decreases or p is constant and δ decreases (solid curves). The dotted curve is Townsend's equation, following Paschen's law.

data taken from Schumann's book (1923). These data are, however, variable in their reliability, and it is necessary to take into account the method by which they were obtained. Presumably, they were obtained with decreasing δ to conform to Fisher's calculation. Thus Fisher noted no departure from observed curves, even at values where streamers must have given way to Townsend's mechanism. This precipitated a rather complicated situation whose interpretation may be clarified by reference to the curve shown in exaggerated form in figure 2. The chosen point of departure for calculation is $p_0\delta_0$. D_p is the point at which the Townsend mechanism and Paschen's law take control for p decreasing. Meek's theory no longer holds. D_s is the point at which Townsend's discharge and Paschen's law take control for δ decreasing. Meek's law no longer holds. The dotted curve is the Townsend curve with a γ following Paschen's law and represents the observed curve up to streamer formation at the two different transition points.

The minima $(p\delta)_m$ for Meek's two curves fall at the same value of $p\delta$ in both cases as they reflect merely the point where $\alpha/p=f(X/p)$ passes through its point of inflection. The value of $(p\delta)_m$ will be lower for Townsend's theory as the quantity γ is increasing markedly with X/p in this region of values of $p\delta$ and will certainly be more effective than the *photo-ionization in the gas*.

With this understanding of what may be expected, one can say that the differences in the calculations of Meek and Fisher indicate the character of the departure from Paschen's law. None of the data which they use are of any value in this region of $p\delta$ to indicate this and thus accurately to confirm theory.

Fortunately, recent results of Skilling and Brenner (1941), and particularly of Howell (1939) and of Trump, Stafford and Cloud (1941) with a large Van de Graaff generator have unequivocally shown the failure of Paschen's law. Mr. C. G. Miller has kindly recalculated and plotted some of their data to show this. Curves of V_s plotted against p for constant $p\delta$ should be horizontal if Paschen's law holds. The curves of Trump, Stafford and Cloud (figure 3) show that with increasing $p\delta$ and increasing V_s there is a marked and increasing slope to the curves. This linear departure is difficult to correlate with the Meek equations (7) and (8) above. If, however, we calculate δ from the data of these curves and plot V_s against δ for constant $p\delta$, we obtain the curves shown in figure 4. Here it is seen that with $p\delta$ constant and increasing δ, V_s increases with δ. This is just what equation

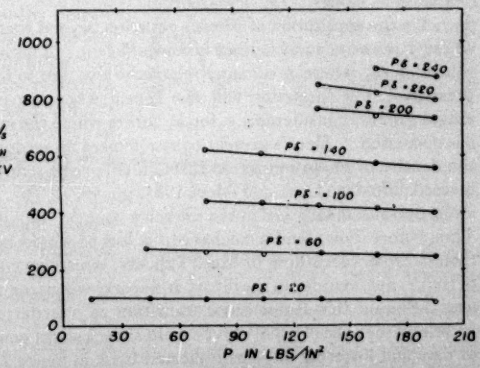

Figure 3. Curves of Trump, Stafford and Cloud showing sparking potential in kv. plotted against pressure in pounds per square inch for constant values of $p\delta$. If Paschen's law held strictly, the indicated curves for $p\delta$ would be straight lines parallel to the axis of abscissae.

(7) indicates.* Here, then, we have our first indication of the deviation from Paschen's law predicted by the streamer theory, and it is observed in regions where p and δ are varied over large ranges of values.

It should be added that in Howell's data with very high p and high V_s, above 400 kv. from the gassy surface used, the appearance of field emission of electrons from the cathode could lead to more efficient breakdown mechanisms and lowered V_s. All Howell's data at above $p\delta = 35$ have such fields and since these are too large they distorted his gap and possibly lowered V_s. The character of the curves reported and the consistency of the data with those of Trump (below field emission) indicate, however, no departure ascribable to field emission in this region. This is doubtless due to Howell's experimental care and choice of results. The findings thus add some urgently needed confirmation to the streamer theory and the use of Meek's equation.

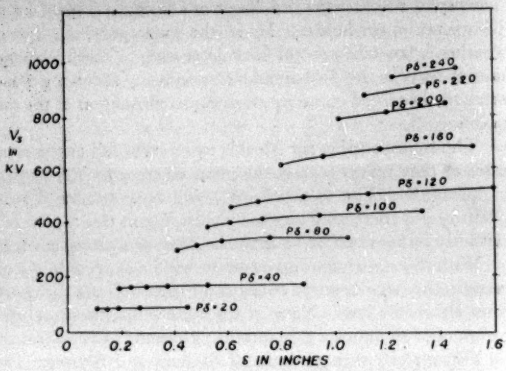

Figure 4. Curves of Trump, Stafford and Cloud as calculated by C. G. Miller with sparking potentials in kilovolts against gap length in inches for various value of $p\delta$ for comparison with Meek's equation. Meek's equation will give analogous curves, but the variation will be distinctly less than observed as indicated by later consideration of Meek's sparking condition.

There is, however, a definite limitation to be expected in the application of Meek's equation beyond that occurring at low $p\delta$ and p where Townsend's mechanism is more efficient. This applies particularly to large values of $p\delta$, where p remains relatively low, i.e. to long sparks at atmospheric pressure. The limitation will also appear when somewhat lower pressures and longer gaps are considered, i.e. for V_s curves where the initial value of δ is large and p is decreased. Meek's present equation takes no account of the effect of lowering the density of photo-ionization through either the reduction of α at low X/p or increased diffusion (Loeb and Meek 1941, pp. 49, 71, 76). Further, both density of ionization and absorption in the sensitive zone $\Delta x'$ rapidly decrease as p decreases. Thus before Townsend's mechanism at low $p\delta$ would normally be more effective than streamers according to Meek's theory, streamers could cease to form because of factors not included in the theory and sparks will occur on the Townsend mechanism. Should this factor cause transition as p is decreased or at low p as δ is increased then the (V_s, $p\delta$) curve would show a slight increase in V_s with scattering of data and lowering of $p\delta$ as indicated by Δ in figure 2. Experimental data are as yet too crude to show this.

* Recent calculation (Miller and Loeb 1947) indicates that in fact Meek's theory predicts the sort of departure observed. It is, however, smaller than the observed departure (1% as against 14%). This is because the pressure sensitive effect present in ϵ is not included in Meek's equation to its full extent.

It is much more important, however, to consider what happens from this circumstance in very long gaps and thus also in lightning discharge (Loeb and Meek 1941, p. 79). If either Townsend's or Meek's equation be studied it is clear that except for slowly varying logarithmic terms, the chief variation is given by $f(V_s/p\delta)p\delta$ which is nearly constant. It yields $V_s/p\delta = f^{-1}(1/p\delta)$. This indicates a hyperbolic type of decrease of $V_s/p\delta$ with increase in $p\delta$. Hence, since $V_s/\delta = X_s$, the sparking field strength, one obtains $X_s/p = f^{-1}(1/p\delta)$. Thus, the important sparking parameter X_s/p should decrease approximately hyperbolically with increasing $p\delta$. In fact, from what data we have (taken mostly at atmospheric pressure with increasing δ), up to $p\delta = 10^4$ mm. × cm., this relation is observed as seen in figure 5. Carrying the data up to 3×10^4 mm. × cm. from the data of Howell and of Trump, Stafford and Cloud, the value X_s/p decreases nearly linearly, within observational error, as p increases to 40 atmospheres. Correlation of the data with $p\delta$, as required by the argument above, is not very good but there is a similar trend with large scatter. In this region, however, Paschen's law deviations are extreme and the scatter with $p\delta$ is caused by the failure of this law in keeping with Meek's equation. For lower pressure regions where Paschen's law deviations are not serious, the value of X_s/p is 33 with $X_s = 25\,000$ v/cm. At 40 atmospheres, the value X_s/p is 21 with $X_s = 650\,000$ v/cm.

The cause for this behaviour is seen if one writes the Meek positive space charge field equation in the exponential form,

$$\frac{X}{p} = \frac{A(\alpha/p)\exp\{(\alpha/p)p\delta\}}{(\delta/p)^{\frac{1}{2}}}. \qquad \ldots\ldots(11)$$

This indicates that, neglecting the non-exponential factors, the equality, and thus the condition for sparking, is maintained if the value of α/p decreases in proportion to increase of $p\delta$. Thus, by increasing δ at p constant as in the conventional studies, α/p can decrease, and hence the value of X_s/p needed can decrease and yet give a spark by Meek's equation. This, interpreted physically, means that with increasing gap length owing to cumulative ionization the number of ions formed per centimetre of length to give the space charge field can decrease and yet yield a spark in a gap of length δ. It is true that α/p as a function of X/p increases rapidly with X/p, so that the decrease in α is not linear with δ in the exponential term. None the less, it is there. Hence, as δ or $p\delta$ increases, $1/\alpha$, the mean distance for ionization in the avalanche, increases. This will have no significance on Meek's theory as formulated. However, as stated, this theory regards *only the space charge field* which, from the slow increase of channel radius due to diffusion, should always be adequate under equation (8). It does not regard the density of photo-ionization (Loeb and Meek 1941, pp. 49, 71, 76). As,

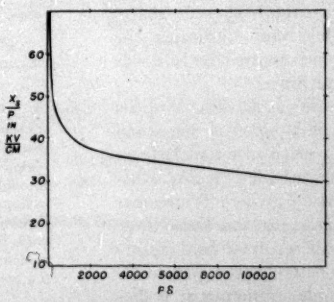

Figure 5. Sparking field strength divided by pressure in kv/cm. plotted against the product $p\delta$ in millimetres times centimetres obtained from various sparking data below the critical gap length δ_0, indicating the decline in sparking field strength with increasing gap length at constant pressure owing to increased ionization.

however, $1/\alpha$ increases, that important density decreases. Thus the photo-ionization in advance of a streamer tip can fall below the critical value if δ is increased at constant pressure. This will prohibit the spark occurring at the values of X predicted by Meek's theory. On the other hand, if path length, and pressure or gas density, i.e. $p\delta$, increase with increasing p, Meek's theory should apply.

It is thus expected to be that in long sparks and in lightning at atmospheric pressure at some critical path length δ_0, Meek's equation should break down (Loeb and Meek 1941, p. 79). What this critical length is we do not know, but Edwards and Smee (1938), with alternating 60 c/s. potentials, observe that at gap lengths between 15 and 20 cm. at 760 mm. Hg the (V_s, $p\delta$) curves pass through a point of inflection, increase and are different in trend for higher values of V. This is what might be expected on the anticipated breakdown of Meek's theory. For an avalanche crossing a gap greater than some critical length δ_0 can no longer produce the photo-ionization necessary, and sparks will not pass until X_s is increased to a point where $1/\alpha$ has the values required to give the needed photo-ionization. Thus, beyond δ_0, X_s/p cannot decrease further and X_s will remain at a constant value X_{δ_0} corresponding to the limiting field at δ_0. Sparking will then occur only at or above a field X_{δ_0}, and V_s will be given by $X_{\delta_0}\delta$ above δ_0, irrespective of δ. The sparking potential curve given by Meek's equation will follow the full curve of figure 6. At δ_0 Meek's equation no longer holds and sparks will pass at a constant field X_{δ_0} such that $V_s = X_{\delta_0}\delta$, which increases linearly with δ as shown by the straight dashed line which is extrapolated back through the origin; the actual transition will not be sharp. This, then, indicates the trend observed by Edwards and Smee.

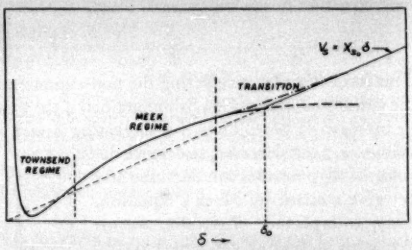

Figure 6. Sparking potential plotting against gap length at constant pressure, the full curve indicating the actual sparking potentials to be expected through the whole régime. Note the transition at δ_0, which extrapolates back through the origin. The dot-dash curve between the two indicates the probable shape of observed sparking potential in the transition region. The Townsend régime holds for the shorter gaps, Meek's equation for the intermediate, and at longer gap lengths the sparking potential is a constant field strength times the gap length.

What actually happens in this region is that when $V_s = X_{\delta_0}\delta$ an avalanche from the cathode proceeds a distance δ_0 where its streamer starts; at the same time, with resultant field distortion, its electrons pass to the anode, initiating at a distance δ_0 or less a new streamer directed towards the cathode, and so on. At path lengths $\delta_0 \sim 20$ cm. the streamer channel will be some 0·2 to 0·5 cm. in radius, which facilitates ionization according to Raether's calculations. The statistical fluctuations in photo-ionization will smooth the range of critical potentials, fields and path lengths about δ_0 so that the transition is not sharp. The sparking potential curves should then appear as in figure 6.

Considerations of the effect of pressure indicate that δ_0 will be a critical function of pressure and rough calculations by Loeb (Loeb and Meek 1941, p. 81) placed δ_0 at 3·8 cm. at half an atmosphere. L. H. Fisher (1947), in Loeb's laboratory,

attempted to observe this in a carefully controlled chamber during the War. His investigation failed owing to field distortion and corona just below the critical gap length. It is urgent that this study be undertaken in some laboratory where high potentials and adequately large spark discharge chambers are available. In carrying out the study extraordinary care must be taken to avoid field distortion. The urgency of the problem will be understood when it is realized that it is the condition that determines flash-over for long static sparks and establishes lightning discharge breakdown fields.

REFERENCES

Allibone, T. E., and Meek, J. M., 1938, *Proc. Roy. Soc.* A, **166**, 97, **169**, 246.

Dunnington, F. G., 1931, *Phys. Rev.*, **38**, 1535.

Edwards, F. S., and Smee J. F., 1938, *J. Instn. Elect. Engrs.*, **82**, 659.

Fisher, L. H., 1946, *Phys. Rev.*, **69**, 530 ; 1947, *Ibid.*, **72**, 423.

Flegler, E., and Raether, H., 1936, *Z. Phys.*, **99**, 625, **103**, 315 ; 1938, *Ibid.*, **110**, 611; 1940, *Arch. Elektrotech.*, **34**, 49.

Hertz, G., 1937, *Z. Phys.*, **106**, 102.

Holst, G., and Oosterhuis, 1923, *Phil. Mag.*, **46**, 1117.

Howell, H. H., 1939, *Trans. Amer. Inst. Elect. Engrs.*, **58**, 193.

Johnson, Gerald W., 1948, " Electron Multiplication in Divergent Fields ", *Phys. Rev.*, **73** (in press).

Laue, M., 1925, *Ann. Phys., Lpz.*, **76**, 261.

Loeb, L. B., 1939, *Fundamental Processes of Electrical Discharge in Gases* (New York : John Wiley and Sons).

Loeb, L. B., and Meek, J. M., 1940, *J. Appl. Phys.*, **11**, 438, 459 ; 1941, *The Mechanism of the Electric Spark* (Stanford Press, U.S.A.).

Meek, J. M., 1940, *Phys. Rev.*, **57**, 722.

Miller, C. G., and Loeb, L. B., 1948, *Phys. Rev.*, **73**, 84.

Raether, H., 1935, *Z. Phys.*, **94**, 567 ; 1940, *Arch. Elektrotech.*, **34**, 49 ; 1941, *Z. Phys.*, **117**, 386, 524.

Schade, R., 1937, *Z. Phys.*, **104**, 487.

Schonland, B. F. J., *et al.*, 1934, *Proc. Roy. Soc.* A, **143**, 654 ; 1935, *Ibid.*, **152**, 595 ; 1937, *Ibid.*, **162**, 175 ; 1938, *Ibid.*, **164**, 132.

Schumann, W. O., 1923, *Elektrische Durchbruchfeldstarke von Gasen* (Springer).

Skilling, H. H., and Brenner, W. C., 1941, *Trans. Amer. Inst. Elect. Engrs.*, **60**, 112.

Snoddy, L. B., Dietrich, J. R., and Beams, J. W., 1937, *Phys. Rev.*, **52**, 739.

Thomson, J. J., 1911, *Conduction of Electricity Through Gases*, 2nd Ed. (Cambridge : University Press), p. 490.

Townsend, J. S., 1915, *Electricity in Gases* (Oxford : University Press), p. 331.

Trump, J. G., Stafford, F. J., and Cloud, R. W., 1941, *Trans. Amer. Inst. Elect. Engrs.*, **60**, 132.

Varney, R. N., Loeb, L. B., White, H. J., and Posin, D. Q., 1935, *Phys. Rev.*, **48**, 818.

White, H. J., 1934, *Phys. Rev.*, **46**, 99.

Wilson, R. R., 1936, *Phys. Rev.*, **49**, 1082.

Zuber, K., 1925, *Ann. Phys., Lpz.*, **76**, 231.

The Electron Trap Mechanism of Luminescence in Sulphide and Silicate Phosphors

By G. F. J. GARLICK and A. F. GIBSON
Department of Physics, University of Birmingham

MS. received 30 *August* 1947; *read* 12 *March* 1948

ABSTRACT. Phosphorescence and thermoluminescence emission from photoconducting impurity activated phosphors have been satisfactorily explained by the storage of electrons, freed from luminescence centres or other atoms of the solid, in metastable energy levels known as electron traps. Electrons escaping from these traps give rise to emission when they recombine with luminescence centres but there is a probability that they may be retrapped in empty electron traps before their final recombination with centres. The present theoretical and experimental studies attempt to determine the extent to which retrapping does occur and what effects it will have in modifying the phosphorescence and thermoluminescence characteristics. Theoretical treatment shows that there are marked differences in these characteristics for conditions when the retrapping process is present and for those when it is negligible. Experimental investigations of the characteristics of specimens of zinc sulphide, zinc silicate and strontium silicate phosphors indicate that, except under special conditions, retrapping of electrons is negligible. These results together with other work can be explained theoretically if it is assumed that electron traps operative in the luminescence process are spatially associated with the immediate neighbourhood of the luminescence centres formed by activating impurities. This new concept is also supported by the relations found between the luminescence characteristics and the dielectric changes in phosphors of the zinc sulphide type.

§1. INTRODUCTION

It is now generally accepted that the phosphorescence and thermoluminescence characteristics of such phosphors as zinc sulphide and zinc silicate activated by suitable specific impurities are governed by the storage mechanism of electron traps which are thermally metastable. Previous workers have developed theoretical models of a luminescent solid which interpret many of the luminescence properties in terms of the trapping of electrons (Johnson *et al.* 1939). Experimental and theoretical studies of a more quantitative nature have been carried out by Randall and Wilkins (1945) and by Garlick and Wilkins (1945). Recently their hypotheses have been extended to explain the origin of the relatively large dielectric changes occurring in zinc sulphide phosphors during the emission of luminescence (Garlick and Gibson 1947).

The theoretical concept of a crystalline phosphor now generally accepted is that based on the "collective electron" model of Bloch which has been developed by various workers (see Mott and Gurney 1940). The allowed energies for electrons in such a phosphor consist of bands of energy states separated by forbidden energy bands as shown in figure 1 for the outermost electrons responsible for luminescence processes. Impurities, lattice defects or other perturbations of the ideal crystal lattice can give rise to discrete energy levels like those of an isolated atom and these may lie in the forbidden regions as shown. While impurity atoms, ions or larger complexes can function as luminescence emission centres the discrete levels of more minor disturbances can provide electron trapping levels just below the conduction levels of the system. These traps have been assumed to be those

responsible for the phenomena of phosphorescence and thermoluminescence. It is also generally assumed that in phosphors of the zinc sulphide type the electron traps are separate entities from the luminescence centres in contrast to the case of potassium chloride activated by thallium where the trapping states are within the thallium centres. Photoconductivity present in zinc sulphide phosphors supports this distinction.

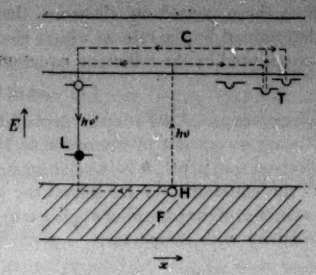

Figure 1. Schematic electron energy diagram for an impurity activated crystalline phosphor.

C. Conduction energy band.
F. Filled energy band.
H. Positive hole.
L. Luminescence centre.
T. Electron traps.
$h\nu$. Absorbed quantum.
$h\nu'$. Emitted quantum.

The mechanism of electron trapping has been investigated in a relatively quantitative way by Randall and Wilkins (1945), and from their experiments they have postulated that, although the luminescence emission is due to recombination of excited electrons with empty luminescence centres, yet the experimental evidence favours assumption of a monomolecular process. As they have pointed out, this assumption is possible in explanations of phosphorescence and thermoluminescence, which are determined then only by the rate of escape of trapped electrons and their return to empty centres, if there is no retrapping of escaping electrons before their recombination with centres. Using the schematic model of figure 1 it is evident that the degree of retrapping will depend at any instant on the relative numbers of empty electron traps and empty luminescence centres and on their relative capture cross sections. Randall and Wilkins have shown that these capture cross sections are approximately equal and for normal phosphorescence conditions the numbers of empty electron traps and empty luminescence centres are about equal. Thus if electron traps and centres are independent entities the absence of retrapping cannot be explained by the model of figure 1.

Some of the conditions under which retrapping is very likely have been given by Garlick and Wilkins (1945) and depend on a high proportion of empty traps compared with the number of empty centres. These conditions occur at high temperatures where all traps are effectively empty, at the beginning of excitation of a previously unexcited phosphor and at very long decay times. The present studies are concerned with the investigation of the occurrence of retrapping under normal conditions as defined above and attempt to provide from experimental data a more correct theoretical model than previous ones for phosphors of the sulphide and silicate classes.

A note on the following studies has already been published (Garlick and Gibson 1946).

§ 2. THEORETICAL STUDIES

For the sake of completeness it is necessary to include and enlarge upon the theoretical developments of Randall and Wilkins (1945) following their assumption that the retrapping of electrons does not occur to any significant extent except for special conditions. If a phosphor contains only traps of one depth E and at any

time these contain n electrons, then the luminescence emission intensity I is determined by the rate at which electrons escape from traps, and the process is represented by the following equations:

$$I = -dn/dt = ns\exp(-E/kT), \qquad \ldots\ldots(1)$$

where $s\exp(-E/kT)$ is the probability per unit time that an electron escapes, s being a constant of the order of $10^{8\pm1}\,\mathrm{sec}^{-1}$ for most phosphors, E being the electron trap depth, k being Boltzmann's constant and T the absolute temperature. If the equations (1) are solved for a uniform rate of rise of temperature after excitation of the phosphor at a low temperature the variation of thermoluminescence intensity with temperature is given by the expression

$$I = n_0 s\exp(-E/kT).\exp\left\{-\int_0^T \frac{s\exp(-E/kT)}{\beta}\,dT\right\}, \qquad \ldots\ldots(2)$$

where β is the rate of warming in deg/sec. Randall and Wilkins (1945) have discussed the effect of the warming rate on the thermoluminescence variation. The

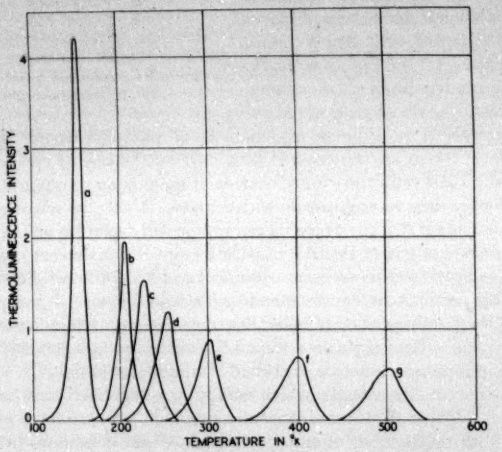

Figure 2 (a). Variation of thermoluminescence with temperature for phosphors with single trap depths after excitation at 90° K. Curves calculated theoretically assuming retrapping to be absent. Warming rate = 2·5°/sec.

(a) E=0·3 ev. : $s=10^9\,\mathrm{sec}^{-1}$. ($d$) E=0·4 ev. : $s=10^7\,\mathrm{sec}^{-1}$. ($f$) E=0·8 ev. : $s=10^9\,\mathrm{sec}^{-1}$.
(b) E=0·4 ev. : $s=10^9\,\mathrm{sec}^{-1}$. ($e$) E=0·6 ev. : $s=10^9\,\mathrm{sec}^{-1}$. ($g$) E=0·4 ev. : $s=10^6\,\mathrm{sec}^{-1}$.
(c) E=0·4 ev. : $s=10^8\,\mathrm{sec}^{-1}$.

graphical form of equation (2) is shown in figure 2 (a) for various values of s and E, n_0 and β remaining fixed (β=2·5°/sec.). The chief characteristics of the curves of figure 2 (a) for the variation of thermoluminescence with temperature when E is single valued are enumerated as follows :—

(a) For given values of s and n_0 and β the temperature at which maximum emission occurs is proportional to the trap depth E.

(b) For given values of E and n_0 the temperature of maximum emission varies with s and with β. For a change in s value from $10^9\,\mathrm{sec}^{-1}$ to $10^7\,\mathrm{sec}^{-1}$ when

$E=0{\cdot}4$ ev. the position of the emission peak moves to higher temperatures by about 50° K. A hundred fold increase in the warming rate will cause the same shift.

(*c*) In all cases the area under the emission–temperature curve is proportional to the number of electrons initially trapped before warming begins, that is to n_0. However, the actual shape of the emission curve is independent of n_0 which also means that the height of the curve at any point is proportional to n_0.

(*d*) The initial rise of the thermoluminescence curve is exponential with temperature following the simple relation

$$I=n_0 s\exp(-E/\mathbf{k}T). \qquad \ldots\ldots(3)$$

This affords a means of determining E from experimental curves of the same form when s is not known.

By means of the above characteristics the experimental results from studies of phosphor specimens may be tested to see whether the phosphors have only one trap depth or a distribution of trap depths according to the above hypothesis.

The above theoretical developments rest on the assumption that retrapping is a negligible process in the phosphor. It is essential however to consider the modification of this theory when an electron escaping from a trap has the same probability of being retrapped as it has of recombining with an empty luminescence centre. There is evidence from previous studies that the two probabilities are about equal (Randall and Wilkins 1945, p. 405). Consider a phosphor containing a total number of electron traps N of which n are filled by electrons at any instant. Then there will be $(N-n)$ empty traps and n empty luminescence centres previously vacated by the trapped electrons (the number of electrons in the conduction band at any instant is assumed to be small compared with n during the phosphorescence and thermoluminescence). The probability that an escaping electron will recombine with an empty luminescence centre and not be retrapped is given by $n/\{(N-n)+n\}=n/N$ and the luminescence process will be given by

$$I=-dn/dt=(n^2/N)s\exp(-E/\mathbf{k}T) \qquad \ldots\ldots(4)$$

with the notation used above. These equations should be compared with the previous equations (2).

The decay of phosphorescence at a fixed temperature is given then by solution of equations (4) and is represented by the equation

$$I=n_0^2 s\exp(-E/\mathbf{k}T)\Big/N\{1+(n_0/N)st\exp(-E/\mathbf{k}T)\}^2. \qquad \ldots\ldots(5)$$

The decay is hyperbolic in form showing that retrapping if present can produce a marked modification of the exponential decay given by equations (1) obtained by neglecting its effect. It will be seen from equation (5) that the form of the decay of phosphorescence will be dependent on n_0 and thus on the conditions of filling of the traps by excitation at the commencement of decay.

If equations (4) are solved to give the thermoluminescence variation with temperature when the phosphor is warmed at a uniform rate after excitation at a low temperature, then the resulting variation is given by the equation

$$I=n_0^2 s\exp(-E/\mathbf{k}T)\Big/N\left\{1+\frac{n_0}{N}\int_0^T\frac{s\exp(-E/\mathbf{k}T)}{\beta}\,dT\right\}^2. \qquad \ldots\ldots(6)$$

This equation corresponds to equation (2) and its graphical forms for various values

of E and n_0 when s and β remain fixed are given in figure 2 (*b*). The main characteristics of thermoluminescence–temperature variation when retrapping occurs are enumerated as follows :—

(*a*) For fixed values of s, n_0 and β the temperature at which the emission reaches its maximum is proportional to the electron trap depth E. For saturation of the traps ($n_0 = N$) and the same values of s the equations (2) and (6) give maxima at the same temperature.

(*b*) For given values of E and n_0 the temperature position of the emission maximum varies with s and β in much the same way as for the case when retrapping is absent.

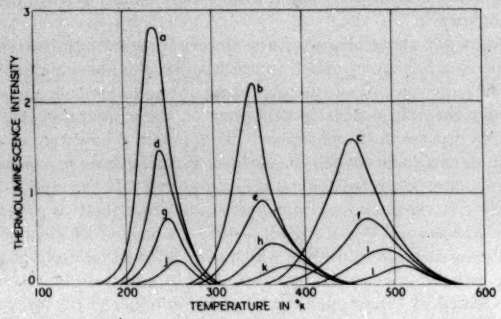

Figure 2 (*b*). Variation of thermoluminescence with temperature for phosphors with single trap depths after excitation at 90° K. Curves calculated theoretically assuming retrapping to be present. Warming rate = 2·5°/sec. $s = 10^8\ \text{sec}^{-1}$; N = total number of traps of depth E; n_0 = number filled.

(*a*) $E = 0{\cdot}4$ ev. : $n_0 = N$.
(*b*) $E = 0{\cdot}6$ ev. : $n_0 = N$.
(*c*) $E = 0{\cdot}8$ ev. : $n_0 = N$.
(*d*) $E = 0{\cdot}4$ ev. : $n_0 = 0{\cdot}5N$.
(*e*) $E = 0{\cdot}6$ ev. : $n_0 = 0{\cdot}5N$.
(*f*) $E = 0{\cdot}8$ ev. : $n_0 = 0{\cdot}5N$.
(*g*) $E = 0{\cdot}4$ ev. : $n_0 = 0{\cdot}25N$.
(*h*) $E = 0{\cdot}6$ ev. : $n_0 = 0{\cdot}25N$.
(*i*) $E = 0{\cdot}8$ ev. : $n_0 = 0{\cdot}25N$.
(*j*) $E = 0{\cdot}4$ ev. : $n_0 = 0{\cdot}1N$.
(*k*) $E = 0{\cdot}6$ ev. : $n_0 = 0{\cdot}1N$.
(*l*) $E = 0{\cdot}8$ ev. : $n_0 = 0{\cdot}1N$.

(*c*) In all cases the area under the emission–temperature curve is proportional to the number of electrons (n_0) initially trapped. However, the actual shape of the curve is dependent on n_0 as shown by equation (6). This is essentially different from the case when retrapping is negligible.

(*d*) The initial rise of luminescence before peak emission is reached follows the simple relation

$$I = (n_0^2/N)s \exp(-E/\boldsymbol{k}T). \qquad \ldots\ldots (7)$$

Comparing this equation with equation (3) it is seen that the power of the n_0 term is different in the two equations, the exponential term being identical. This provides a further means of experimental correlation with theory.

The above characteristics obtained by the two different assumptions of retrapping and no retrapping show the marked effect which retrapping may have on the phosphor characteristics. For most phosphors which have complex electron trap distributions the above treatment must be extended to traps of many depths. This is relatively simple if retrapping is neglected as shown by Randall and Wilkins for particular trap distributions. For example if the number of traps decreases

exponentially with depth (i.e. $N \propto e^{-\alpha E}$) then the phosphorescence decay for initial saturation of the traps involved is of the form $I \propto t^{-(\alpha kT+1)}$ where t is the decay time. The trap distributions may be obtained by means of thermoluminescence experiments and in the above case the theory verified by correlation of the results with phosphorescence measurements at different fixed temperatures, since the index of t should vary linearly with the temperature. This particular case shows that the hyperbolic decays characteristic of zinc sulphide phosphors can be explained by the sum of exponential terms whose constants are known from experiments. The derivation of phosphorescence characteristics for phosphors with complex distributions when retrapping is present becomes difficult as electrons escaping from traps of one depth may be retrapped in traps of different depths. Solutions have not yet been obtained for these conditions.

It is necessary to consider the way in which the trapping processes are affected by the conditions of excitation of the phosphor both with and without the presence of retrapping of escaping electrons. As a simple case that of steady excitation of a phosphor at fixed temperatures will be considered.

(i) *The filling of traps by constant excitation with no retrapping*

The considerations below make a fundamental change in the theoretical model of figure 1. They assume that each luminescence centre has an electron which on excitation is raised into electron traps which are in the immediate neighbourhood of the centre or are metastable trapping levels within the centre. Then if ultra-violet light of intensity J excites aJ electrons per second and in equilibrium the number of electrons trapped is n_0 in the N available traps of depth E then the equilibrium is represented by

$$dn_0/dt = 0 = abJ(N - n_0) - n_0 s \exp(-E/\boldsymbol{k}T) \qquad \ldots\ldots(9)$$

where b is the probability of electron capture by a trap. This gives the relation between n_0 and N for different intensities of ultra-violet radiation, temperatures and trap depths as

$$n_0 = N/\{1 + (s/abJ)\exp(-E/\boldsymbol{k}T)\}. \qquad \ldots\ldots(10)$$

This equation may be tested experimentally by both thermoluminescence and phosphorescence experiments. It may be extended to apply to complex trap distributions as has been done in the theoretical treatment of dielectric changes due to electron traps in phosphors (Garlick and Gibson 1947). For the purposes of the present experimental studies equation (10) is rearranged to show the simple relation between n_0 and J for fixed trap depth and temperature

$$(N/n_0) - 1 = (s/abJ)\exp(-E/\boldsymbol{k}T). \qquad \ldots\ldots(11)$$

(ii) *The filling of electron traps when retrapping is present*

With the above notation and assuming retrapping to be present as in the derivation of equations (4), (5) and (6), the filling of the N available traps by constant excitation J at a fixed temperature may be determined. If aJ electrons are raised into the conduction band per second by the excitation and in equilibrium m_0 electrons are in the band, n_0 being in traps, then $(n_0 + m_0)$ centres are empty and the equilibrium equations are

$$dm_0/dt = 0 = aJ - \beta m_0(m_0 + n_0),$$
$$dn_0/dt = 0 = bm_0(N - n_0) - n_0 s \exp(-E/\boldsymbol{k}T),$$

where b is the probability of capture of an electron by an empty trap and β the

probability of electron recombination with an empty luminescence centre. Solution of these equations shows that below saturation level for the traps (i.e. $N>n$) both m_0 and n_0 are root functions of the excitation intensity J. Thus when retrapping is present the simple relation between n_0 and J as in equations (10) and (11) is not found and the examination of trap filling thus provides a means of testing the above relations for validity.

The above theoretical developments have been compared with the results of experimental studies on typical phosphors as described below and these comparisons provide evidence for the relative importance of retrapping.

§3. EXPERIMENTAL STUDIES AND RESULTS

(i) *Experimental methods*

The experiments consisted essentially of measurements of thermoluminescence and phosphorescence characteristics of selected specimens under many different but known conditions of excitation and temperature. For all these experiments the phosphor was mounted *in vacuo* in a thin layer on a rhodium-plated copper surface forming part of a metal Dewar vessel described in a previous paper (Garlick and Wilkins 1945). The specimens could be excited by monochromatic radiation of wavelengths 2537 A. or 3653 A. by means of a mercury arc source. The methods of measuring thermoluminescence curves and phosphorescence curves have also been previously described (Randall and Wilkins 1945). The rate of warming in all thermoluminescence experiments was kept fixed at 2·5°/sec.

(ii) *Experimental results and theoretical correlations*

For the experimental investigations three phosphor specimens have been chosen with narrow trap distributions giving a peak in their saturated thermoluminescence curves which are shown in figures 3 (*a*), 3 (*b*) and 3 (*c*). The specimen corresponding to figure 3 (*a*) is a zinc sulphide phosphor activated by copper and excited by 3653 A. radiation. It has two peaks in its thermoluminescence curve but in experimental studies use was made of the peak due to deeper traps only. Figure 3 (*b*) is the thermoluminescence curve for a zinc silicate phosphor activated by manganese and excited by 2537 A. radiation having a single peak in its emission curve. In both figures 3 (*a*) and 3 (*b*) the theoretical curves obtained by substitution of suitable values of s and E in equation (6) are shown by broken curves. The experimental curves show remarkably good agreement with the calculated curves for which retrapping has been assumed. However, on the basis of "no trapping" these phosphors would have a distribution of trap depths. Both specimens are typical of their class and are photoconductors. The third specimen studied is a strontium silicate phosphor with europium impurity as activator. Its thermoluminescence curve has one main peak as shown in figure 3 (*c*) and this represents a single trap depth as shown by the agreement with the theoretical curve, the broken curve of figure 3 (*c*), derived from equation (2) assuming no retrapping. This phosphor is excited by ultra-violet light of both wavelengths used but thermoluminescence and the corresponding phosphorescence of long duration only occurs after excitation by 2537 A. radiation. The unique characteristics of the luminescence of this phosphor are described and discussed later. The following experiments attempt to correlate the characteristics of each phosphor with one or other of the theoretical hypotheses. By this means the extent to which retrapping occurs may be defined.

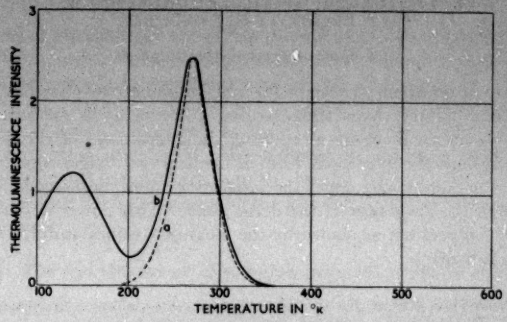

Figure 3 (*a*). ZnS—Cu phosphor. Thermoluminescence characteristics after excitation at 90° K.

(*a*) Theoretical curve assuming retrapping to occur. (*b*) Experimental curve.

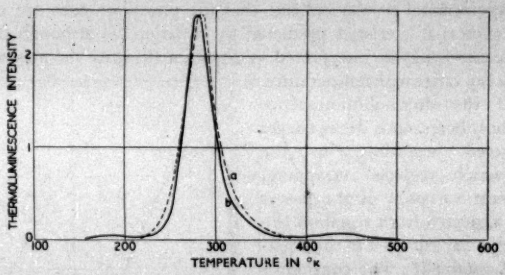

Figure 3 (*b*). Zn_2SiO_4—Mn phosphor. Thermoluminescence characteristics after excitation at 90° K.

(*a*) Theoretical curve assuming retrapping to occur. (*b*) Experimental curve.

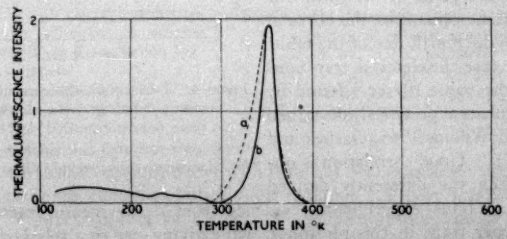

Figure 3 (*c*). $SrSiO_3$—Eu phosphor. Thermoluminescence characteristics after excitation at 90° K.

(*a*) Theoretical curve assuming retrapping to be absent. (*b*) Experimental curve.

§4. THE DECAY OF PHOSPHORESCENCE AT FIXED TEMPERATURE

(i) *Copper-activated zinc sulphide*

The decay of phosphorescence of the zinc sulphide phosphor has been measured at several different fixed temperatures. The decay as measured at room temperature is shown in figure 4, curve *a*, the coordinates of the graph being logarithmic to show the hyperbolic form of the decay, at longer times. At room temperature for these longer times the intensity of phosphorescence is inversely proportional to the 2·2 power of the decay time. This power is found to vary linearly with temperature as shown by the measured values at different temperatures given in table 1.

Table 1. Power law indices for the phosphorescence decay of ZnS–Cu phosphor

Temperature (° K.)	265	292	318	355
Power law index ($\alpha kT+1$)	2·07	2·2	2·32	2·5
α (ev^{-1})	47	47·7	48	49
α from thermoluminescence measurements (ev^{-1})	49	49	49	49

These experimental results indicate that the phosphor does not exhibit the phosphorescence characteristics predicted by equation (5) although its thermoluminescence curve may be interpreted by equation (6) since the final asymptotic form of the decay varies with temperature. However, if the thermoluminescence curve and phosphorescence decay curves are interpreted according to the hypothesis which neglects retrapping, then the linear variation of the power law index is expected from equation (8), and from the decay curves α of the equation may be obtained. The constant α may also be obtained from the exponential form of the thermoluminescence curve at its higher temperature end given in figure 3 (*a*). Values of α derived from the decay curves are given in the third line of table 1 and the value from the curve of figure 3 (*a*) in the fourth line of the table. In the latter case the electron trap constant s had the value $10^8\ sec^{-1}$ found by other experiments as previously described (Randall and Wilkins 1945, Garlick and Gibson 1947). Good correlation is obtained between the differently derived values of α. Thus experimental evidence from decay measurements shows that the deeper traps in this phosphor, while giving rise to a relatively narrow thermoluminescence–temperature curve, have a distributed range of depths and that agreement of experimental results with theory necessitates the assumption that retrapping is negligible.

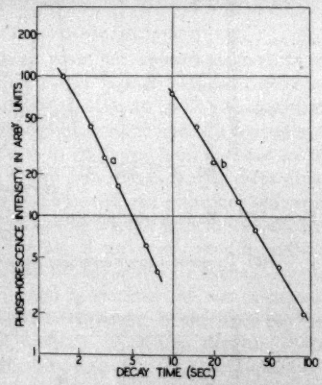

Figure 4. Decay of phosphorescence with time for zinc sulphide and zinc silicate phosphors at room temperature (291° K.).
(*a*) Copper activated zinc sulphide specimen.
(*b*) Manganese activated zinc silicate specimen.

(ii) *Manganese-activated zinc silicate*

The decay of phosphorescence of this specimen at room temperature is shown by curve (*b*) of figure 4. It is of the similar hyperbolic form to curve (*a*), at longer decay times its power law index being 1·7. By use of equation (8) this gives the trap distribution constant α as 28·0 ev^{-1}. Derivation from the thermoluminescence curve of figure 3 (*b*) gives α as 25 ev^{-1}. Again agreement with theory is good when retrapping is neglected. The value of the power law index is found to increase linearly with temperature as in the case of the zinc sulphide phosphor. These facts provide the data supporting the theoretical hypothesis that retrapping is not important.

(iii) *The phosphorescence of europium-activated strontium silicate*

This phosphor may be excited to give fluorescence and phosphorescence by radiation of either 3653 A. or 2537 A. However, there is no long duration phosphorescence or any thermoluminescence when the longer wavelength radiation is

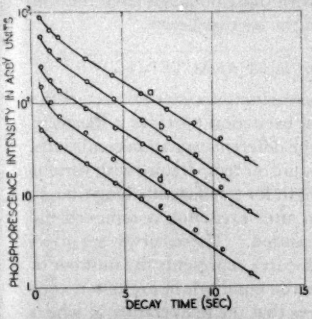

Figure 5 (*a*). Phosphorescence decay of $SrSiO_3$—Eu phosphor at various temperatures after excitation by 3650 A. radiation.
(*a*) 476° K. (*d*) 192° K.
(*b*) 398° K. (*e*) 90° K.
(*c*) 294° K.

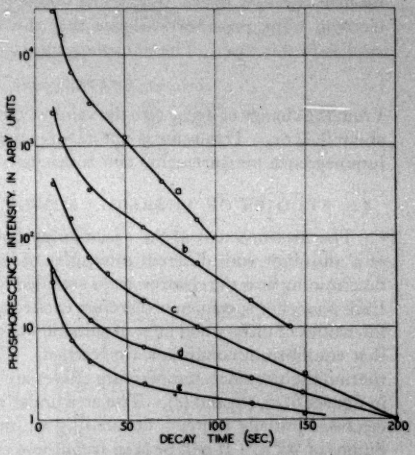

Figure 5 (*b*). Phosphorescence decay of $SrSiO_3$—Eu phosphor at various temperatures after excitation by 2537 A. radiation.
(*a*) 387° K. (*d*) 340° K.
(*b*) 373° K. (*e*) 320° K.
(*c*) 358° K.

used. The phosphorescence decay with time has been measured after excitation by each of these wavelengths of ultra-violet radiation. Figure 5 shows the results obtained. Figure 5 (*a*) shows the form of the phosphorescence decay after excitation by radiation of 3635 A. wavelength at different temperatures from 90° K. to 476° K. The initial decay is rapid, occupying a small fraction of a second. The subsequent decay has an exponential form, the decay rate being independent of temperature. The half-value period of the decay at different temperatures from

90° K. to 476° K. is included in the figure, its mean experimental value being 2·25 sec. Since this decay rate is independent of temperature it cannot be due to thermally metastable electron energy levels. This is also supported by the absence of thermoluminescence and photoconductivity when the 3650 A. is used. Thus the phosphorescence must be due to a forbidden optical transition within the europium luminescence centre, the life time of the state being abnormally large. Similar decay characteristics have been observed in other studies of the phosphorescence of adsorbed dyestuffs made according to the method of Travnicêk (1937).

When radiation of wavelength 2537 A. is used to excite the specimen the latter exhibits both photoconductivity and thermoluminescence. Its phosphorescence decay at various temperatures is given in figure 5 (*b*). The initial decay is due to the same two components which are present when 3653 A. irradiation is used, but the decay includes also phosphorescence of long duration decaying exponentially with time over the range measured but having a decay rate markedly dependent on temperature. This decay must be due to electron traps with a single depth or at the most a very narrow spread of trap depths as indicated by the thermoluminescence curve of figure 3 (*c*). The absence of a hyperbolic decay due to these electron traps provides evidence that the hypothesis of Randall and Wilkins applies in this case. The phosphorescence decay is thus of the form :—

$$I = c \exp(-ste^{-E/kT}). \qquad \ldots\ldots(14)$$

From the change of decay rate the value of E has been calculated and is found to be about 0·32 ev. This value is not in agreement with those obtained from thermoluminescence measurements and is discussed in the section below.

§ 5. STUDIES OF THERMOLUMINESCENCE CHARACTERISTICS

The measurement of the variation of the thermoluminescence characteristics of a phosphor with different intensities of initial excitation provides a means of determining how the electron traps are filled for the different excitation conditions. Each phosphor specimen is therefore excited at liquid air temperature with various intensities of ultra-violet light of suitable wavelength for a sufficiently long time so that equilibrium conditions are reached. Then after excitation is removed the thermoluminescence–temperature curves are measured. These curves are given in figures 6 (*a*), (*b*) and (*c*). The area under each curve represents the number of electrons initially trapped, denoted by n_0, under the equilibrium excitation conditions at 90° K. It will be seen from these curves that the temperature at which maximum emission occurs does not alter appreciably as the excitation intensity is varied.

In order to compare these experimental results with the theoretical predictions represented by equations (11) and (14) the area under each curve is taken as n_0, the number of electrons initially trapped, and the area under the curve for very high intensities as the saturation value N. Then for each specimen the experimentally derived values of $((N/n_0)-1)$ are plotted against the inverse of the excitation intensity J. These plots are given in figures 7 (*a*), (*b*) and (*c*) for the three specimens respectively. From inspection it is found that the experimental results follow the relations given by equation (11), i.e. retrapping assumed to be absent.

A further correlation of experiment with theory can be made by considering the portion of the thermoluminescence curve at some temperature lower than that at which peak emission occurs. As shown by the equations (3) and (7) the shape

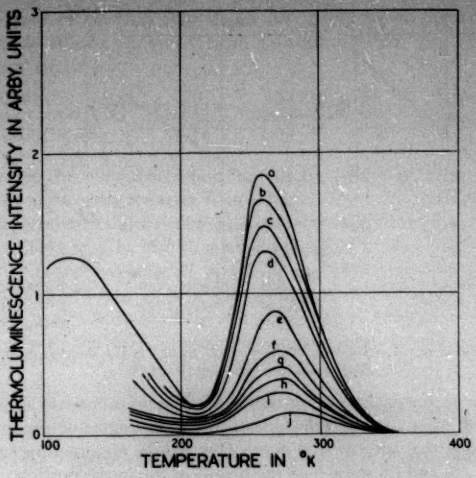

(*a*). Zinc sulphide—Copper-activated phosphor.

(*a*) $J=1740$. (*e*) $J=3$. (*h*) $J=0{\cdot}97$.
(*b*) $J=69$. (*f*) $J=1{\cdot}6$. (*i*) $J=0{\cdot}93$.
(*c*) $J=27$. (*g*) $J=1{\cdot}0$ (*j*) $J=0{\cdot}53$.
(*d*) $J=9$.

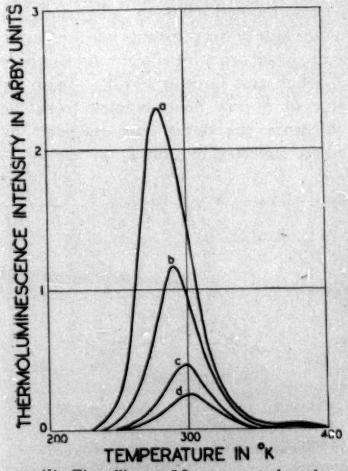

(*b*) Zinc silicate—Manganese-activated phosphor.

(*a*) $J=27$. (*c*) $J=3$.
(*d*) $J=9$. (*d*) $J=1$.

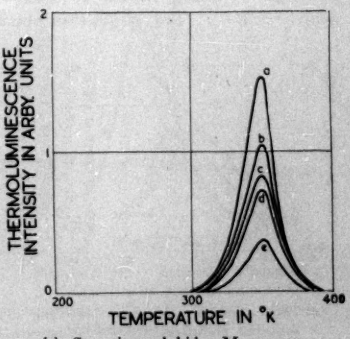

(*c*) Strontium sulphide—Manganese-activated phosphor.

(*a*) $J=100$. (*d*) $J=3$.
(*b*) $J=27$. (*e*) $J=1$.
(*c*) $J=9$.

Figure 6. Variation of thermoluminescence of sulphide and silicate phosphors with intensity of excitation (J) at 90° K.

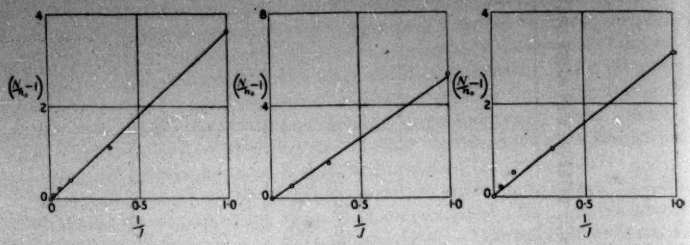

(*a*) Zinc sulphide—Copper-activated phosphor.

(*b*) Zinc silicate—Manganese-activated phosphor.

(*c*) Strontium sulphide—Europium-activated phosphor.

Figure 7. Variation in the number of trapped electrons (n_0) in the number of available traps (N) with excitation intensity (J) at 90° K.

of this portion of any curve will depend upon the degree of retrapping present. From this shape the value of trap depth may also be obtained for each specimen. Figures 8 (*a*), (*b*) and (*c*) show how the height of the initial portion of the curve at some selected fixed temperature varies with the number of electrons initially trapped, as given by the total area under the curve. Results for each of the three specimens show that equation (3) is adhered to. Calculations of the trap depth from the curve shape have been made for the strontium silicate specimen where the depth is almost single-valued. The depth thus obtained is 0·68 ev. By using this value and the temperature of peak emission the value of the constants may be found. This is calculated to be 10^9 sec^{-1} which is of the usual order for silicate and sulphide phosphors (Randall and Wilkins 1945, Garlick and Gibson 1947). Again by using this value of the constant the value of E may be calculated from the phorescence decay curves of figure 5 (*b*) since the decay rate is given by $s\exp(-E/\boldsymbol{k}T)$. The values thus obtained are collected in table 2.

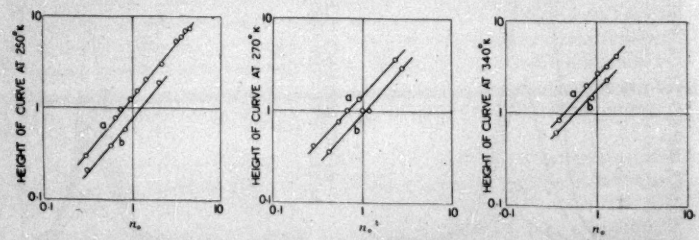

(*a*) Zinc sulphide—Copper-activated phosphor.

(*b*) Zinc silicate—Manganese-activated phosphor.

(*c*) Strontium silicate—Europium-activated phosphor.

(*a*) Steady excitation.
(*b*) Pulse excitation.

(*a*) Pulse excitation.
(*b*) Steady excitation.

(*a*) Pulse excitation.
(*b*) Steady excitation.

Figure 8. Variation in height of initial portion of thermoluminescence curve with the number of electrons (n_0) initially trapped by excitation at 90° K.

Table 2. Values of electron trap depth for specimen of europium-activated strontium silicate obtained from phosphorescence characteristics with constant $s = 10^9\,\text{sec}^{-1}$.

Temperature (° K.)	320	340	358	373	387
Decay rate $s \exp(-E/kT)$	0·00935	0·013	0·021	0·031	0·05
Electron trap depth E (ev.)	0·74	0·74	0·75	0·77	0·77

As shown by the phsophorescence curves the values of E given in table 1, while agreeing approximately with that obtained from the thermoluminescence curve, do not correlate with the value obtained from the change of decay rate with temperature. This may be due to a small spread of E values for this specimen similar to that found by Randall and Wilkins (1945) for potassium chloride activated by thallium. Otherwise if E is considered single valued the value of the constant s must be of the order of $10^4\,\text{sec}^{-1}$ according to decay rate changes, which does not agree with the value obtained from the thermoluminescence measurements.

(ii) *Changes in thermoluminescence characteristics during phosphorescence decay and after pulse excitation*

The following experiments provide further data to distinguish between retrapping and no-retrapping processes in the phosphor specimens and follow the method used in earlier studies (Garlick and Wilkins 1948). Each specimen is excited at liquid oxygen temperature by a pulse of ultra-violet light whose duration can be varied. After such excitation the variation of the thermoluminescence with temperature is measured. The curves obtained are shown in figures 9(*a*), (*c*) and (*e*) for the three phosphor specimens respectively. The specimens are also excited at room temperature (291° K.) and allowed to phosphoresce after removal of excitation for various selected times after which periods the specimen is suddenly cooled and then warmed at the unifrom rate of 2·5°/sec., its thermoluminescence

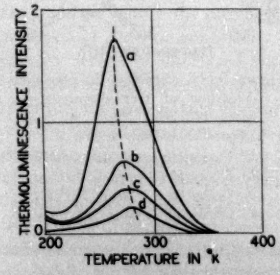

Figure 9(*a*). ZnS—Cu phosphor. Variation of thermoluminescence with duration of pulse excitation at 90° K.
(*a*) Steady excitation.
(*b*) Medium length pulse.
(*c*) Short pulse.
(*d*) Very short pulse.

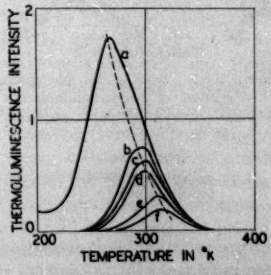

Figure 9(*b*). ZnS—Cu Phosphor. Variation of thermoluminescence after different times of phosphorescence decay at 291° K.
(*a*) Excitation at 90° K.
(*b*) Decay for 1 sec. at 291° K.
(*c*) Decay for 2 sec. at 291° K.
(*d*) Decay for 3 sec. at 291° K.
(*e*) Decay for 10 sec. at 291° K.
(*f*) Decay for 20 sec. at 291° K.

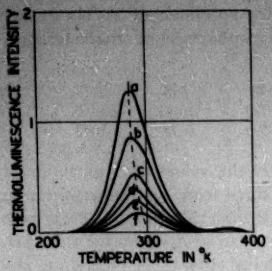

Figure 9 (*c*). Zn_2SiO_4—Mn phosphor. Variation of thermoluminescence with duration of pulse excitation at 90° K.

(*a*) Steady excitation.
(*b*) Long pulse.
(*c*) Medium pulse.
(*d*) Short pulse.
(*e*) Short pulse.
(*f*) Very short pulse.

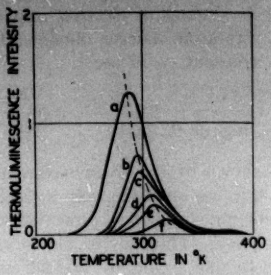

Figure 9 (*d*). Zn_2SiO_4—Mn phosphor. Variation of thermoluminescence after different times of phosphorescence decay at 291° K.

(*a*) Excitation at 90° K.
(*b*) Decay for 1 sec. at 291° K.
(*c*) Decay for 4 sec. at 291° K.
(*d*) Decay for 10 sec. at 291° K.
(*e*) Decay for 20 sec. at 291° K.
(*f*) Decay for 60 sec. at 291° K.

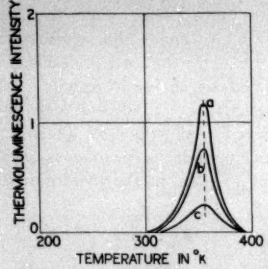

Figure 9 (*e*). $SrSiO_3$—Eu phosphor. Variation of thermoluminescence with duration of pulse excitation at 90° K.

(*a*) Steady excitation.
(*b*) Medium pulse.
(*c*) Short pulse.

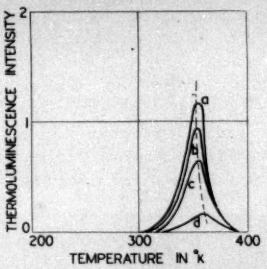

Figure 9 (*f*). $SrSiO_3$—Eu phosphor. Variation of thermoluminescence after different times of phosphorescence decay at 291° K.

(*a*) Excitation at 90° K.
(*b*) Decay for 30 min. at 291° K.
(*c*) Decay for 1·5 hr. at 291° K.
(*d*) Decay for 16 hr. at 291° K.

temperature variation being measured during warming. The curves so obtained are given in figures 9 (*b*), (*d*) and (*f*) and represent the distribution of electrons in traps at different stages of phosphorescence decay. Cross comparison between curves 9 (*a*), and (*b*), (9 *c*) and (*d*) and (9 *e*) and (*f*) respectively shows that change in duration of pulse excitation affects the number of trapped electrons but the shape of the thermoluminescence curves and their maxima positions are not markedly altered. However, phosphorescence decay does cause a shift of the maximum position of these curves at higher temperatures as the decay proceeds for the specimens of zinc sulphide and zinc silicate. The strontium silicate phosphor characteristics in curves 9 (*e*) and 9 (*f*) show no change in the maximum position

with the number of trapped electrons either during phosphorescence or due to pulse excitation.

These results confirm the hypothesis that retrapping is a negligible process in these phosphors. As stated in the theoretical section above the thermoluminescence curve shape for a single trap depth when retrapping is present depends on the number of trapped electrons (figure 2 (*b*)) but is independent of the process of filling or emptying, whether by pulse excitation or phosphorescence decay. Thus for a given area under the curve the shape should be fixed. As shown by comparison of curves (*a*) and (*b*), (*c*) and (*d*), (*e*) and (*f*) respectively of figure 9 the experimental results do not agree with this prediction but are in agreement with the supposition that a distribution of trap depths is present and that retrapping is negligible. This means that pulse excitation of the previously unexcited phosphor will fill traps of all different depths with equal probabilities, the number filled thus depending only on the number available. Thus the shape of the thermoluminescence curve is little affected. However, when phosphor-decay proceeds the shallower traps are emptied leaving only the deeper ones filled with the consequence observed in the curves of figure 9 (*b*), (*d*) and (*f*), that is, a temperature shift of the emission maxima.

§ 6. CONCLUSION

The experimental results described above have been obtained from studies of three typical phosphor specimens of three different classes. In each case the specimen has been selected because it affords suitable thermoluminescence and phosphorescence properties to determine how far retrapping of electrons escaping from electron traps was a major part of the mechanism. The evidence presented has shown that the characteristics measured are in agreement with the simple theoretical treatment originally due to Randall and Wilkins which assumes retrapping to be negligible. This could be understood in terms of the model of figure 1 if, as in the case of the thallium activated alkali halide phosphors, the electron traps are within the luminescence centres to which the phosphorescence processes would then be confined. However, the specimens all exhibit photoconductivity which is associated with the thermoluminescence and phosphorescence processes and therefore electrons must leave luminescence centres during the process. This means that the luminescence process involves a recombination of electrons with luminescence centres after escaping from electron traps which are not in the luminescence centres themselves. Previous experiments due to Randall and Wilkins (1945) have given estimates of the capture cross sections of empty luminescence centres and electron traps which appear to be of the same order. Thus retrapping of escaping electrons from traps will be an integral part of the mechanism if traps are quite independent of luminescence centres. It is therefore more probable that the impurity centres while not containing the trapping energy states cause perturbations in their environment (i.e. in the surrounding local lattice) which give rise to the trapping states. If this is so then the absence of retrapping of electrons may be more readily understood since electrons escaping from traps adjacent to empty luminescence centres will have a higher probability of recombining with the centres than of moving to other empty traps and being recaptured. It is not possible to provide a detailed treatment of this assumption as no studies of the complex potential configurations around impurity centres in a matrix lattice have been made. However, the postulate of association between traps and

luminescence centres is supported by other and independent studies of the effect of one or more different impurities and also of the preparation conditions (firing temperature, fluxes etc.) on the electron trap distributions of phosphors (Garlick 1947). These experimental investigations show that introduction of specific impurities gives rise to particular electron trap configurations. Other studies of the dielectric changes in zinc sulphide and other phosphors show good agreement between theory and experiment when retrapping is neglected (Garlick and Gibson 1947).

To summarize, the experimental and theoretical developments described above show that the simple electron trap theory due to Randall and Wilkins (1945) which neglects retrapping is in better agreement with experiment than that in which retrapping is assumed to be present. This evidence, combined with that from other investigations leads to a new concept of the origin and spatial location of electron traps in phosphors. They appear to be formed by the perturbations due to the impurity activator in the matrix crystal lattice immediately surrounding the centre.

ACKNOWLEDGMENTS

Our thanks are due to Professor M. L. Oliphant, F.R.S., for the provision of facilities for this work and to the Ministry of Supply (D.C.D.) under whose research projects it has been carried out.

REFERENCES

GARLICK, G. F. J., 1947, *Monograph of Cornell Conference on Luminescence* (New York: John Wiley).

GARLICK, G. F. J., and GIBSON, A. F., 1946, *Nature, Lond.*, **158**, 704; 1947, *Proc. Roy. Soc.* A, **188**, 485.

GARLICK, G. F. J., and WILKINS, M. H. F., 1945, *Proc. Roy. Soc.* A, **184**, 408.

DE GROOT, W., 1939, *Physica*, **6**, 275.

JOHNSON, R. P., 1939, *J. Opt. Soc. Amer.*, **29**, 387.

MOTT, N. F., and GURNEY, R. W., 1940, *Electronic Processes in Ionic Crystals* (Oxford: University Press).

RANDALL, J. T., and WILKINS, M. H. F., 1945, *Proc. Roy. Soc.* A, **184**, 366.

TRAVNICĚK, M., 1937, *Ann. Phys., Lpz.*, **30**, 224.

The Moving Coil Galvanometer as a Circuit Element

BY N. F. ASTBURY

G.K.N. Research Laboratories, Wolverhampton

MS. received 2 *September* 1947; *read* 6 *February* 1948

ABSTRACT. An account is given of a simplified calculus applicable to a moving-coil galvanometer in which use is made of the concept of motional impedance. The fundamental galvanometer equations are presented in a novel and very simple form. Examples of the use of the formulae are given, notably with reference to the ultimate "noise level" of a galvanometer.

§1. INTRODUCTION

THE moving-coil galvanometer, one of the oldest and most familiar of our laboratory instruments, has recently found considerable application in various systems for direct-current amplification, amongst which may be noted those described by D. C. Gall (1942, 1945). It is hoped to publish

shortly descriptions of other systems developed by the present writer, but in the meantime it may be noted that the problem of D.C. amplification is one of very great technical importance and one which is most admirably met by the use of a moving-coil galvanometer in a preamplifying stage. In the course of development work on problems of this type it occurred to the writer that the mathematics of a moving-coil galvanometer could be considerably simplified for many purposes of circuit analysis, and it is the purpose of this paper to show how the behaviour of a galvanometer as a circuit element can be succinctly expressed in terms of its motional impedance, which can in turn be expressed in terms of experimentally determined constants.

While the concept of motional impedance applied to galvanometers is by no means new, it is believed that the present treatment is novel. Butterworth (1912) showed that a galvanometer can be represented by a parallel combination of a pure inductance, a capacitance and resistance placed in series with a resistance equal to that of the instrument coil, and that in this equivalent circuit the current in the inductance branch is homologous with the angular deflection of the coil. Kennelly showed that the impedance circle diagram was applicable to a galvanometer. A note on these points is given in the *Dictionary of Applied Physics* (Vol. II, p. 976).

It is proposed in the present paper to put forward the motional impedance concept and to illustrate it by applications to various circuit problems.

§ 2. PRÉCIS OF STANDARD RESULTS

It is convenient to start with a précis of well-known results for the galvanometer.

Let α, β and γ be respectively the moment of inertia of the moving system, the mechanical damping factor and the torque control constant of the galvanometer, and let k be the product of the total area of the coil and the control field, i.e. the "area-turns-field" constant. Then, if the galvanometer form part of a closed circuit of total resistance R (and of zero reactance) in which an E.M.F. e is acting, the current i and the angular deflection θ of the moving system are related to e by the torque and E.M.F. equations

$$(\alpha D^2+\beta D+\gamma)\theta = ki, \qquad \ldots\ldots(2.1)$$

$$Ri + kD\theta \quad = e, \qquad \ldots\ldots(2.2)$$

where D stands for d/dt.

Eliminating i, we have

$$\{\alpha D^2+(\beta+k^2/R)D+\gamma\}\theta = ke/R, \qquad \ldots\ldots(2.3)$$

from which we find S, the critical resistance, as

$$S \simeq k^2/2\alpha\omega_0 \qquad \ldots\ldots(2.4)$$

where ω_0 is the free frequency of the instrument and is given by

$$\omega_0 = (\gamma/\alpha)^{\frac{1}{2}}(1-\beta^2/4\alpha\gamma)^{\frac{1}{2}} \simeq (\gamma/\alpha)^{\frac{1}{2}}. \qquad \ldots\ldots(2.5)$$

The logarithmic decrement, λ, is, if $T = 2\pi/\omega$,

$$\lambda = (\beta+k^2/2R)(T/2\alpha) \qquad \ldots\ldots(2.6)$$

and

$$\lambda_0 = \beta\pi/\alpha\omega_0, \qquad \ldots\ldots(2.7)$$

where λ_0 is the value of λ for the open circuit condition. We may define the damping factor, δ, by

$$\delta = \lambda_0/\pi = \beta/\alpha\omega_0. \qquad \ldots\ldots(2.8)$$

Finally, we may define the direct current sensitivity, μ, by

$$\mu = k/\gamma \qquad \ldots\ldots(2.9)$$

and then express all our coefficients in terms of the experimentally observable quantities S, ω_0 and μ, obtaining

$$\alpha = 2S/\omega_0^3\mu^2, \qquad \ldots\ldots(2.10)$$

$$\beta = 2S\lambda_0/\pi\omega_0^2\mu^2, \qquad \ldots\ldots(2.11)$$

$$= 2S\delta/\omega_0^3\mu^2, \qquad \ldots\ldots(2.12)$$

$$\gamma = 2S/\mu^2\omega_0, \qquad \ldots\ldots(2.13)$$

$$k = 2S/\mu\omega_0. \qquad \ldots\ldots(2.14)$$

These results can be used to express Butterworth's (1912) formulae in simple forms. If L, C and P are respectively the inductance, capacitance and shunt resistance of his equivalent circuit, we have

$$L = 2S/\omega_0, \qquad \ldots\ldots(2.15)$$

$$C = 1/2S\omega_0, \qquad \ldots\ldots(2.16)$$

$$P = 2S/\delta. \qquad \ldots\ldots(2.17)$$

§ 3. THE MOTIONAL IMPEDANCE

We can now proceed to a discussion of the motional impedance of the galvanometer, but we may note before so doing that it is proposed to regard the circuit in the static condition as non-reactive. There is no loss of generality in this, because the dynamic reactance of the instrument is always so much greater than the static value that the inclusion of the latter in the discussion would be a mere algebraic *tour de force*.

Eliminating θ from equations (2.1) and (2.2), we find

$$e = \{R + k^2D/(\alpha D^2 + \beta D + \gamma)\}i. \qquad \ldots\ldots(3.1)$$

It is evident that the second term in the bracket represents the contribution made to the effective impedance of the circuit by the moving galvanometer coil. This term we call the *motional impedance* (more precisely it is the motional impedance operator) and we denote it by I. Then

$$I = k^2D/(\alpha D^2 + \beta D + \gamma) \qquad \ldots\ldots(3.2)$$

$$= 2S\omega_0 D/\{(D^2 + \omega_0^2) + \delta\omega_0 D\}, \qquad \ldots\ldots(3.3)$$

using equations (2.4), (2.5), (2.8) and (3.1).

From (2.1) and (3.2) we find

$$\theta = \frac{I}{k}\frac{1}{D}\,i = \frac{I}{k}\int i\,dt, \qquad \ldots\ldots(3.4)$$

while from (3.1) and (3.4) we have

$$\theta = \frac{1}{k}\cdot\frac{I}{I+R}\frac{1}{D}\,e = \frac{1}{k}\cdot\frac{I}{I+R}\int e\,dt. \qquad \ldots\ldots(3.5)$$

Equations (3.4) and (3.5) present the equations of the moving-coil galvanometer in a novel and simple form which is of considerable value in circuit analysis. Equation (3.5) is of particular interest, because it holds the key to the problem of the behaviour of a galvanometer as a fluxmeter and shows at once that for flux measurement the condition is that the motional impedance shall dominate the static resistance of the circuit.

The expression $I/(I+R)$ may be regarded as the "response operator" of the instrument and its circuit, and may conveniently be rewritten as a function of D, ω_0 and σ, where $\sigma = S/R$ may be called the "degree of damping" of the instrument. We have

$$\frac{I}{I+R} = \frac{2\omega_0\sigma D}{D^2+\omega_0{}^2+\omega_0\sigma D(2\sigma+\delta)}. \qquad \ldots\ldots(3.6)$$

While we shall discuss later the application to particular forms of time-variation of e, the form taken by I for sinusoidal variations, which is useful in connection with vibration galvanometers, is interesting. If ω be the frequency of e, then we have at once from (3.2)

$$I = \frac{2j\omega_0\omega S}{(\omega_0{}^2-\omega^2)+j\omega\omega_0\delta},$$

where j is the operator rotating through a right angle. This may be written

$$I = \frac{2S\delta}{z^2+\delta^2} + \frac{2jSz}{z^2+\delta^2}$$

where $z = (\omega_0/\omega) - (\omega/\omega_0)$, showing the existence of a motional resistance term, R_M, and a motional reactance term, X_M, given by

$$R_M = 2S\delta/(z^2+\delta^2) \; ; \quad X_M = 2Sz/(z^2+\delta^2).$$

It is easy to show that the locus of the end of the vector $R_M + jX_M$ is a circle of diameter $2S/\delta$, passing through the origin and with its centre on the R axis. Except very near to resonance, we can disregard δ and then X_M assumes the very simple form $X_M = 2S/\{(\omega_0/\omega) - (\omega/\omega_0)\}$, and this quantity can, in fact, be taken in many problems as representing the motional impedance of the instrument.

§4. ILLUSTRATIVE EXAMPLES

Two of the most interesting examples of the application of the galvanometer equations in the form derived above are to be found in the calculation of the inherent "noise level" of a galvanometer (that is, the background deflection due to spontaneous voltage fluctuations in the circuit) and the calculation of the response of an amplifier using a galvanometer.

(i) *Noise level*

From equation (3.5) we may write

$$D\theta = \frac{1}{k}\frac{I}{I+R}e.$$

Here e will be the spontaneous E.M.F. of the circuit, and in any frequency range df we may write

$$|D\theta|^2 = \frac{1}{k^2}\left|\frac{I}{I+R}\right|^2 \overline{e^2} \qquad \ldots\ldots(4.1)$$

where mean square quantities are indicated by the bars.

By Nyquist's theorem (Moullin 1938, p. 13) we may put

$$\overline{e^2} = 4R\boldsymbol{k}T\,df, \qquad \ldots\ldots(4.2)$$

where $\boldsymbol{k}$ is Boltzmann's constant and T is the absolute temperature. We

therefore have, for the mean kinetic energy of the suspended system arising from spontaneous fluctuations in the range df,

$$\begin{aligned}\tfrac{1}{2}\alpha|D\theta|^2 &= \tfrac{1}{2}\frac{\alpha}{k^2}\left|\frac{I}{I+R}\right|^2\bar{e}^2 \\ &= \tfrac{1}{2}\frac{\alpha}{k^2}\frac{4\omega^2\omega_0^2\sigma^2}{(\omega^2-\omega_0^2)^2+4\omega^2\omega_0^2\sigma^2}\cdot 4R\boldsymbol{k}T\frac{d\omega}{2\pi} \\ &= \frac{2\omega_0\sigma\boldsymbol{k}T}{\pi}\frac{\omega^2}{(\omega^2-\omega_0^2)^2+4\omega^2\omega_0^2\sigma^2}d\omega, \qquad \ldots\ldots(4.3)\end{aligned}$$

from (2.10) and (2.14).

The total energy, E, is thus given by

$$E=\frac{2\omega_0\sigma\boldsymbol{k}T}{\pi}\int_0^\infty\frac{\omega^2}{(\omega^2-\omega_0^2)^2+4\omega^2\omega_0^2\sigma^2}\,d\omega=\tfrac{1}{2}\boldsymbol{k}T. \qquad \ldots\ldots(4.4)$$

This may also be set equal to the mean potential energy, $\frac{1}{2}\gamma|\theta|^2$, so that

$$|\theta|^2=\boldsymbol{k}T/\gamma. \qquad \ldots\ldots(4.5)$$

Using (2.13) we may write, for the mean deflection $\bar{\theta}$,

$$\bar{\theta}=\mu(\pi\boldsymbol{k}T/S\tau)^{\frac{1}{2}}, \qquad \ldots\ldots(4.6)$$

where $\tau=2\pi/\omega_0$ is the free period of the instrument. This corresponds to an R.M.S. current $\bar{i}$ given by

$$\bar{i}=\bar{\theta}/\mu=(\pi\boldsymbol{k}T/S\tau)^{\frac{1}{2}}. \qquad \ldots\ldots(4.7)$$

Ising (1926) has given a similar result (but restricted to the case of critical damping) deduced from considerations of the effect of Brownian movement of gas molecules on the suspension. As Moullin (1938, p. 217) has pointed out, we must suppose that the total background noise arises from the combination of the two effects, and we would expect therefore a background corresponding to $\bar{i}\sqrt{2}$, that is, to

$$\bar{i}\sqrt{2}=(2\pi\boldsymbol{k}T/S\tau)^{\frac{1}{2}}. \qquad \ldots\ldots(4.8)$$

Taking $\boldsymbol{k}=1{\cdot}4\times10^{-16}$ ergs per degree and $T=290$, we have

$$\bar{i}\sqrt{2}\simeq 5\times10^{-7}(S\tau)^{-\frac{1}{2}} \text{ absolute amperes.} \qquad \ldots\ldots(4.9)$$

(ii) *Galvanometer amplifier*

If we consider an amplifying system such as that described by Gall (1942, 1945), the essential circuit of which is shown in figure 1, the response can be calculated very readily by the present method.

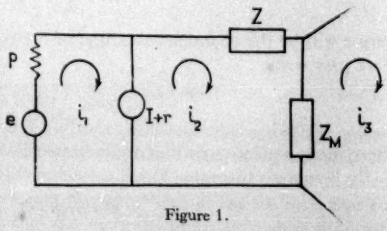

Figure 1.

Referring to figure 1, the galvanometer is represented by $I+r$, where r is its D.C. resistance, Z and Z_M are elements of a feedback circuit, and i_3 is the amplified current arising from the application of an E.M.F. e through a resistance P to the galvanometer.

We then have the following equations

$$e = Pi_1 + (I+r)(i_1 - i_2),$$
$$0 = (I+r)(i_2 - i_1) + Zi_2 + Z_M(i_2 - i_3),$$
$$i_3 = g\theta \; ; \quad \theta = (I/kD)(i_1 - i_2),$$

where g is the gain factor for the amplifying device. Solving for i_3, we get for the current amplification

$$\frac{i_3}{i_1} = \frac{Z+Z_M}{Z_M} \cdot \frac{1}{1+\xi} \qquad \ldots\ldots(4.10)$$

where

$$\xi = kD(I+r+Z+Z_M)/gIZ_M. \qquad \ldots\ldots(4.11)$$

The quantity ξ is a non-dimensional complex number. In any practical case it is easy to evaluate, and generally the two components are of the order of 0·01.

The effective input impedance, I', of the galvanometer is given by

$$I' = (I+r)\frac{kD}{gI} \cdot \frac{Z+Z_M}{Z_M} \cdot \frac{1}{1+\xi} \qquad \ldots\ldots(4.12)$$

$$= (I+r)\,\frac{\text{Effective current gain}}{\text{Gain without feedback}}. \qquad \ldots\ldots(4.13)$$

Thus in general $I' \ll I+r$.

In Gall's amplifier, Z and Z_M were pure resistances, Z/Z_M being of the order of 10^4. If Z_M be of the form $S+MD$, i.e. a combination of mutual inductance M and resistance S, and if Z be a large resistance P, we have, disregarding ξ,

$$i_3/i_1 = (P+S+MD)/(S+MD), \qquad \ldots\ldots(4.14)$$

so that i_3 can be made to record the *integral* of i_1 over certain ranges of D. It is easy to make S/M about 0·001 (say with $M = 1$H, $S = 0{\cdot}001\ \Omega$) and thus to secure an integrating time constant of the order of 1000 seconds (Astbury 1948).

(iii) *Galvanometer response problems*

The present calculus leads very readily to the operational method for the solution of certain response problems. We may take as simple examples the problem of determining the response to suddenly applied E.M.F. or flux signals. In the former case, let the E.M.F. be $H(t).e$, where $H(t)$ is the unit operator. Then from (3.5), we have

$$\theta = \frac{1}{k} \cdot \frac{I}{I+R} \cdot \frac{1}{D}\, H(t).e. \qquad \ldots\ldots(4.15)$$

Writing $I/(I+R)$ as $f(D)$, we have (Jeffreys 1931)

$$\theta = \frac{1}{k} \cdot f(D) \cdot \frac{1}{D} \cdot H(t).e$$

$$= \frac{1}{k} \cdot \frac{e}{2\pi j} \int_{c-j\infty}^{c+j\infty} \frac{e^{\lambda t}}{\lambda^2} f(\lambda).d\lambda. \qquad \ldots\ldots(4.16)$$

For the second case, if the applied flux is $H(t).\Phi$, we have

$$\theta = \frac{1}{k} \cdot \frac{I}{I+R} \cdot H(t).\Phi$$

$$= \frac{1}{k} \cdot \frac{\Phi}{2\pi j} \int_{c-j\infty}^{c+j\infty} \frac{e^{\lambda t}}{\lambda} f(\lambda) d\lambda. \qquad \ldots\ldots(4.17)$$

The complex integral in both cases is taken round a curve from $c-j\infty$ to $c+j\infty$, c being positive and finite. The evaluation of the integrals is straightforward, since $f(\lambda)$ has simple poles at the roots of $\lambda^2+2\sigma\omega_0\lambda+\omega_0{}^2=0$.

(iv) *Two galvanometers in series*

Finally, we may note the easy way in which we can write down the solution to the problem of two galvanometers in series, an arrangement suggested by Butterworth for filtering. If I_1 and I_2 are the motional impedances of the instruments and R the static resistance of the circuit, the current i is given by

$$i=e/(R+I_1+I_2) \qquad \ldots\ldots(4.18)$$

and the deflections θ_1, θ_2 are given by

$$\theta_{1,2}=\frac{1}{k_{1,2}}\cdot\frac{I_{1,2}}{R+I_1+I_2}\int e dt$$

and

$$\left|\frac{I_{1,2}}{R+I_1+I_2}\right|=\frac{2S_{1,2}/z_{1,2}}{\{R^2+4(S_1/z_2+S_2/z_2)^2\}^{\frac{1}{2}}}, \qquad \ldots\ldots(4.19)$$

where the zs are as defined in (3.8).

ACKNOWLEDGMENTS

The writer is indebted to the Chief of the Royal Naval Scientific Service for permission to publish this paper, which formed part of work done during the war.

REFERENCES

Astbury, N. F., 1948, in preparation.
Butterworth, S., 1912, *Proc. Phys. Soc.*, **24**, 88.
Gall, D. C., 1942, *J. Instn. Elect. Engrs.*, **89**, Pt. II, 434 ; 1945, *J. Sci. Instrum.*, **22**, 218.
Ising, 1926, *Phil. Mag.*, Ser. 7, **1**, 827.
Jeffreys, H., 1931, *Operational Methods in Mathematical Physics* (Cambridge : University Press).
Moullin, E. B., 1938, *Spontaneous Fluctuations of Voltage* (Oxford : Clarendon Press).

DISCUSSION

Mr. J. F. W. Bell. I have recently been making use of the equivalent electrical circuit concept of the moving coil galvanometer as deduced by Butterworth. When a condenser is placed across the terminals there is an increase in the period, as would be expected if the galvanometer is looked upon as a parallel *LCR* network. The change in period gives the ratio k^2/gamma. From a knowledge of the unloaded period and the current sensitivity the constants α, β and k can be calculated. This method of determining the constants of a galvanometer has given good agreement with nominal values.

There are possible applications of the galvanometer as an electromechanical resonator at power and low frequencies, similar to the use of the piezoelectric crystal resonator at radio frequencies. Its use in an electronically maintained sine wave generator is of particular interest.

Mr. J. C. Willmott. I would like to ask Mr. Astbury if the formula $\bar{\theta}=\mu\sqrt{\pi kT/sT_0}$ for the mean deviation is applicable whatever the resistance of the circuit connected across the galvanometer.

Author's reply. I had originally intended to include as an example in the paper the problem quoted by Mr. Bell, and perhaps I may be allowed to show how simply the result can be obtained. If r be the d.c. resistance of the galvanometer, then the impedance, Z, obtained by connecting a capacitance C in shunt with the instrument, is given by

$1/Z=1/(r+I)+j\omega C$ or $Z=(r+I)/[1+j\omega C(r+I)]$. The maximum deflection will occur when $j\omega CI+1=0$, from which $\omega^2=\omega_0^2/(1+2SC\omega_0)$. Here ω_0 is the natural frequency of the instrument and ω the frequency as modified by the presence of the capacitance.

I feel that measurements of μ, S and ω_0 should be sufficient to provide estimates of all the other constants required, although I might mention that during the war I did devise a method for testing galvanometers based on a potentiometric method for measuring R_M and X_M at various frequencies. I agree with Mr. Bell that applications do exist for the galvanometer as he suggests, and I would like to add that it is good to see an appreciation of the galvanometer as a scientific instrument and not merely as a hack for null-detection work.

In reply to Mr. Willmott, the analysis given in the paper certainly leads to the result that the noise level is independent of R. We have made records of background signals which show that the level is substantially independent of R for values between critical resistance and one-fifth of this value, but the level observed was always higher by about 50% than that given by equation (4.9).

LETTERS TO THE EDITOR

The Structure of Carbon Monoxide

In both the molecular orbital and pairing approximations it is easily shown that the four π electrons of carbon monoxide are completely equivalent, so that the distinction between bonding and non-bonding electrons recently introduced by Long and Walsh (1947) is invalid. The symmetry of the molecule is most simply exhibited by Mulliken's formulation (1932):

$$(K)(K)(z\sigma)^2(y\sigma)^2(w\pi)^4(x\sigma)^2, \quad {}^1\Sigma^+,$$

where $(w\pi)$ is doubly degenerate.

The existence of the $(w\pi)^4$ shell, while indicating that four equivalent π electrons are concerned in $\pi\pi$ bonding, by no means implies that the molecule is best represented by a triple-bonded structure, as Long and Walsh seem to suppose. Indeed, analysis shows (Moffitt, to be published) that of the conventional structures

$$\overset{-}{\mathrm{C}}\equiv\overset{+}{\mathrm{O}} \text{ I}, \qquad \mathrm{C}=\mathrm{O} \text{ II}, \qquad \overset{+}{\mathrm{C}}-\overset{-}{\mathrm{O}} \text{ III},$$

II is the most important, and I is less important than III.

The rotational analysis (Schmid 1932) of the $(CO)^+$ produced by the first ionization of the molecule has shown it to have the symmetry ${}^2\Sigma$. Consequently the first ionization potential of CO, ${}^1\Sigma^+$ corresponds to the removal of a σ electron. The removal of a π electron, as postulated by Long and Walsh, would lead to $(CO)^+$, ${}^2\Pi$, and Mulliken (1928) has cited evidence to show that this ionization occurs near 17 ev. and not near 14 ev.

It is difficult to follow Long and Walsh in their reasoning that the removal of a π electron should lead to a strengthening of the bonding in the resulting $(CO)^+$. Introducing the wave-function symmetrization necessary to give significance to their structure, the ionization of an electron which accounts for a quarter of the considerable $\pi\pi$ bond strength in CO would surely lead to a weakening; and this is actually observed for CO^+, $A^2\Pi$ (Sponer 1935). The "three-electron bonding function" involving one π and two σ electrons, invoked in this connection, has, as far as I am aware, no precedent.

The low dipole moment of CO is well known; calculations (Moffitt, to be published) based on Long and Walsh's structure indicate, however, that the molecule should be highly polar. Further, the electron donor properties of CO are hardly to be attributed to the "inert pair" $(2s_C)^2$, whose ionization potential is expected to be near 20 ev., as assumed by these authors.

The real difficulty in describing the carbon monoxide molecule does not lie in the specification of the LCAO forms for the $(w\pi)^4$ shell, but in characterizing the nature of the three different σ-type orbitals. A plausible assignment of the six σ electrons to there localized molecular orbitals has been devised (Moffitt, to be published). Retaining Mulliken's notation, $(z\sigma)^2$ now corresponds essentially to $(2s_0)^2$ and $(y\sigma)^2$ refers to an electron pair

bond between some sp-type hybrid carbon orbital and a predominantly $2p\sigma$ oxygen orbital. The third pair of electrons $(x\sigma)^2$ are localized near the carbon atom and are nearly non-bonding. The ionization potential of a $(x\sigma)$ electron is estimated at near 14 ev., and, therefore, accounts for the first ionization potential and electron donor properties of carbon monoxide. The $(y\sigma)^2$ electron pair bond is shown to be largely homopolar.

The effect of the s-p hybridization gives rise to a compromise between strong $\sigma\sigma$-type bonding and the promotion required to produce the appropriate carbon valence state. This compromise has been shown to lead to an asymmetry in σ electron distribution, whose direction is opposite and whose magnitude is approximately equal to that of the π electrons ; the low dipole moment of carbon monoxide is no longer surprising.

The ionization of a non-bonding $(x\sigma)$ electron leads to a strengthening of the $\pi\pi$ bonding in as much as $(CO)^+$, $X^2\Sigma$ now becomes more nearly triple-bonded in the conventional sense. Further, the properties of the excited $A^1\Pi$ state of CO (Sponer 1935), in particular its weak bond strength, are accounted for by the formulation

$$(K)(K)(z'\sigma)^2(y'\sigma)^2(w'\pi)^4(x'\sigma)(\overline{w'\pi}),\ ^1\Pi,$$

where $(\overline{w'\pi})$ is the antibonding orbital corresponding to $(w'\pi)$. A full account of this work is being prepared for publication.

The author would like to acknowledge the receipt of a grant from the Board of the British Rubber Producers' Research Association.

New College, Oxford. WILLIAM MOFFITT.
5 March 1948.

LONG L. H., and WALSH, A. D., 1947, *Trans. Faraday Soc.*, **43**, 342.
MULLIKEN, R. S., 1928, *Phys. Rev.*, **32**, 205 ; 1932, *Rev. Mod. Phys.*, **4**, 1.
SCHMID, R., 1932, *Phys. Rev.*, **42**, 182.
SPONER, H., 1935, *Molekülspektren* (Berlin: Springer).

A Note on the Shape of the Polepieces of a Synchrotron Magnet

The Birmingham synchrotron magnet has recently been described (Oliphant, Gooden and Hide 1947), and an interesting problem connected with its magnetic field has arisen. For certain reasons it is desirable that the magnetic field strength H along the central radius of the gap between the polepieces of a synchrotron ring magnet should, in any normal section of the ring, be related to the radius vector r drawn from the centre of the ring by an equation of the form $H=ar^{-\frac{1}{3}}$. What shape should the polepieces have to give such a field? If the direct field due to the current in the coils be neglected, an approximate solution of the problem can be obtained by regarding it as a two-dimensional one. This is justified by the large mean radius of the ring, which is 450 cm. in the Birmingham magnet.

Once the method of conformal transformations has been adopted, the fact that the integral of $r^{-\frac{1}{3}}\,dr$ is equal to $3r^{\frac{1}{3}}$ suggests the trial of

$$W=Az^{\frac{1}{3}} \qquad \ldots\ldots (1)$$

as a possible solution. A is a constant and W is the complex potential of the form $W=U+iV$ and $z=x+iy=re^{i\theta}$. Applying equation (1), we get

$$W=Ar^{\frac{1}{3}}e^{i\theta/3}=Ar^{\frac{1}{3}}\cos\theta/3+iAr^{\frac{1}{3}}\sin\theta/3.$$

Take V as the potential and U as the stream function, then, since

$$U=Ar^{\frac{1}{3}}\cos\theta/3\ ;\quad V=Ar^{\frac{1}{3}}\sin\theta/3,$$

equipotentials are given by

$$r^{\frac{1}{3}}\sin\theta/3=B \quad\text{or}\quad r=C\,\mathrm{cosec}^3\,\theta/3, \qquad \ldots\ldots (2)$$

and lines of force are given by

$$r^{\frac{1}{3}}\cos\theta/3=D \quad\text{or}\quad r=E\sec^3\theta/3. \qquad \ldots\ldots (3)$$

Figure 1 represents sets of such curves.

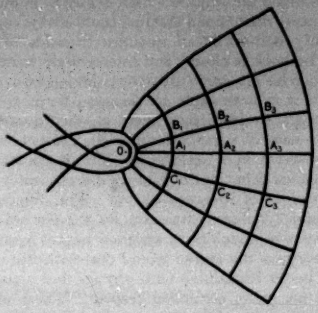

Figure 1. Section of field of " ideal " synchrotron magnet (right side only). Lines such as $B_1B_2B_3$, $C_1C_2C_3$ are equipotentials and possible polepiece profile curves. Lines such as $B_1A_1C_1$, $B_2A_2C_2$ are lines of force. Beams of particles pass normal to the plane of the figure through points on $A_1A_2A_3$.

The radial field strength $H_r=-\partial V/\partial r=-(Ar^{-\frac{1}{3}}\sin\theta/3)/3$, and the tangential component $H_\theta=-\partial V/r\partial\theta=-(Ar^{-\frac{1}{3}}\cos\theta/3)/3$. The resultant field strength is $H=-Ar^{-\frac{1}{3}}/3$. Along the central radius $\theta=0$; thus along that line $H_r=0$, $H_\theta=H=-Ar^{-\frac{1}{3}}/3$. Hence the field satisfies the desired condition. At any point $H_r/H_\theta=\tan\theta/3$, showing that for small values of θ, H_r is very small compared with H_θ.

The polepieces are to be made with profile curves $r=C\,\mathrm{cosec}^3\,\theta/3$, for they are themselves magnetic equipotentials.

The complete curves given by (2) and (3) consist of closed loops with " wings " extending to infinity. The two sets of curves are of the same shape but the lines of force are obtained by rotating the other set through 270° about an axis through the origin normal to the plane of the figure. The necessity of making the real polepieces finite in length instead of infinite increases the discrepancy between theory and experiment, but in the middle of the gap the difference should not be great.

The " basic " shape of the profile curves of the Birmingham synchrotron magnet, obtained empirically by the aid of the Peierls tank, appears to be very close to that suggested by equation (2).

University College, Nottingham. N. Davy.
23 February 1948.

Oliphant, M. L., Gooden, J. S., and Hide, G. S., 1947, *Proc. Phys. Soc.*, **59**, 666.

REVIEWS OF BOOKS

The A Priori in Physical Theory, by Arthur Pap. Pp. x+102. (New York: King's Crown Press, 1946.) 13*s.* 6*d.* net.

This book deals with a problem which, mainly through the assertions of the late Sir Arthur Eddington and Professor E. A. Milne, has in recent years become of much interest to physicists, namely the question whether or not the laws of nature are *a priori*, i.e. derivable by reason apart from experience and so not liable to falsification by experience. The author does not, however, attempt to solve the ultimate problem, but points out that in practice physical laws are often treated as " functionally " *a priori* ; thus, if an experiment or observation appears to violate a law we sometimes do not abandon the law but regard the experiment as not providing a fair example of it. Thus, when Uranus appeared to violate

Newton's law of gravitation, the law was not changed but Uranus was held to be disturbed. Laws sufficiently well grounded can acquire a high degree of immunity in this way. It was on such grounds that Poincaré maintained that one could always regard space as euclidean by attributing any apparently non-euclidean qualities to fields of force or non-rectilinear propagation of light. The book is clearly and interestingly written, though one feels that the author tends to continue his argument after the point has been adequately explained.

With the main thesis it is impossible to disagree, for it simply records what every physicist knows to be true. It inevitably raises another question, however, which the author does not consider—namely, what determines the choice between abandonment of the law and rejection of the observation as irrelevant? This is a pertinent question because, for example, while the anomalous behaviour of Uranus did not upset Newton's law of gravitation, the anomalous behaviour of Mercury did so. The difference was not merely that Neptune was observed and "Vulcan" was not, for the law was retained in spite of the irregularities of certain stars to which were assigned purely hypothetical companions. It would be interesting to see how the author would deal with this extension of his problem.

Mr. Pap is evidently better acquainted with physics than some philosophers who write on physical theory, and his views command respect. There are a few slips, however, which might be worth mentioning. The principle of conservation of mass is not rendered invalid by the discovery that mass depends on velocity (p. 61); it is, in fact, in order to maintain that principle that we must make mass depend on velocity. Again, neither in Newton's nor in Einstein's language is it true to say that force means $m\,dv/dt$ (p. 65); it means $d(mv)/dt$. An injustice is done to Galileo on p. 85 where it is said that he regarded the string of his pendulum as having no mass. He considered the effect of its mass very interestingly in the *Dialogues Concerning the Two Great Systems of the World*. Finally (p. 22), the author, apparently following Lenzen, seems to think that there is a "vicious circle" in making the length of a standard measuring rod depend on its temperature and defining a temperature scale in terms of length—a circle which needs a series of "successive approximations" to break it. This is not so, however, for a *thermoscope* is sufficient to make the prescription of the standard measuring rod definite, leaving us free to choose whatever type of *thermometer* we wish. Nor, in fact, do we ever measure temperature in terms of *measures* of length; the marks on our glass tube containing mercury are arbitrary so far as the unit of length measurement is concerned, which is why it is possible (though not necessary) to regard length and temperature as independent fundamental measurements in dimensional theory.

HERBERT DINGLE.

Five-figure Tables of Natural Trigonometrical Functions, prepared by H.M. Nautical Almanac Office. Pp. 124+iv. (London: H.M. Stationery Office, 1947.) 15*s.* net.

Tables of the natural values of the four trigonometrical functions: sine, tangent, cotangent, cosine, for every 10 seconds of arc, and an auxiliary table for the cotangent for every second of arc to 7° 30′.

A. C. S.

Logarithmic and Trigonometric Tables, by J. B. DALE. Pp. 42+vi. (London: Edward Arnold and Co., 1947.) 2nd Edition. 2*s.* 6*d.*

A new edition, completely reset in very clear form.

A. C. S.

Note. Details of binding cases will be given in the July issue of the *Proceedings*.

INDEX

PAGE

Alkali halides, polarization of second order Raman effect in 498
Ammonia, collision broadening of inversion spectrum 540
Ammonia, pressure broadening of inversion spectrum : disturbance of thermal equilibrium 83
Andrade, E. N. da C. : Device for maintaining constant stress in rod undergoing plastic extension 304
Arc discharges, transient, cathode spot behaviour in 424
Astbury, N. F. : Calibration of hydrophones and crystal transceivers 193
Astbury, N. F. : Moving-coil galvanometer as circuit element 590

Band overlap, and thermionic emission constants 360
Barkhausen effect 370
Bates, L. F., and Davis, J. H. : Effect of temperature on heat changes in magnetization of Ni–Si alloy 307
Bates, L. F., and Harrison, E. G. : Adiabatic temperature changes accompanying magnetization of ferromagnetic alloys 213, 225
Belin, R. E. : Radiosonde method for atmospheric potential gradient measurements . 381
β-ray measurements, correction for self-weakening in 460
β-ray spectrum of ThC″D 466
Birks, J. B. : Measurement of permeability of low-conductivity ferromagnetic materials at cm. wavelengths 282
Blackman, M., and Michiels, J. L. : Efficiency of counting systems 549
Bleaney, B., and Penrose, R. P. : Collision broadening of inversion spectrum of ammonia : III. cross-sections for self-broadening and for mixtures with non-polar gases 540
Bleaney, B., and Penrose, R. P. : Paramagnetic resonance at low temperatures in chromic alum 395
Bleaney, B., and Penrose, R. P. : Pressure broadening of inversion spectrum of ammonia : II. disturbance of thermal equilibrium at low pressures 83
Bond lengths and electronic structure of coronene and pyrene 309
Book reviews 114, 212, 308, 398, 499, 599
Brewer, A. W., Cwilong, B., and Dobson, G. M. B. : Measurement of absolute humidity in extremely dry air 52
Broda, E., Grummitt, W. E., Guéron, J., Kowarski, L., and Wilkinson, G. : Correction for self-weakening in β-ray measurements 460
Broda, E., *see* Zając, B.
Bush, H. D., and Tebble, R. S. : Barkhausen effect 370

Calibration of hydrophones and crystal transceivers 193
Campbell, N. R., and Hartshorn, L. : Experimental basis of electromagnetism : II. electrostatics 27
Carbon monoxide, structure 597
Cathode spot behaviour in transient arc discharges 424
Cavity resonator method of measuring dielectric constant of polar liquids . . 71
Chaudhri, M., and Fenton, A. G. : Experiments with adjustable Geiger-Müller counters 183
Clegg, J. A., *see* Lovell, A. C. B.
Collie, C. H., Hasted, J. B., and Ritson, D. M. : Cavity resonator method of measuring dielectric constants of polar liquids in centimetre band 71
Collie, C. H., Hasted, J. B., and Ritson, D. M. : Dielectric properties of water and heavy water 145
Collision broadening of inversion spectrum of ammonia 540
Contacts, electrical behaviour, influence of surface films 315

PAGE

Corcoran, N., and Hough, J. M. : Computation of polar diagram of radio aerial, flat earth and vertical screen 203
Corrigenda 308
Cosmic-ray intensity, semi-diurnal variation 509
Coulson, C. A. : Excited electronic levels in conjugated molecules, u.v. absorption of naphthalene etc. 257
Coulson, C. A., *see* Duncanson, W. E.
Coulson, C. A., *see* Moffitt, W. E.
Counters, Geiger-Müller, adjustable, experiments with 183
Counting systems, efficiency of 549
Cwilong, B., *see* Brewer, A. W.

Davis, J. H., *see* Bates, L. F.
Davy, N. : Shape of polepieces of synch-otron magnet 598
δ-radiation, Kapitza's theory, extension 453
Désirant, M., and Shoenberg, D. : Penetration of magnetic field into super-conductors, measurements on thin cylinders 413
Diagrams, solid, to illustrate resonance phenomena 132
Dielectric constant measurement, of polar liquids by cavity resonator method . 71
Dielectric films, electric strength 243
Dielectric properties of water and heavy water 145
Dilworth, C. C. : Influence of surface films on electrical behaviour of contacts . 315
Disintegration of nitrogen by deuterons, neutrons emitted in 523
Dissociation energy of NO molecule 533
Dobson, G. M. B., *see* Brewer, A. W.
Donovan, B. : Specific heat of linear ionic lattice 325
Duncanson, W. E., and Coulson, C. A. : Electron momenta in atoms . . . 175

Efficiency of counting systems 549
Eigenvalue problems, solution of 481
Electric strength of dielectric films 243
Electromagnetism, experimental basis : electrostatics 27
Electron bunching for mμsec. pulse generation 397
Electronic levels, excited, in conjugated molecules : symmetry and multiplicity of molecular states 270
Electronic levels, excited, in conjugated molecules : u.v. absorption of naphthalene . 257
Electronic structure and bond lengths of coronene and pyrene 309
Electron momenta in atoms 175
Electron trap mechanism of luminescence in sulphide and silicate phosphors . 574
Electrostatics—experimental basis of electromagnetism 27
Emission, thermionic, constants, and band overlap 360
Energy levels in insulators, and work function 13
Energy levels, in oxide cathode coatings 22
Evans, W. M., *see* Pack, D. C.

Feather, N. *see* Zajac, B.
Fenton, A. G., *see* Chaudhri, M.
Ferretti, B., and Krook, M. : Solution of scattering and related problems . . . 481
Fisher, D. G. : Molecular structure and arrangement in stretched natural rubber . 99
Frank, F. C. : Isotopic abundance rule, and origin of nuclei 211
Froome, K. D. : Rate of growth of current and behaviour of cathode spot in transient arc discharges 424

Galvanometer, moving-coil, as circuit element 590
γ-radiation from polonium, study of 501
Garlick, G. F. J., and Gibson, A. F. : Electron trap mechanism of luminescence in sulphide and silicate phosphors 574
Gerő, L., and Schmid, R. : Dissociation energy of NO molecule 533

PAGE

Gibson, A. F., *see* Garlick, G. F. J.
Gibson, W. M., and Livesey, D. L. : Neutrons emitted in disintegration of nitrogen by deuterons 523
Gold in silver, heat of solution and residual resistance 161
Grummitt, W. E., *see* Broda, E.
Guéron, J., *see* Broda, E.

Harrison, E. G., *see* Bates, L. F.
Hartshorn, L., *see* Campbell, N. R.
Hasted, J. B. : Milli-microsecond pulse generation by electron bunching . . 397
Hasted, J. B., *see* Collie, C. H.
Heavy water, and water, dielectric properties 145
Helium, liquefaction, expansion method 405
Horton, G. K. : Angular distribution in internal pair creation 457
Hough, J. M., *see* Corcoran, N.
Hsü, Yun-Kuei, *see* Martin, D. G. E.
Huang, Kun : Quantum mechanical calculation of heat of solution and residual resistance of gold in silver 161
Humidity, absolute, measurement in extremely dry air 52
Hydrophones, and crystal transceivers, calibration 193

Impedance measurement, Lecher wire method 388
Insulators, energy levels in, and work function 13
Internal pair creation, angular distribution in 457
Isotopic abundance rule, and origin of nuclei 211

James, H. J., *see* Pack, D. C.

Kapitza's theory of δ-radiation, extension 453
Kikuchi-line patterns, interpretation and application : I. crystal unit cell . . 341
Kowarski, L., *see* Broda, E.
Krook, M., *see* Ferretti, B.
Kun Huang, *see* Huang

Lattices, ionic, linear, specific heat of 325
Lead sulphide and lead selenide photosensitive deposits, structure, and effect of sensitization by oxygen 117
Livesey, D. L., *see* Gibson, W. M.
Loeb, L. B. : Certain aspects of mechanism of spark discharge 561
Longuet-Higgins, H. C. : Excited electronic levels in conjugated molecules : symmetry and multiplicity of molecular states 270
Lovell, A. C. B., and Clegg, J. A. : Characteristics of radio echoes from meteor trails : I. intensity and electron density 491
Luminescence, electron trap mechanism, in sulphide and silicate phosphors . . 574

Magnetization of ferromagnetic alloys, adiabatic temperature changes accompanying 213, 225
Magnetic field, penetration into superconductors 413
Magnetization of Ni–Si alloy, effect of temperature on heat changes . . . 307
Magnetization, variation of Young's modulus for Co with 236
Martin, D. G. E., Richardson, H. O. W., and Hsü, Yun-Kuei : β-ray spectrum of ThC″D 466
Menzies, A. C., and Skinner, J. : Polarization of second order Raman effect in alkali halides 498
Metals, slip at grain boundaries and grain growth 391
Meteor trails, characteristics of radio echoes from : I. intensity and electron density . 491
Michiels, J. L., *see* Blackman, M.
Moffitt, W. : Structure of carbon monoxide 597

PAGE

Moffitt, W. E., and Coulson, C. A.: Electronic structure and bond lengths of coronene and pyrene 309
Molecular states, symmetry and multiplicity 270
Molecular states, and u.v. absorption of naphthalene etc. 257
Molecular structure and arrangement in stretched natural rubber 99
Mott, N. F.: Slip at grain boundaries, and grain growth in metals 391
Moving-coil galvanometer as circuit element 590

Nicolson, P., and Sarabhai, V.: Semi-diurnal variation in cosmic-ray intensity . 509
Nitrogen, disintegration by deuterons, neutrons emitted in 523
NO molecule, dissociation energy 533
Nuclear physics, internal pair creation, angular distribution 457

Optical instruments, perfect 293
Oxide cathode coatings, energy levels in 22

Pack, D. C., Evans, W. M., and James, H. J.: Propagation of shock waves in steel and lead 1
Paramagnetic resonance, in chromic alum, at low temperatures 395
Penrose, R. P., *see* Bleaney, B.
Permeability of low-conductivity ferromagnetic materials at cm. wavelengths, measurement 282
Phosphors, sulphide and silicate, electron trap mechanism of luminescence . . 574
Photosensitive PbS and PbSe deposits, structure 117
Pickard, G. L., and Simon, F. E.: Quantitative study of expansion method for liquefying helium 405
Plessner, K. W.: Electric strength of dielectric films 243
Polar diagram of radio aerial, flat earth and vertical screen, computation of . . 203
Polar liquids, dielectric constant measurement by cavity resonator method . . 71
Polonium, study of γ-radiation from 501
Potential gradient, atmospheric radiosonde method of measurement 381
Pressure broadening of inversion spectrum of ammonia: II. disturbance of thermal equilibrium at low pressures 83
Prowse, W. A.: Solid diagrams illustrating resonance phenomena 132
Pulse generation, milli-microsecond, by electron bunching 397

Quantum mechanical calculation of heat of solution and residual resistance of gold in silver 161

Radiosonde method for atmospheric potential gradient measurement 381
Raman effect in alkali halides, polarization 498
Reflectivity, metallic, variation with temperature 8
Resonance, paramagnetic, at low temperatures in chromic alum 395
Resonance phenomena, solid diagrams illustrating 132
Richardson, H. O. W., *see* Martin, D. G. E.
Ritson, D. M., *see* Collie, C. H.
Rubber, natural, stretched, molecular structure and arrangement in 99
Rubber, stresses and birefringence in, when subjected to strain 135

Sarabhai, V., *see* Nicolson, P.
Scattering problems, solution of 481
Schmid, R., *see* Gerö, L.
Self-weakening in β-ray measurements, correction for 460
Shoenberg, D., *see* Désirant, M.
Shock waves, propagation in steel and lead 1
Sillitto, R. M.: Extension of Kapitza's theory of δ-radiation 453
Simon, F. E., *see* Pickard, G. L.

PAGE
Sinha, S. P.,: Blue and ultra-violet bands of K_2 436
Sinha, S. P. : Ultra-violet bands of Li_2 443
Sinha, S. P. : Ultra-violet bands of NaK 447
Skinner, J., *see* Menzies, A. C.
Slip at grain boundaries and grain growth in metals 391
Smith, T. : Perfect optical instruments 293
Spark discharge, mechanism of 561
Specific heat of linear ionic lattice 325
Spectrum, inversion, of ammonia, collision broadening 540
Spectrum, inversion, of ammonia, pressure broadening 83
Spectra, blue and ultra-violet bands of K_2 436
Spectra, ultra-violet bands of Li_2 443
Spectra, ultra-violet bands of NaK 447
Street, R. : Variation with magnetization of Young's modulus for cobalt . . 236
Stress, constant, maintenance in rod undergoing plastic extension 304
Stresses and birefringence in rubber subjected to strain 135
Superconductors, penetration of magnetic field: measurements on thin cylinders . 413
Surface films, influence on electrical behaviour of contacts 315
Synchrotron magnet, shape of polepieces 598

Tebble, R. S., *see* Bush, H. D.
Temperature changes, adiabatic, accompanying magnetization of ferromagnetic alloys 213, 225
Temperature, variation of metallic reflectivity with 8
ThC″D, β-ray spectrum of 466
Transceivers, crystal, and hydrophones, calibration 193
Treloar, L. R. G. : Stresses and birefringence in rubber subjected to homogeneous strain 135

Ultra-violet bands of K_2, Li_2, NaK 436, 443, 447

Water, and heavy water, dielectric properties 145
Weil, R. : Variation with temperature of metallic reflectivity 8
Wilkinson, G., *see* Broda, E.
Williamson, M. : Lecher wire method of measuring impedance 388
Wilman, H. : Interpretation and application of electron-diffraction Kikuchi-line patterns : I. crystal unit cell 341
Wilman, H. : Structure of photosensitive PbS and PbSe deposits and effect of sensitization by oxygen 117
Wohlfarth, E. P. : Thermionic emission constants and band overlap 360
Work function, and energy levels in insulators 13
Wright, D. A. : Energy levels in oxide cathode coatings 22
Wright, D. A. : Work function and energy levels in insulators 13

Young's modulus for cobalt, variation with magnetization 236

Zajac, B., Broda, E., and Feather, N. : Further study of γ-radiation from polonium . 501

INDEX TO REVIEWS OF BOOKS

PAGE

Boucher, Paul E.: *Fundamentals of Photography with Laboratory Experiments* . 402
Bouwers, A.: *Achievements in Optics* 212

Chase, C. T.: *The Evolution of Modern Physics* 403
Cork, J. M.: *Radioactivity and Nuclear Physics* 400
Cosslett, V. E.: *The Electron Microscope* 404
Culver, Charles A.: *Theory and Applications of Electricity and Magnetism* . . 499

Dale, J. B.: *Logarithmic and Trigonometric Tables* 600

Evans, David T.: *Frontiers of Astronomy* 404

Griffiths, Ezer: *Methods of Measuring Temperature* 308

Lovell, Bernard (Editor): *Electronics and their Applications in Industry and Research* 114

Mathematical Tables Project of the National Bureau of Standards: *Table of the Bessel Functions $J_0(z)$ and $J_1(z)$ for Complex Arguments* 401
Mathematical Tables Project of the National Bureau of Standards: *Tables of Spherical Bessel Functions* 401

Nautical Almanac Office: *Five-figure Tables of Natural Trigonometrical Functions* 600
Nimmo, R. R.: *Atomic Energy* 403

Pap, Arthur: *The A Priori in Physical Theory* 599
Poynting, Thomson and Todd: *A University Text-Book of Physics, Volume I: Properties of Matter* 404

Ridenour, Louis N. (Editor): *Radar System Engineering* 398

Snoek, J. L.: *New Developments in Ferromagnetic Materials* 116

Ubbelohde, A. R.: *Time and Thermodynamics* 402